Title
Non-Thermal Irreversible Electroporation in Heterogeneous Tissues

Author
Daniels, Charlotte Sara

Publication Date
2011

Peer reviewed|Thesis/dissertation

Non-Thermal Irreversible Electroporation in Heterogeneous Tissues

By

Charlotte Sara Daniels

A dissertation submitted in partial satisfaction of the

requirements for the degree of

Doctor of Philosophy

in

Engineering – Mechanical Engineering

in the

Graduate Division

of the

University of California, Berkeley

Committee in charge:

Professor Boris Rubinsky, Chair

Professor Lisa A. Pruitt

Professor Steven Conolly

Fall 2011

Abstract

Non-Thermal Irreversible Electroporation in Heterogeneous Tissues

by

Charlotte Sara Daniels

Doctor of Philosophy in Engineering – Mechanical Engineering

University of California, Berkeley

Professor Boris Rubinsky, Chair

Non-thermal irreversible electroporation (IRE) is a new minimally invasive surgical technique that is part of the emerging field of molecular surgery which holds the potential to treat diseases with unprecedented accuracy. IRE utilizes electrical pulses delivered to a targeted area, producing irreversible damage to the cell membrane. While electroporation is not fully understood to date, evidence indicates that this damage is induced by the increased transmembrane potential due to high voltage pulses affecting the lipid bilayer. Because IRE does not cause thermal damage, the integrity of all other molecules and only effects cellular structures, collagen and elastin in the targeted area is preserved.

Previous theoretical studies have only examined IRE in homogeneous tissues. However, tissues can be heterogeneous in two different capacities: 1) they can be intrinsically heterogeneous due to anatomy, and 2) they can be extrinsically heterogeneous due to external factors. This investigation of heterogeneous tissues studies both cases in order to expand the depth and breadth of the field of electroporation.

Intrinsic Heterogeneous Tissues

Because biological structures are complex collections of diverse tissues it becomes imperative to consider intrinsic heterogeneities. In order to develop electroporation as a precise treatment in clinical applications, realistic models for pre-surgical planning are necessary. In this way, the study of heterogeneous tissues will enable refinement of electroporation as a treatment. In this chapter, three different intrinsic heterogeneous structures were taken into account: nerves, blood vessels and lactiferous ducts. The subsequent results made it clear that heterogeneities significantly impact both the temperature and electrical field distribution in surrounding tissues, indicating that heterogeneities should not be neglected. While the surrounding tissue experienced a high electrical field, the axon of the nerve, the interior of the blood vessel and the ducts experienced no electrical field. This indicates that blood vessels, nerves and lactiferous ducts adjacent to a tumor treated with electroporation have the potential to survive, while the cancerous lesion is ablated. This clearly demonstrates the importance of considering heterogeneity in IRE applications.

Extrinsic Heterogeneous Tissues

Extrinsic heterogeneous tissues can be induced by various external factors. One such factor is an applied temperature gradient. Two different temperature gradients were considered in this investigation: 1) subzero temperatures, induced by cryosurgery, and 2) cooling temperatures.

Cryosurgery, tissue ablation by freezing, is a well-established minimally invasive surgical technique. The goal of this investigation was to study extrinsic heterogeneous tissues induced by externally applied subzero temperatures by combining cryosurgery and electroporation. Analysis of the electric field and temperature distribution during simultaneous tissue treatment with cryosurgery and irreversible electroporation (cryoIRE) was used to study the effect of tissue freezing on electric fields. The results indicate that this combination may resolve some of the major disadvantages that occur in each technology when used alone. Because of decreased electrical conductivity in the frozen tissue, this region experienced temperature induced magnified electric fields in comparison to IRE delivered to unfrozen tissue, the control case. This suggests that freezing confines and magnifies the electric fields to those regions; a targeting capability unattainable in traditional electroporation. This analysis also shows how temperature induced magnified and focused IRE can be used to ablate cells in the high subzero freezing region of a cryosurgical lesion, in which cells can be resistant to freezing damage.

The next heterogeneous tissues that were studied were heterogeneities extrinsically produced by cooling. This chapter explores the hypothesis that non-subzero temperature dependent electrical parameters of tissue can also be used to modulate the outcome of IRE protocols, providing a new means for controlling and optimizing this minimally invasive surgical procedure. This chapter investigates two different applications of cooling temperatures applied during IRE. The first case utilizes an electrode which simultaneously delivers electric fields and cooling temperatures. The subsequent results demonstrate that changes in electrical properties due to temperature produced by this configuration can substantially magnify and confine the electric fields in the cooled regions while almost eliminating electric fields in surrounding regions. This method can be used to increase precision in IRE procedures, and eliminate muscle contractions and damage to adjacent tissues. The second configuration considered introduces a third probe that is not electrically active and only applies cooling boundary conditions. This second configuration demonstrates that with this probe geometry the temperature induced changes in electrical properties of tissue substantially reduce the electric fields in the cooled regions. This novel treatment can potentially be used to protect sensitive tissues from the effect of IRE.

Perhaps the most important conclusion of this investigation is that temperature is a powerful and accessible mechanism to modulate and control electric fields in biological tissues and can therefore be used to optimize and control IRE treatments.

TABLE OF CONTENTS

Chapter 1: Introduction

1.1 Electroporation

1.1.1 Introduction to Electroporation

Electroporation is the phenomenon in which the permeability of a lipid bilayer is affected by an increased transmembrane potential induced by high voltage pulses (J. Weaver & Mintzer 1981). While the molecular mechanism of electroporation is not yet fully understood, theoretical models and experimental results both suggest that permeability is altered due to the formation of pores, also known as electropores, in the lipid bilayer (J. Weaver 1993). The formation of pores is affected by various parameters, including pulse number, length and frequency, but is primarily affected by electric field. These parameters can be varied in order to accomplish two different kinds of electroporation: reversible electroporation and irreversible electroporation. When the permeability of the membrane is only temporary, and the cell membrane reseals, reversible electroporation has occurred. If permeability remains permanent, irreversible electroporation has occurred and the cell will experience necrosis (J. Weaver & Chizmadzhev 1996a). Reversible electroporation is used for drug delivery and gene therapy and to transfer proteins or other macromolecules into cells (Neumann et al. 1982),(Okino & Mohri 1987). Irreversible electroporation functions as sterilization and focal tissue ablation (AJ Sale & WA Hamilton 1967),(AJ Sale 1968).

1.1.2 History of Electroporation

Studies on the effect of a voltages applied to tissue were initiated over a century ago. However, the experiments that lead to the theory of electroporation began in the 20th century. In the mid 20th century, Frankenhaeuser and Widén conducted a study in which electrical pulses were applied to the nodes of nerve tissue in order to investigate the phenomenon of *anode break excitation* (Frankenhaeuser & Widén 1956). They found that there was electrical damage to the nodes, as well as inactivation of the nerves. However, they also noted that the damage seemed reversible (Hodgkin 1951).

In the 1960s, Sale and Hamilton published a series of three papers which became the foundation of the field of electroporation (Ivorra & Rubinsky 2010). The goal of the first paper was to prove that cells can be killed by high DC electric pulses, without thermal effects. They used ten, 2-10μs pulses of a frequency higher than 1Hz to minimize a change temperature. They found that the parameters which effect cell death were electrical field magnitude and length of the applied field (AJ Sale & WA Hamilton 1967).

In their second paper, Hamilton and Sale attempted to determine how electric fields kill cells. In their study, light spectroscopy demonstrated leakage of Escherichia Coli cell content into the extracellular medium. They concluded that the method of ablation is through the irreversible loss of the membranes function as a semipermeable barrier (WA Hamilton & AJH

Sale 1967). Their third paper demonstrated that the magnitude of the electric field required to achieve cell lysis ranges from 3.1-17kV/cm in various organisms. They utilized 10 pulses of 20μs length with the requirement for lysis being an ablation of 50% of the population. However, the corresponding transmembrane potentials were 0.7-1.15V (AJ Sale & WA Hamilton 1968).

The 1980s were the decade in which electroporation gained wide recognition in the field of modern biotechnology. In 1982 the term *electroporation* was first established to describe the membrane breakdown discussed in a paper by Neumann and his collaborators. In this paper, the use of electroporation to introduce genes into cells is first presented. Gene therapy specifically utilizes reversible electroporation, and therefore this study strongly cautions irreversible electroporation. For two decades after this study, irreversible electroporation was studied primarily as an upper boundary to reversible electroporation (Neumann et al. 1982).

Mir published two seminal papers in 1991 that used reversible electroporation to treat cancer by facilitating the penetration of chemotherapy drugs such as bleomycin into cancer cells. In the first paper, he introduced the term *electrochemotherapy* to the field of electroporation in order to describe this treatment (Mir et al. 1991). Electrochemotherapy is currently being used to treat cancer patients in clinical settings (Mir et al. 2006).

Following Mir's work, the field of electroporation took off. Numerous experimental and theoretical studies on reversible and irreversible electroporation in various mammalian and bacterial cells and tissues have contributed to the field, leading to new discoveries and potential applications. Additionally, numerous theories have been introduced and developed in an attempt to explain the mechanism behind electroporation.

1.1.3 Mechanism of Electroporation

To date, electropores have not yet been imaged on the membrane level. However, implicit evidence gathered from mathematical analysis, cellular imaging, experimental studies and other investigations all corroborate the transient aqueous pore model. For this reason, in the field of electroporation, the widely accepted explanation for cellular response to the application of high voltage pulses is electropores. According to experimental observations and transient aqueous pore mechanism hypothesis (Neumann et al. 1989),(Chang et al. 1992),(J. Weaver 1993),(J. Weaver & Chizmadzhev 1996a),(Zimmerman 1996),(J. Weaver 2000),(T. Tsong 1991) the process of electroporation follows a series of six stages:

1. Electroporation is catalyzed by the application of short (micro, milli or even nanosecond) electrical pulses which create an elevated transmembrane potential of approximately 1V (RP Joshi & K. Schoenbach 2002), (Vernier et al. 2008).
2. The elevated transmembrane potential charges the lipid bilayer membrane as a result of ion flow.
3. The membrane then undergoes rapid, localized, structural rearrangements which can be termed 'hydrophobic' pores.
4. The membrane then establishes stable 'hydrophilic' pores.

5. Due to the formation of hydrophilic pores, which act as aqueous pathways between the extracellular and intracellular space, ionic and molecular transport through the membrane increases.
6. Depending on pulse parameters, the hydrophilic pores are either reversible or irreversible. If reversible, the cell membrane reseals. If irreversible, the cell is ablated.

These six stages are currently viewed as governing the process of electroporation (J. Weaver 2003).

A cell membrane is a bilayer of organized amphiphilic phospholipid molecules, which each have distinct hydrophobic and hydrophilic regions, in an aqueous electrolyte. Amphiphilic phospholipid molecules are composed of a triglycine head attached to two fatty acid hydrocarbon chains by ester linkages. The triglycine head is hydrophilic and the hydrocarbon chains are hydrophobic. As a result, the phospholipids arrange themselves with hydrophilic triglycine heads exposed to the aqueous extracellular environment, sequestering the hydrophobic hydrocarbon chains away from the aqueous phase efficiently packed in parallel (as shown in Figure 1.1). One of the major roles of the cellular membrane is, in fact, an electrical mechanism; impeding or permitting ion flow through various embedded proteins. As a result, a potential difference of 100mV is typically maintained across a membrane (Lewis 2003).

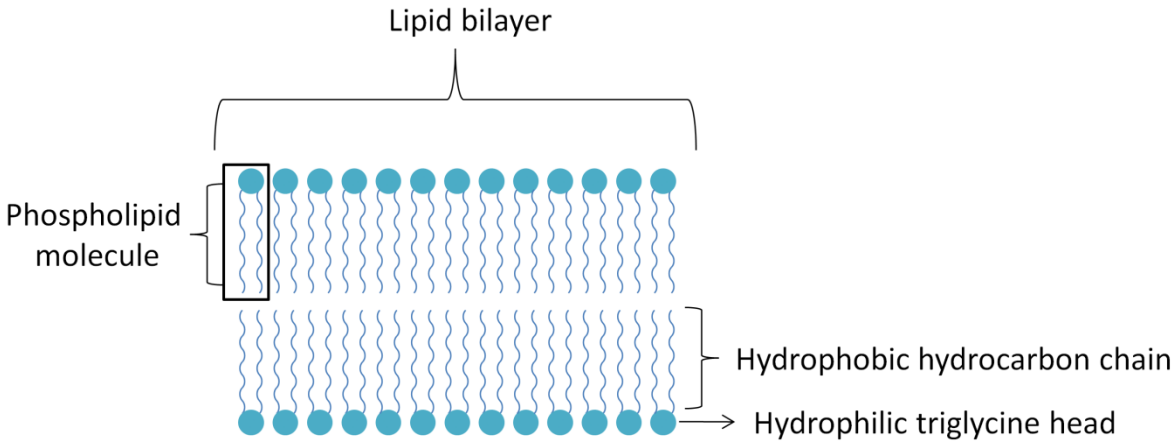

Figure 1.1: The geometric configuration of a cell membrane. Shown here is a cross section of the cell membrane lipid bilayer. The lipid bilayer is composed of two rows of amphiphilic phospholipid molecules. Phospholipid molecules arrange themselves with their hydrophilic triglycine head outwards, adjacent to the surrounding aqueous environment and cluster the hydrophobic hydrocarbon chains sandwiched within. This protects the hydrophobic system from the aqueous environment.

The charges or electric dipoles of the lipid molecule render a lipid bilayer susceptible to the influence of an externally applied electric field. This allows the lipid molecules to reorient themselves under an intense electric field, which ultimately can lead to the creation of new

hydrophobic pores followed by the formation of structurally more stable hydrophilic pores (T. Tsong 1991).

In a normal cell, pores occur stochastically in the lipid bilayer as a result of thermal fluctuations. However, the application of a transmembrane potential lowers the energy necessary to form them (Saulis & Venslauskas 1993). Once a pore is formed, the stability depends on pore energy, which is the sum of mechanical and electrical energy contributions. As a result, the creation of a pore occurs when the transmembrane electric field exceeds the dielectric strength of the membrane. This leads to the rapid formation of hydrophobic pores (Figure 1.2a). Depending on the electrical parameters, hydrophobic pore expansion may occur (Figure 1.2b). If the local transmembrane potential reaches a metastable state, pores can stabilize and transition from a hydrophobic to hydrophilic configuration (Figure 1.2c). Hydrophilic pores allow the introduction of macromolecules into a cell. In the case of reversible electroporation, once the external electric field is removed, the lipid bilayer is capable of rearranging and returning to its original configuration (Figure 1.2d). In the case of irreversible electroporation, once the external electric field is removed, the cell no longer is capable of rearranging and returning to its original state. In this case, it then undergoes cell death (J. Weaver & Chizmadzhev 1996b),(J. Weaver 2003).

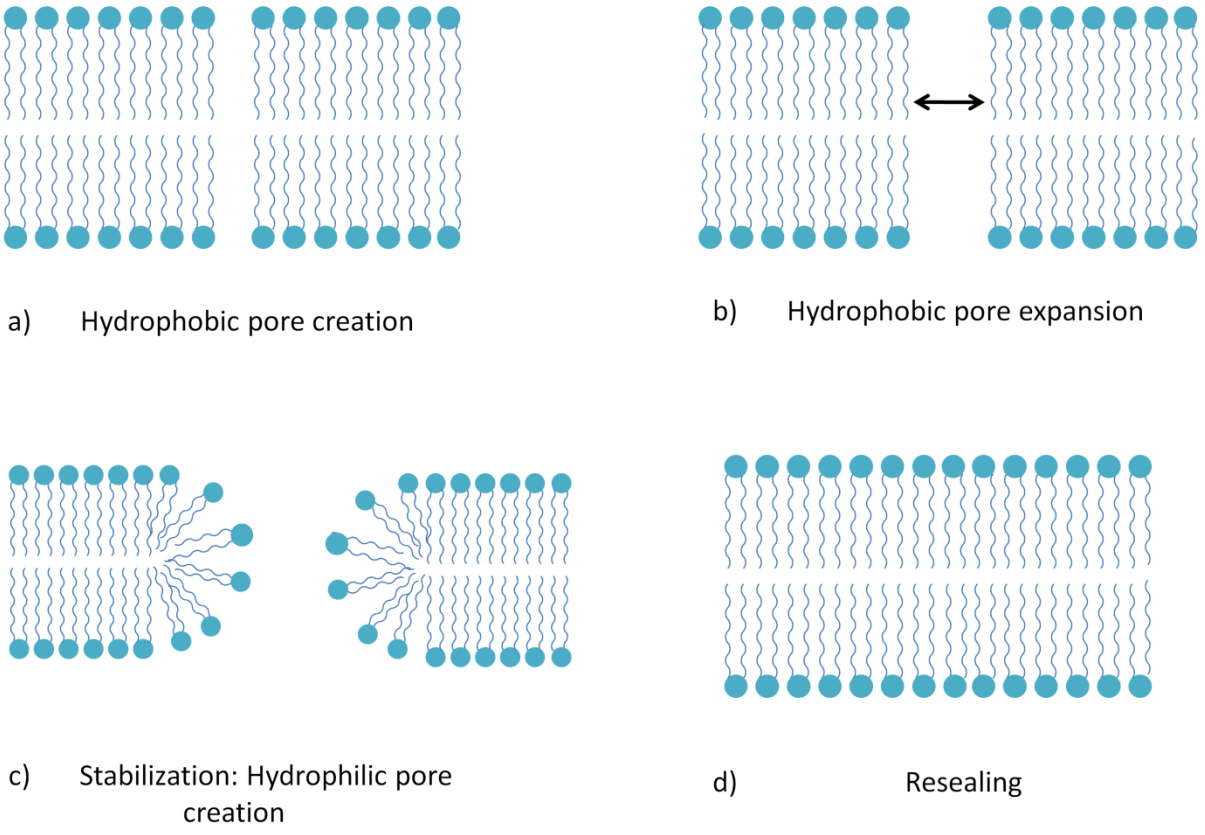

Figure 1.2: a) When the transmembrane electric field exceeds the dielectric breakdown strength of the membrane, hydrophobic pores form. b) Hydrophobic pore expansion occurs if the electric parameters are sufficient. c) If the local transmembrane potential reaches a metastable state, hydrophobic pores rearrange into hydrophilic pores. d) Once the

external electric field is removed, the lipid bilayer returns to its original configuration in the case of reversible electroporation.

Figure 1.2 illustrates the progression of events that occur in the lipid bilayer during reversible electroporation. During irreversible electroporation, the same process depicted in Figure 1.2 is followed, except step four (resealing) is replaced with membrane rupture and eventual cell death (Kinosita & K. Tsong 1977). Therefore, both reversible and irreversible electroporation undergo hydrophobic pore creation, hydrophobic pore expansion and hydrophilic pore creation and stabilization.

The onset of electroporation is a function of multiple parameters (discussed in section 1.1.5), one of which is electric field. The electric field required for reversible electroporation is typically lower than the values required for irreversible electroporation. Irreversible electroporation requires an electric field of approximately 100V/m, whereas reversible electroporation requires an electric field of 10V/m. With an applied voltage, a membrane passes through at least two stages:

1) A steady state current stage, and
2) A fluctuating current stage.

In the case of reversible electroporation, the membrane recovers from the region of pre-breakdown fluctuations and if the pulse length is not too long, returns to its original, intact state (J. Weaver 2003). With an electric field of sufficient proportions, stabilization of hydrophilic pores leads to expansion. Expansion of pores leads to instability in the membrane and results in cell death.

The mechanism of cell death due to irreversible electroporation has been shown to be due to both necrosis and apoptosis, otherwise known as programmed cell death. Necrosis, or cell lysis, happens relatively immediately in a cell. However, apoptosis requires a more sophisticated cascade of cellular responses, and therefore can take hours to days to complete. It has been shown that electroporation can trigger apoptosis in cancer cells, which no longer have the ability to go through programmed cell death independently (Al-Sakere et al. 2007). Other studies have found that cell death becomes more extensive as time progresses after an electroporation treatment, peaking after 24 hours. This indicates the occurrence of apoptosis in electroporation ablation methods (Hjouj & Rubinsky 2010).

Resealing is currently even less understood than the poration phase. As the transmembrane voltage slows and then decreases, the ionic conductance of the pores also decreases. This is the beginning of the resealing process. As the electrical impact fades due to local membrane discharge via pores as well as the lowering of the transmembrane potential, pore expansion slows. After pore expansion slows, pore size begins to decrease, finalizing the resealing process (J. Weaver 2003).

1.1.4 Applications of Electroporation

Because electroporation has been effectively demonstrated in research scenarios throughout its stages of development, electroporation has generated uses in various different settings. Reversible and irreversible electroporation both have practical applications in medicine, biology and the food industry as well as other fields. Additionally, because electroporation is a relatively simple procedure to perform, it has gained acceptance even in smaller laboratory settings.

1.1.4.1 Reversible Electroporation

The field of electroporation began with the discovery and development of reversible electroporation. And even currently, reversible electroporation is by far the most common application of electroporation technology. Two common applications of reversible electroporation, as mentioned previously, are drug delivery and gene therapy (also known as transfection).

Reversible electroporation can be used to facilitate drug delivery. It has been shown that the combination of anticancer drugs and electroporation reduces the weight of tumors more effectively than anticancer drugs alone. Okino and Mohri demonstrated in 1987 that by applying pulsed electric fields to a cellular medium while simultaneously administering the anticancer drug, bleomycin, the weight of tumors in rats were reduced on average by 56% as compared to bleomycin administered alone (Okino & Esato 1990). This application is known as electrochemotherapy when it is utilized with the drug bleomycin to target tumor cells. The application of electroporation catalyzes the development of electropores, which provide a pathway for external drugs to enter a cell. Electrophoresis may play a role in transporting drugs through such pathways into the cell. Once the electric field is removed, the cell reseals (because reversible electroporation is being utilized) encapsulating the particular drug (Dev et al. 2000).

Diseases that are caused by the mutation of a single gene, such as cystic fibrosis or hemophilia, could be reduced by long term expression of the correct form of the gene. Gene therapy, or DNA transfection, can be accomplished with reversible electroporation by introducing the sufficient quantity of DNA into target cells. This way, desired expression levels of the encoded gene can be achieved (Knoell & Yim 1998).

Electroencapsulation is a general term for the introduction of nontoxic, nonnucleic acid material into any cell, such as white blood cells and platelets. Electroencapsulation has been widely studied for various different therapies, and has been found to be particularly useful in cardiology and vascular therapy. For example, electroencapsulation of inositol hexaphosphate has been shown to improve tissue oxygenation during cardiopulmonary bypass operations on patients with respiratory problems (Mouneimne et al. 1990). Iloprosts, an antiproliferative agent, have been electroencapsulated inside platelets to reduce restenosis after blood vessel injury (Crawford & Chronos 1996).

Electroinsertion is another application of reversible electroporation. It occurs when a molecule is inserted into the membrane of a cell instead of the cytoplasm. This insertion is

accomplished when a sub-critical voltage is applied. One application of electroinsertion is the incorporation of glycophorin into a cell membrane. The protein was shown to be correctly oriented, fully functional and capable of binding to antibodies (Mouneimne et al. 1991).

1.1.4.2 Irreversible Electroporation

While reversible electroporation is the most commonly utilized and researched, irreversible electroporation is a newer technology with emerging novel applications. Initially, during the development of reversible electroporation, irreversible electroporation was viewed as a negative side effect. However, the field of irreversible electroporation has come into its own, and now has many useful applications. Because irreversible electroporation permanently damages the cell membrane and leads to cell death, two of the most common uses for irreversible electroporation are sterilization and tissue ablation.

One of the first theorized applications of irreversible electroporation was sterilization in the food industry (Doevenspeck 1961). Because of the environmental need to reduce waste and byproducts, irreversible electroporation presents a viable alternative to traditional methods. Additionally, irreversible electroporation can address the growing concern of consumers for fresh, natural and organic foods (Mattson & Sonesson 2003). Irreversible electroporation also could require lower energetic input and fewer resources (Andersson & Ohlsson 1999).

Electroporation has recently been introduced as an alternative method to chemical sterilization of water (Narsetti et al. 2006). This is a particularly attractive option in developing nations because clean drinking water is not an accessible resource to all. Electroporation presents a promising alternative to chemical sterilization in regions of developing nations which desire to preserve the environment. Utilizing irreversible electroporation for water sterilization is specifically relevant to the treatment of Legionella. Legionella are bacteria that are deleterious when inhaled by humans. Chlorine and heat shock treatment have been proposed as potential treatments of high risk water, however, only an online treatment will allow the critical level of safety to be achieved (J. Teissie et al. 2002). Irreversible electroporation was already been found to be an effective mechanism of ablation for *B. subtilis* spores and *Escherichia coli* in water (Narsetti et al. 2006). It was determined that at peak electric fields of 164kV/cm, only 0.85J/cm^3 of energy was required to achieve one-log reduction of *E. coli* in tap water with 60ns pulses (H. Schoenbach et al. 2000).

Since the development of irreversible electroporation for sterilization of food and water, it has recently been introduced as a potential method for sterilizing pharmaceutical drugs. It has been found that because irreversible electroporation can be delivered without potentially negative effects on temperature and pH, it could be an effective method for bacterial control of drugs in solution (Golberg et al. 2009). Because contamination of drugs can have potentially deleterious effects on the health of the patients using them, preservatives are a necessary additive (Jimenez 2007). However, preservatives in eye drops, such as benzalkonium chloride, have been shown to cause chronic dry eyes in glaucoma patients. Using irreversible electroporation to sterilize eye drops for glaucoma patients instead of preservatives could potentially solve this problem (Leung et al. 2008). More recently developed preservatives may be less damaging to the

eyes, but they are still not free of complications (Labbé et al. 2006). Additionally, it has been found that preservatives such as Merthiolate in pediatric vaccinations have been linked to neurovascular disorders such as autism (D. Geier et al. 2007). Merthiolate contains 49.55% mercury, and was eliminated from topical treatments in the 1980's because of its demonstrated infectiveness and toxicity. However, Merthiolate is still present in some vaccines (Advisory Committee on Immunization Practices 2006). While the connection between Merthiolate and neurological disorders remains controversial, public concern could be mitigated by replacing chemical sterilization techniques with the use of irreversible electroporation for sterilization of vaccines.

Irreversible electroporation also has applications in medicine, specifically tissue ablation. Because irreversible electroporation leads to cell death, tissue ablation is a particularly relevant application that could be used to eliminate pathogenic tissue. One specific use of irreversible electroporation for tissue ablation is the treatment of cancerous tumors. Experiments have demonstrated the success of irreversible electroporation as a treatment method for cancer. An in vivo study on irreversible electroporation in rats for the treatment of liver cancer found a demarcated boundary between necrotic congestion in the treated region and the unaffected, untreated region. Three hours after the procedure, in all cases, treated areas in perfusion-fixed livers displayed microvascular occlusion, endothelial cell necrosis, and diapedeses, resulting in ischemic damage to parenchyma and massive pooling of erythrocytes in sinusoids. However, large blood vessel architecture was preserved, which was demonstrated by the successful flushing of blood through these vessels (Edd et al. 2006). Electroporation effects only the cell membrane, therefore molecular scaffolding and proteins are unaffected by the electric fields. In addition, nerves, blood vessels and lactiferous ducts have been shown to also be unaffected by the fields both mathematically (Daniels & Rubinsky 2009) and experimentally (G Onik et al. 2007),(Schoellnast et al. 2011),(Rubinsky et al. 2007). An experimental study on male dogs demonstrated the potential of irreversible electroporation to achieve focal tissue ablation of the prostate while sparing the urethra, rectum, blood vessels and nerves (G Onik et al. 2007). This data suggests that tumors can be treated while sparing adjacent molecular scaffolding, rectum, urethra, lactiferous ducts, nerves and blood vessels.

Irreversible electroporation can be used for a wide range of tissue ablation applications. In addition to cancerous tissues, irreversible electroporation can be used to prevent restenosis by ablating vascular smooth muscle cells. The gold standard in treating a myocardial infarction (“heart attack”) is reperfusion. Reperfusion can be accomplished pharmacologically (intravenous thrombolytic therapy), surgically (bypass surgery), or mechanically (balloon angioplasty). Post angioplasty, distension of the diseased artery can cause damage to the lumen of the blood vessel, which triggers the body’s inflammatory response. The immune response of the body leads to the formation of scar tissue, in the form of excess vascular smooth muscle cells. In some cases, the excessive growth of vascular smooth muscle cells can overcompensate and in turn actually block the blood vessel. This leads to a reoccurrence of artery blockage and myocardial infarction and is termed restenosis. Irreversible electroporation has been investigated as a method to prevent restenosis by abating vascular smooth muscle cells and has been found to be an efficient minimally invasive endovascular approach. The benefit of using irreversible electroporation for restenosis, as compared to other techniques, lies in its potential use as a preventative method. While treating a myocardial infarction, a balloon catheter can be used, as is typical in balloon angioplasty procedures. However, after the blockage is cleared, electrodes attached to the

catheter can then deliver electric fields to the arterial wall to accomplish irreversible electroporation. This has been shown to sufficiently prevent the excess growth of vascular smooth muscle cells, effectively preventing restenosis (Maor, Ivorra & Rubinsky 2008b),(Maor et al. 2009).

1.1.5 Electroporation Parameters

As previously discussed, there are various parameters that can be modified in order to control the outcome, intensity and extent of an electroporation procedure. These parameters include voltage magnitude, pulse length, pulse frequency and number of pulses.

1.1.5.1 Voltage Magnitude

Voltage magnitude plays an important role in the efficiency of electroporation. This is because as voltage increases, the electric field rises exponentially. However, other parameters merely have a linear effect on electroporation efficacy.

Voltage magnitude also initiates pore formation. When the transmembrane potential reaches a threshold value of 0.2-1V, electroporation occurs (J. Teissie & Rols 1993). Therefore, below this threshold value, electroporation cannot occur. However, voltage magnitude also effects the location of pores. It has been shown that pores are concentrated at the poles (the part of the sphere closest to each of the electrodes) of a cell (Kinosita et al. 1988). However, increasing the voltage magnitude beyond this threshold does not directly translate into an increase in transmembrane potential because the rapid accumulation of pores at the poles of the cell depressed the current across the membrane.

The voltage magnitude is affected by the presence of the membrane, which plays a role in amplifying the electric field. The potential distribution from an applied electric field in the region surrounding a spherical cell with an insulating membrane is described by the Laplace equation with applicable boundary conditions. This equation has the following solution:

$$U = 1.5 r_{cell} E cos\theta, \qquad (1.1)$$

where U is the transmembrane voltage, r_{cell} is the radius, and θ is the angle between the site on the cell membrane where U is measured and the direction of E. At the poles (where $\theta = 0, \pi$) 75% of the potential drop occurs across the cell membrane. The amplification is $\frac{E_{transmembrane}}{E} = 1.5 r_{cell}/h$. Where h is the membrane thickness and $E_{transmembrane}$ is the transmembrane electric field. With appropriate values, this equation evaluates to an amplification of 2E3. This results because the intracellular region is an equipotential (J. Weaver 1993).

1.1.5.2 Pulse Length

Different pulse lengths can accomplish different goals. For example, long, moderate transmembrane potentials applied to a cellular medium lead to irreversible breakdown and membrane rupture. However, larger voltage magnitudes paired with shorter pulses do not rupture the membrane. Instead, large, short pulses cause reversible electrical breakdown by creating a high conductance state that rapidly discharges the membrane before it can rupture (Benz et al. 1979),(J. Weaver 2003). In this way, the pulse length can be used to control whether electroporation is irreversible or reversible.

The function of pulse length is primarily to control the pore expansion mechanism. Experiments on Chinese hamster ovary cells generated results that 1) validated Teissié and Rols 1993 experiment, and 2) provided data on the effects of pulse length. Regarding the first point, it was verified that the local electric field magnitude played a role in determining the pore formation location. Regarding the second point, it was found that at a constant electric field magnitude, longer pulses lead to an increase in pore formation (Gabriel & Teissié 1997).

1.1.5.3 Other Parameters

Other parameters that are utilized during an electroporation procedure to control outcome include: number of pulses, and pulse frequency (Gehl & Mir 1999). The number of pulses applied during electroporation effects pore lifetime. The higher the number of pulses, the longer the pore lifetime, and the inverse is also true. This parameter is important when specifically dealing with reversible electroporation, because it allows control over the introduction and transport of molecules into a cell. Pulse frequency is important because the time in between pulses can eliminate Joule heating by allowing the temperature of the tissue to fall. Joule heating is discussed in more detail in section 1.1.6, below.

1.1.6 Joule Heating

High electric fields can lead to Joule heating (Belov 1978),(Lee 2005), which is the result of energy absorption by tissues because they are inherently resistive. Joule heating can lead to thermal damage in tissues. There are many therapeutic treatments that use Joule heating to ablate undesirable tissue, such as focused ultrasound (Foster et al. 1993), radio frequency (Organ 1976), and laser tissue ablation (Bown 1983). However, thermal effects such as these harm all structures in the treated zone indiscriminately, including blood vessels and connective tissue. Electroporation, on the other hand, causes no thermal damage and affects only the cellular membrane, leaving molecular scaffolding unharmed. For this reason, electroporation can be an ideal treatment because it can selectively target malignant tissue.

Electroporation causes no thermal damage because the treatment is designed to minimize Joule heating. Joule heating is determined by an analysis of thermal damage experienced by the electroporated tissue using a kinetic model based on the Arrhenius equation (Agah et al. 1994). The Arrhenius equation is the principal method for determining such damage:

$$\Omega = \int_0^\tau \left(A e^{-E/RT} \right) dt, \qquad (1.2)$$

where Ω is a dimensionless parameter indicating the level of thermal damage, A is a measure of molecular collision frequency, E is an energy barrier that must be overcome, R is the gas constant, T is the temperature, and t is the time. Both A and E are dependent on tissue type and are determined experimentally. Values of Ω below 1 indicate negligible thermal damage.

1.1.7 Electroporation Models

1.1.7.1 Aqueous Pore Model

The Aqueous Pore theory is currently the most widely accepted model for electroporation (J. Weaver & Chizmadzhev 1996a). Despite this, controversy still exists in the field. This is primarily due to the fact that pores have never been viewed on a membrane level and strictly speaking, our knowledge is phenomenological (J. Weaver & Chizmadzhev 1996b). The only pores that have ever been imaged were on the cellular level in an experiment conducted by Chang and Reese (Chang & Reese 1990). It remains controversial to this day because of the inconclusive images. In Figure 1.3, the images achieved from rapid-freezing electron microscopy in their experiment show a cell before and after electroporation.

While the images in Figure 1.3 make it clear that the cellular membrane changes after the application of an electric field, the exact mechanism of this change is not clear. The electron microscopy reveals volcanic shapes with apexes pointed outwards. However, whether or not the structures visible in the electron microscopes are pores remains to be determined. Chang and Reese observed that these inverted volcanic shapes were the only changes in the cell after electroporation (Chang & Reese 1990). Additionally, such physical deformations were not present in any of the control studies. In their study, they state that it is unclear as to whether this geometric heterogeneity is an electropore or a cross-fractured neck of an elongated membrane evagination. As a result, the mechanism of electroporation is still controversial. As a result, the first electroporation model presented here will be the most widely accepted: the aqueous pore model, followed by other existing theories in the field.

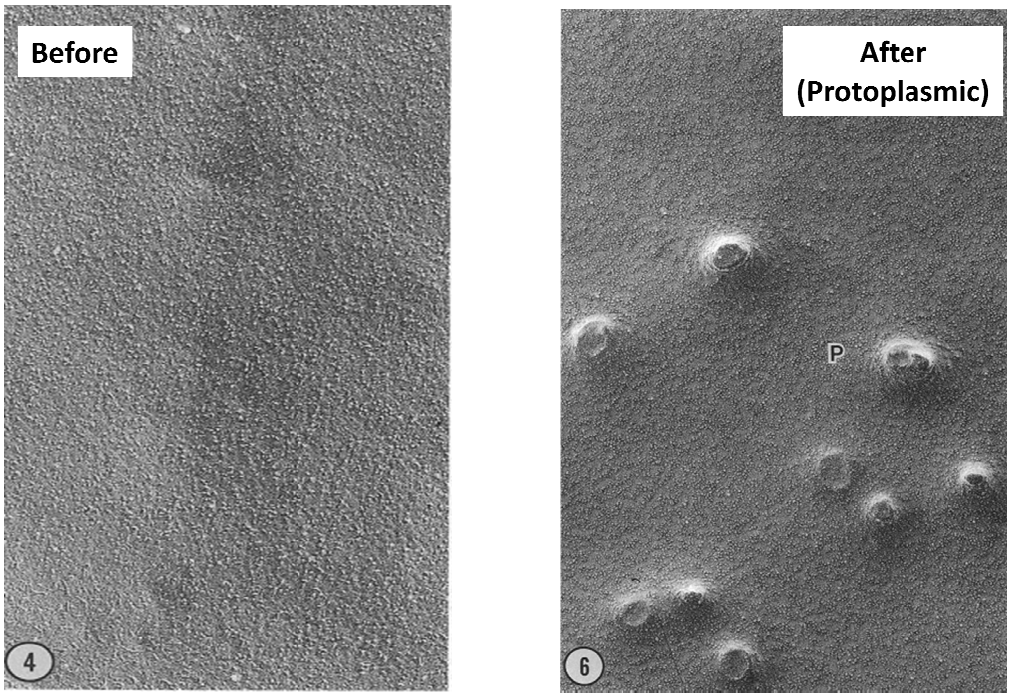

Figure 1.3: Electron microscope images of a red blood cell before and after electroporation. Left: external membrane face of an electroporated human red blood cell frozen at 40ms after the application of an electric pulse. 60,000x magnification. Right: protoplasmic membrane face of an electroporated human red blood cell frozen at 220ms after the application of the electrical pulse. 60,000x magnification.

The basic concept of the transient aqueous pore model was established first in soap films (Deryagin & Gutop 1962). A pore has electrical energy associated with the change of its specific capacitance, *C*, as lipid is replaced with water in the formation of a pore (Abidor et al. 1979). The passage of ions through small pores in a low dielectric membrane is unlikely, and as a result the pore is represented by a water filled capacitor, instead of an electrolyte filled capacitor. With the application of a transmembrane electric field, the free energy of pore formation is characterized by:

$$\Delta W_p(r, U) = 2\pi\gamma r - \Gamma\pi r^2 - 0.5CU^2\pi r^2, \qquad (1.3)$$

where the function $\Delta W_p(r, U)$ is a large parabolic barrier. This means that spontaneous thermal fluctuations may create pores, but the probability of surmounting the barrier is low. *U* is the spatially averaged transmembrane voltage, r is pore radius, γ is edge energy of a pore and Γ is surface tension at the interface between the non-conducting and conducting liquids. The change of the pore's specific capacitance as water displaces lipid to form a pore is:

$$C = \left(\frac{\epsilon_w}{\epsilon_m} - 1\right) C_0, \qquad (1.4)$$

where the permittivity of pure water, $\epsilon_w = K_w \epsilon_0$, and $\epsilon_m = K_m \epsilon_0$ is the permittivity of the lipid interior of the membrane. The constant C_0 is the capacitance per area of a membrane without pores, where $C_0 = \epsilon_m / h$, with h representing the membrane thickness, as stated before in equation 1.1. It is common for $K_m \approx 2$ and $K_w \approx 80$, which means that $\Delta W_p(r, U)$ decreases as U increases (J. Weaver & Chizmadzhev 1996b). The function of $\Delta W_p(r, U)$ is demonstrated in Figure 1.4. This figure illustrates that $\Delta W_p(r, U)$ acts as a barrier function. This means that the energy required for pore formation increases as pore radius increases. Therefore, the creation of hydrophobic pores that are very small in radius is easy to accomplish because the pore formation energy is low. However, as the pore radius increases, and hydrophobic pores develop into hydrophilic pores, the pore formation energy increases, providing a barrier to larger pore formation.

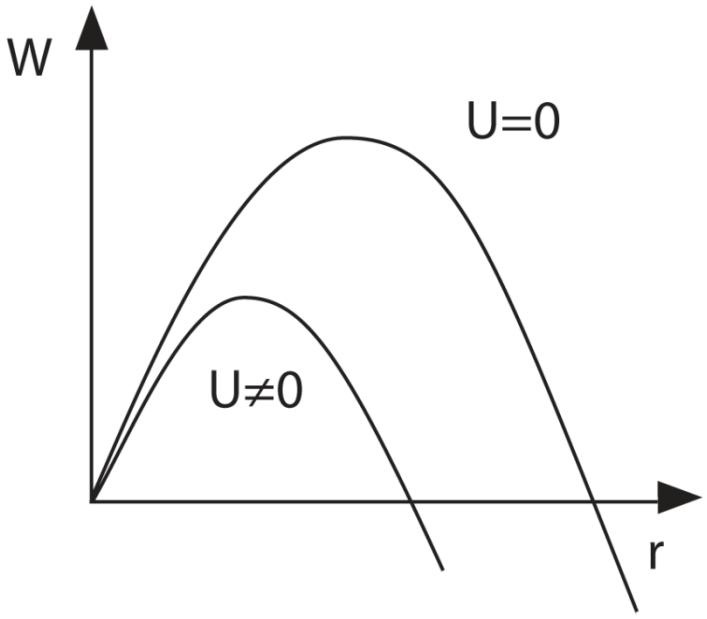

Figure 1.4: Formation energy, W, of electropores as a function of pore radius. The upper curve represents pore formation energy without an applied pulse (U=0). The lower curve represents pore formation energy with an applied pulse (U≠0, or U>0). However, this diagram is only a rough approximation. It neglects 1) the transition from hydrophobic pores into hydrophilic pores and 2) the effect of surrounding pores on surface tension of a particular pore.

Figure 1.4 also elucidates the behavior of pore formation energy with and without an applied pulse. Without an applied voltage, the energy barrier to pore formation is higher. However, once a voltage is applied the energy barrier is lowered. And when the voltage is increased, the energy barrier is decreased. This provides a clear visual explanation for planar membrane rupture. The probability of a membrane developing supra-critical pores, $r > r(U)_c$,

increases as voltage increases. The presence of a single supra-critical pore is sufficient to cause rupture because one pore can expand until it reaches the macroscopic aperture that defines the planar membrane. As U is increased, the critical pore radius decreases. More importantly, the corresponding pore formation energy also decreases (J. Weaver & Chizmadzhev 1996b).

Equation 1.2 and Figure 1.4 are a good first order approximation for the behavior of the lipid bilayer and pore formation energy. However, they do not take into account two more advanced processes of electroporation: 1) the transition from hydrophobic pores into hydrophilic pores and 2) the effect of surrounding pores on surface tension of a particular pore.

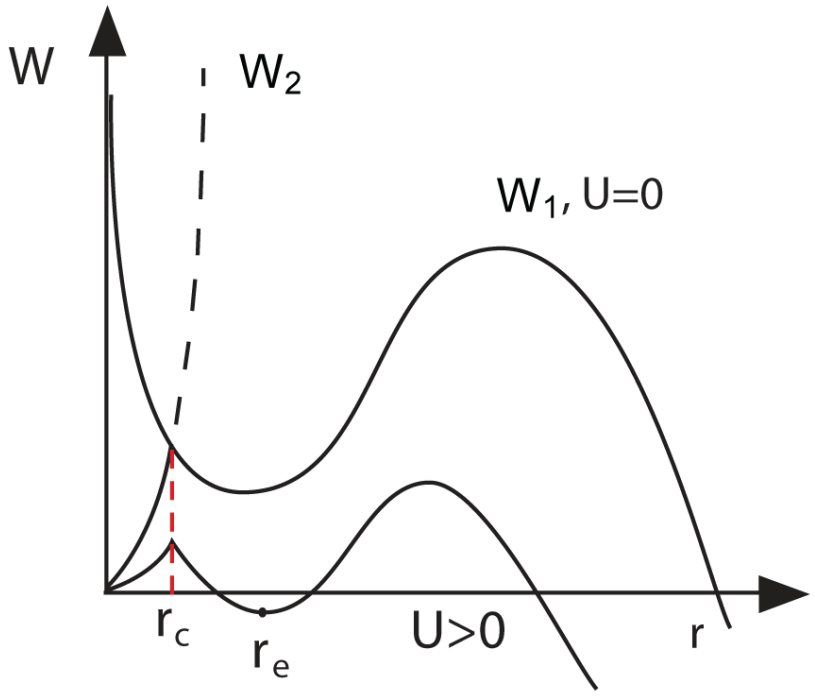

Figure 1.5: Pore formation energy, taking into account hydrophobic pores and surface tension of surrounding pores, is depicted above. W_1 represents the hydrophilic pore formation energy as a function of radius with ($U \neq 0$) and without ($U=0$) an applied pulse. W_2 represents the hydrophobic pore formation energy as a function of radius.

The arrangement of the lipids along the toroidal walls of hydrophilic pores leads to deformation of the molecular order (Glaser et al. 1988). This alteration to pore energy is the most influential when the pore radius is closest to the radius of the lipid heads (Petrov 1980). In addition, at this scale hydration interactions cause repulsion between the hydrophilic components at the edge of the pore wall. Both of these effects lead to an increase in pore formation energy, W, at small radii. The dependence of pore formation energy on radius, taking points 1 and 2 into consideration, is qualitatively depicted in Figure 1.5.

Figure 1.5 elucidates the fact that it is energetically favorable to have hydrophobic pores of a smaller radius. Hydrophobic pores are formed by lateral thermal fluctuations of the lipid molecules. However, at a critical radius, r_c, a transformation in the configuration of the phospholipids is energetically favorable. This transformation is the reconfiguration of

hydrophobic pores into hydrophilic pores, and occurs when $W_1(r_c)=W_2(r_c)$ (Glaser et al. 1988). The radius r_c is the highest energy barrier required to form hydrophilic pores. Once this barrier is overcome, equilibrium pore radius r_e is easily achieved. This is the lowest possible energy achieved by a hydrophilic pore. Additionally, note that in Figure 1.5 the same trend as in Figure 1.4 is visible; the application of an external voltage lowers the energy required for pore formation. This is clear from the plot because: $W_1(U > 0) < W_2(U = 0)$.

The first order validation of the transient aqueous pore model has been achieved through experimental evidence. Early models utilized the simplest pore configuration for mathematical simplicity; a cylindrical pore with a circular base with sharp edges at 90º. However, this was determined to be a crude and inaccurate representation (Petrov et al. 1979). As illustrated in Figure 1.2c, it is more likely that pores have curved edges, and therefore a toroidal shape (Petrov 1980). Although more accurate in terms of allowing fluctuations in pore size and shape, toroidal geometry has not yet been included in models that are capable of predicting measurable behavior.

In experiments done on planar lipid bilayers, it was found that the membrane lifetime, defined as the time from voltage application to drastic current rise, varied between different experiments. Additionally, the character of the fluctuations and the duration of the fluctuating stage were different. This indicates that the membrane conductance and lifetime both exhibit stochastic behavior. This is an important conclusion, because it indicates that a purely deterministic mechanism cannot play a role.

The transient aqueous pore model uses a combination of diffusion and electrical and interfacial forces to govern pore formation. Diffusion fundamentally involves fluctuations; therefore, pores of various sizes are expected. This can be taken into account by a probability density function. This function also indicates that pore formation is dependent on pore formation history. This corroborates the experimental evidence that pores are stochastic. And as a result, thresholds for the onset of electroporation reflect both the transmembrane voltage amplitude and the electrical history of the lipid bilayer. Therefore, a simple model utilizing a critical voltage is inaccurate according to the transient aqueous pore theory and experiments.

1.1.7.2 Electrocompression Model

It was first suggested that rupture might be caused by an electromechanical collapse due to compression of the entire membrane (Crowley 1973),(J. Weaver & Chizmadzhev 1996a). Early on, it was found that the capacitance of the membrane remains constant until the moment of breakdown. This data indicated that the prebreakdown current fluctuations are not associated with significant changes in membrane thickness *h*. Therefore, large scale membrane electrocompression can be eliminated as a possible method for membrane rupture. In fact, the data are consistent with pore theories, discussed in section 1.1.7.1.

The electrocompression model predicts a critical voltage one order of magnitude too large (J. Weaver & Mintzer 1981). This is a second indication that the electrocompression model does not best represent the mechanics of electroporation. However, the deficit greatest in magnitude of the electrocompression model is that it predicts that rupture does not occur below critical voltage.

However, experiments show that rupture is a stochastic process, with a range of lifetimes for a given voltage magnitude.

1.1.7.3 Electrohydrodynamic Instability Model

The problem of electrohydrodynamic instability of a planar layer of nonconducting liquid separated by two charged conducting liquids has already been investigated (Michael & O'Neill 1970),(Taylor & Michael 1973). The information gleaned from these studies can be extended to the process of electroporation because this system is similar to a membrane. Therefore an analogy can be drawn between the stability of a planar dielectric layer and electrical breakdown of the lipid bilayer. According to this model, the membrane would become unstable with respect to long wave perturbations if the following inequality is true:

$$U^2\epsilon_m > \frac{1}{2}\Gamma h, \tag{1.5}$$

where U is the transmembrane voltage, ϵ_m is the permittivity of the lipid interior of the membrane, $\frac{\Gamma}{2}$ is the surface tension at the interface between the non-conducting and conducting liquids and h is the membrane thickness. This implies a breakdown voltage of:

$$U_c = \left(\frac{\Gamma h}{2\epsilon_m}\right)^{1/2}, \tag{1.6}$$

where U_c is the critical transmembrane potential. When using relevant values, this equation yields $U_c = 0.375V$. This critical voltage is on the same order of magnitude as experimental results. However, this liquid-layer model does not account for either the stochastic nature of rupture, or the strong dependence of membrane lifetime on voltage (J. Weaver & Chizmadzhev 1996a). The origin of instability considered in the electrohydrodynamic model is the same as the electrocompression model. The difference between the two models is that the electrocompression model contributes the increase in system energy to elastic compression energy of the membrane. In the electrohydrodynamic instability model it is attributed to the work required to form a new membrane surface.

1.1.7.4 Wave Instability Model

The difference between the wave instability models and those previously mentioned is that the analysis of wave instabilities in membranes takes into account their viscoelastic properties (Steinchen et al. 1982),(Maldarelli et al. 1980). The elastic properties of the membrane material

in the wave instability analysis were described within the framework of models of Kelvin and Maxwell, which also considered the compression of the membrane due to van der Waals attraction forces. It is predicted that both the surface tension and the viscosity will increase membrane lifetime. As a result, wave instability models yield very different results than electrocompression and electrohydrodynamic models, where an increase in surface tension decreases membrane lifetime.

In this model the bilayer membrane is analyzed in terms of the time evolution of symmetric waves. This analysis results in the characteristic time of the process, $\tau_{elastic}$ which depends on the wavenumber, *k*.

$$\tau_{elastic} = \left(-\frac{Y_m}{3\mu_m} + \frac{\epsilon_m U^2 k^2}{12\mu_m} - \frac{\Gamma h^2 k^4}{24\mu_m}\right)^{-1}, \qquad (1.7)$$

where Y_m is the constant for Hooke's Law and μ_m is the effective membrane viscosity. However, this model fails to describe the stochastic aspect of rupture, and the strong dependence of voltage on lifetime.

1.1.7.5 Electroporation Models Summary

The short comings of the non-pore theories all have several commonalities. The non-pore theories discussed in sections 1.1.7.2, 1.1.7.3 and 1.1.7.4 as a group do not explain the following mechanics of electroporation:

1. Rupture is stochastic; a distribution of membrane lifetimes has been consistently experimentally observed for the same transmembrane voltage (Abidor et al. 1979).
2. The magnitude of an approximate critical voltage at which the probability of rupture becomes large (Benz et al. 1979),(J. Weaver & Chizmadzhev 1996a).

However, these phenomena can be quantitatively explained by transient aqueous pore theory. This indicates that at this point time, transient aqueous pore theory is the most accurate model of the electroporation phenomenon and best predictor of lipid bilayer rupture. Therefore, the remainder of this dissertation will reflect the fact that the current most accurate theory is the transient aqueous pore model.

1.2 Motivation and Dissertation Overview

1.2.1 Motivation

1.2.1.1 Motivation to Study Irreversible Electroporation

Currently, cancer is the 2nd most leading cause of death in the United States (Kochanek et al. 2011). Cancer cells are able to mutate and thwart pharmaceuticals and drugs, which are designed to alter cell surface receptors. Because of this, it becomes necessary to design second, third, and so on, generations of drugs to handle the cell mutations that follow. This is one of the many reasons it is paramount to pursue focal tissue ablation techniques.

Current available techniques for the treatment of cancer include radiofrequency (RF) ablation, high intensity focused ultrasound (HIFU), radiation/brachytherapy and chemotherapy, in addition to countless others. However, there are still existing challenges with each procedure. RF ablation and HIFU are thermal ablation modalities, which means that they ablate all tissue in a given treatment zone indiscriminately (Goldberg et al. 2000),(Wu et al. 2003). This can be dangerous for adjacent nerves, blood vessels and organs. Brachytherapy, while more targeted than radiation, still is most effective only when used in conjunction with other treatments methods (Ragde et al. 2008). And lastly, chemotherapy has side effects that are detrimental to quality of life (Love et al. 1989).

Non-thermal Irreversible Electroporation (NTIRE), a relatively new tissue ablation method, has recently emerged as a promising method of minimally invasive surgery for treatment of cancer, as well as other soft tissue lesions. Because IRE is administered through needle electrodes, it is a minimally invasive procedure. Compared to surgery, it is extraordinarily less invasive (Davalos et al. 2004). There is only one currently used treatment method that is less invasive, and that is HIFU. HIFU delivers acoustic waves from outside the body, which are focused on narrow target. Intervening tissue is said to be unharmed, however, some amount of acoustic energy is absorbed by the tissues and depending on the tissue and treatments, can be negatively affected (Bailey et al. 2003).

IRE has the capability of selective ablation, a quality not ascribed to any of the other available treatment modalities. IRE only affects the cellular membrane, so molecular scaffolding is left undamaged. For example, collagen and elastin are unaffected by electric fields (Phillips et al. 2011). Nerves, blood vessels and lactiferous ducts have been shown to also be unaffected by the fields (Daniels & Rubinsky 2009),(G Onik et al. 2007),(Schoellnast et al. 2011). This is advantageous in comparison to thermal ablation modalities such as RF and HIFU, because they do not have this capability of selective ablation.

Previous experiments have demonstrated the success of IRE as a treatment method for cancer. IRE proved successful in long term studies involving rat (Edd et al. 2006) and pig livers (Rubinsky et al. 2007). An experiment performed in a small rodent study illustrated that IRE can treat cancer (Al-Sakere et al. 2007). Another experimental study demonstrated the potential of IRE to achieve focal tissue ablation of the prostate while sparing the urethra and nerves (G Onik et al. 2007). In addition, recent clinical studies have shown electroporation's ability to treat prostate cancer in humans (G Onik & Rubinsky 2010).

It is well known that cancer cells no longer have the capability of going through apoptosis, or programmed cell death. This is one of the reasons cancer is defined as the uncontrolled growth, or mitosis, of cells (Reed 1999). In an unprecedented study, it was shown that irreversible electroporation can trigger apoptosis in cancer cells (Al-Sakere et al. 2007), a capability unachieved by any other cancer treatment. Researchers used an apoptotic stain to demonstrate that cancer cells were actually experiencing apoptosis and not just necrosis after treatment. This discovery sets irreversible electroporation apart from any other cancer treatment method.

Treatment planning for irreversible electroporation has major advantages in comparison to other cancer treatment modalities. One problem with pre-surgical planning and modeling of radiofrequency ablation and high intensity focused ultrasound, which are thermal treatments, is that the analysis of the effects of blood flow on heat transfer is more complicated than is currently understood. The Pennes Bioheat equation is conventionally used in heat transfer analyses in the body, but there is widespread concern over its precision (Wissler 1998). In fact, Pennes' model of heat transfer in perfused tissue has been criticized for various reasons over the last 50 years.

One reason for the controversy is that Pennes assumed uniform metabolic heating, perfusion rate and thermal conductivity. Additionally, the method used to plot temperature curves is not, when tested by third parties, achieved by averaging his experimental data, which puts his plots into question. His experimental data is at variance with his theoretical results, which is a substantial problem. Pennes studied heat transfer between capillary blood and tissue, but it is easily demonstrated that the temperature of blood in precapillary arterioles and postcapillary venules is close to the temperature of surrounding tissue. This proximity in temperature magnitudes indicates that the heat transfer between the two structures may not be significant enough to draw conclusions. Pennes also made another simplistic assumption: that the perfusion effect is isotropic, which it probably is not. Additionally, Pennes did not take into consideration vascular architecture, especially the countercurrent arrangement of the circulatory network and the gradually tapering characteristics of the vascular bed (Charny 1992),(Wulff 1974).

Treatment planning of electroporation procedures is simpler that thermal ablation modalities. Treatment planning of irreversible electroporation consists of the analysis of electric fields in tissue. Because electric fields are determined through electrostatic equations, there are no transients. This simplifies the analysis, and increases the accuracy of electroporation procedures, especially in comparison to RF ablation and HIFU, which must use the controversial Pennes Bioheat equation.

Treatment planning for electroporation consists of designing pulses that produce electric fields above the lower threshold for irreversible electroporation and below the upper threshold to avoid thermal damage. This is a powerful method, because it allows analysts to overcome the lack of precise information available regarding tissue properties. In the case of thermal modeling for other treatments, such as RF ablation and HIFU, the most critical sites where cells survive are near blood vessels because of their convective effect on heated tissue. Because of the heat transfer complexities in the vicinity of blood vessels and the inaccuracy of the Pennes Bioheat equation, this is exactly where thermal models fail.

1.2.1.2 Motivation to Study Heterogeneous Tissues

Previous theoretical research has only explored electroporation in homogeneous tissues (Davalos et al. 2003),(Davalos et al. 2002),(Davalos & Rubinsky 2008). However, the anatomy surrounding a tumor site is, in reality, not actually homogeneous. Nerves, blood vessels, glands, and other organs that should be protected may surround any given tumor. Therefore, to preserve these vital structures but also to ablate a tumor, it becomes pertinent to investigate the effect of IRE in heterogeneous tissues. This dissertation investigates the impact of anatomical heterogeneous tissues on electric fields due to IRE pulses and the resulting impact on malignant tissue treatment strategy.

Heterogeneous tissues occur naturally due to the anatomy of our organs. However, extrinsic factors can create heterogeneous tissues as well. For example, an applied temperature gradient will create a temperature induced heterogeneity. Electrical fields are dependent upon electrical conductivity, which is a function of temperature (this is discussed in further detail in Chapter 3). Therefore, an externally applied temperature gradient will create extrinsic heterogeneous tissues and impact the electric field due to IRE. This impact on electric field distribution could potentially impact the treatment strategy for malignant tissue. Therefore, this dissertation investigates extrinsic heterogeneous tissues in addition to intrinsic anatomical heterogeneous tissues.

1.2.2 Dissertation Overview

This dissertation provides a preliminary assessment of the impact of intrinsic and extrinsic heterogeneous tissues on the electric fields due to IRE and the subsequent consequences for treatment strategies. The emphasis of this investigation is on a fundamental theoretical analysis in order to establish a preliminary foundation for the field of IRE in heterogeneous tissues.

Chapter 2 investigates a theoretical model of the electric field distribution in anatomically intrinsic heterogeneous tissues. The temperature distribution is also analyzed in order determine the impact of Joule heating due to the presence of the applied voltage of high magnitude. Specifically, prostate and breast tissue are considered. The heterogeneities considered are: included nerves, blood vessels and lactiferous ducts.

Extrinsic heterogeneous tissues are investigated in Chapter 3. This study, like Chapter 2, investigates on a theoretical level. In this case, heterogeneous tissues are induced through the application of freezing temperatures through a cryoprobe. The resulting electric fields are studied in terms of ablation capabilities. Additionally, the temperature distribution due to freezing is investigated and correlated to electrical conductivity.

The final chapter of this dissertation, Chapter 4, follows the theoretical framework of Chapter 3. In this case, however, applied temperatures are raised from freezing to cooling. The effect of temperature on electric fields is investigated on tissues at low temperatures and

compared to results in Chapter 3. The resulting implications for treatment methodology, imaging and surgical procedure are analyzed in terms of both freezing and cooling temperatures.

Chapter 2: Non-Thermal Irreversible Electroporation in Intrinsic Heterogeneous Tissues

2.1 Introduction

Standard surgical techniques only function at the tissue and organ level. However, molecular surgery can treat diseases on a cellular and molecular scale. Molecular surgery will allow local treatment of disease by utilizing devices to target individual cells in the body. In the field of molecular surgery, non-thermal irreversible electroporation (NTIRE) has recently emerged as a novel method of minimally invasive surgery (Edd et al. 2006). Electroporation utilizes high voltage pulses delivered through electrodes to create an electrical field across cellular membranes. This field permeabilizes the membrane and exposes the cytoplasm of the cell to the extracellular space. When permeability is only temporary, and the cell membrane reseals, reversible electroporation has occurred. If permeability remains permanent, irreversible electroporation has occurred and the cell will experience necrosis. Reversible electroporation is used for drug delivery and gene therapy. Irreversible electroporation functions as focal tissue ablation. However, irreversible electroporation is an anomaly among tissue ablation techniques because it only affects the cell membrane, while proteins and collagen remain unaffected. IRE can ablate cancerous tumors by inserting electrodes near the tumor and applying periodic voltage pulses of specific amplitude and frequency.

High electric fields can lead to Joule heating (Belov 1978),(Lee 2005), which is the result of energy absorption by tissues because they are inherently resistive. Joule heating may cause thermal damage in tissues. Focused ultrasound (Foster et al. 1993), radio frequency (Organ 1976) and laser tissue ablation (Bown 1983) use thermal damage to ablate tissue. However, thermal effects harm all structures in the treated section indiscriminately, including blood vessels and connective tissue. IRE, on the other hand, causes no thermal damage and affects only the cell membrane, leaving molecular scaffolding unharmed. Therefore, IRE is the ideal treatment because it can selectively target malignant tissue.

Previous experiments have demonstrated the success of IRE as a treatment method for cancer. IRE proved successful in long term studies involving rat (Edd et al. 2006) and pig (Rubinsky et al. 2007) livers. An experiment performed in a small rodent study illustrated that IRE can treat cancer (Al-Sakere et al. 2007). Another experimental study demonstrated the potential of IRE to achieve focal tissue ablation of the prostate while sparing the urethra and nerves (G Onik et al. 2007).

Previous theoretical research has only explored electroporation in homogeneous tissues (Davalos et al. 2003),(Davalos et al. 2002),(Davalos & Rubinsky 2008). However, the anatomy surrounding a tumor site is, in reality, not actually homogeneous. Nerves, blood vessels, glands and other organs that should be protected may surround any given tumor. Therefore, to preserve these vital structures, but also ablate a tumor, it becomes pertinent to investigate the effect of IRE in heterogeneous tissues.

In this study the first model of IRE on lesions in complex tissues is introduced. The purpose of this study is to demonstrate the importance of developing IRE models that accurately depict human anatomy and the significant effect of tissue heterogeneities. This will accomplish several important objectives that could potentially lead to widespread clinical applications. Firstly, heterogeneous tissue models will yield results that are far more accurate than current models. Secondly, more accurate models will allow the possibility to treat the cancer without harming any other structure in the body. Such latent potential demonstrates the importance of pursuing heterogeneous models.

Two tissue regions were used to demonstrate IRE in heterogeneous models. The first was in the prostate. Any treatment of prostate cancer poses a threat to the surrounding nerves which control urinary and erectile function. In fact, despite new techniques for nerve sparing prostatectomy, the success rate of such surgeries has been low (Montorsi 1997). Impotence is a common postoperative result, undermining the success of the treatment. The preservation of these nerves is necessary to retain the patient's quality of life. Therefore, if IRE could leave these nerves unharmed, it could present a promising treatment for prostate cancer. To determine the effect of irreversible electroporation on the surrounding nerves, the model of prostate cancer included the pelvic plexus nerve structure.

The second example was in the breast. Within the breast's fatty tissue are lactiferous ducts and lobes that are necessary for milk production. The preservation of duct functionality is possible, but only with conservative surgeries performed on early-stage cancers (Higgins & Hafty 1994). In other cases, such as mastectomy, functionality is eliminated, the body image of the patient is threatened and the probability of depression rises (Lasry 1987). The function of these ducts is of extreme importance to an individual's wellbeing. To determine the effect of irreversible electroporation on ducts, the breast cancer model included mammary ducts.

Because the subject of this chapter has never been investigated before, the primary goal of this study is to introduce the concept of modeling IRE in tissues with heterogeneities. As a first order study, it was sufficient to demonstrate this subject with single heterogeneities in two dimensions.

2.2 Methods

The models were generated using numerical analysis executed by Comsol Multiphysics (version 3.4). This initial study utilized 2-dimensional models because these were sufficient to demonstrate the significant difference between homogeneous and heterogeneous models. Two equations were solved simultaneously in Comsol. The first was the Laplace equation which solved for the potential distribution associated with an electric pulse:

$$-\nabla \cdot d(\sigma \nabla V - J^e) = dQ_j \qquad (2.1)$$

where σ is electrical conductivity, V is voltage, J^e is external current density, d is thickness and Q_j is the current source. For all boundaries the external current density and the current source were set to zero, and thickness was set to one. The electric field was solved in order to illustrate the electrical effects of IRE in the tissue. The electric field was solved for in the AC/DC Conductive Media module using a transient analysis. Each biological structure was given a different electrical conductivity. The values are shown in Tables 2.1 and 2.2. While conductivities are subject to change with a change in temperature, it is not necessary to consider this variation here because the models were designed to yield low increases in temperature. Additionally, it is important to note that biological tissues may exhibit slight variation from the tabulated values.

Table 2.1: Values of electrical conductivity for the structures in the prostate cancer Conductive Media model used to solve for the electric field induced by electroporation

Structure	Electrical Conductivity (σ) [S/m]	Reference
Prostate tissue	0.42	(Andreuccetti et al. 1997)
Myelin	3.45E-6	(Villapecellin-Cid et al. 2003)
Axon	1.44	(Roth & Wikswo 1985)

Table2.2: Values of electrical conductivity for the structures in the breast cancer Conductive Media model used to solve for the electric field induced by electroporation

Structure	Electrical Conductivity (σ) [S/m]	Reference
Fatty breast tissue	0.024	(Andreuccetti et al. 1997)
Breast myoepithelial cell	10^{-7}	(Hassan 2003)
Breast gland	0.52	(Andreuccetti et al. 1997)
Breast tumor	2.31	(Campbell & Land 1992)
Blood	0.31	(Andreuccetti et al. 1997)

The thermal effects of electroporation were determined from the solution of the Pennes Bioheat equation, which was solved simultaneously with the electrical potential equation. The Pennes Bioheat equation took the following form:

$$\nabla \cdot (k\nabla T) + \rho_b w_b c_b (T_a - T) + q''' = \rho c_p \frac{\partial T}{\partial t} \qquad (2.2)$$

where k is the thermal conductivity, T is the temperature, w_b is the blood perfusion, c_b is the heat capacity of blood, T_a is the arterial temperature, ρ is the tissue density, c_p is the tissue heat capacity and $q''' = Q_{met} + Q_{ext}$. The term Q_{met} is the metabolic heat generation, which is assumed to be negligible here. Also, $Q_{ext} = \sigma|\nabla\phi|^2$, which accounts for Joule heating, where ϕ

is electrical potential and σ is electrical conductivity of the tissue. Heat transfer in living organisms is more complex than in other circumstances. Metabolism and blood flow are important in addition to conduction, convection, radiation and evaporation. For this reason, the Bioheat equation, which includes terms that account for blood flow and metabolism, was used. In addition, the Bioheat equation solves for the temperature and ascertains the impact of the Joule effect. The result of the Bioheat equation determines if the tumor was also being treated by resistive heating, or only by IRE. The values utilized in the Bioheat equation for the corresponding structures in the prostate and the breast are shown in Tables 2.3, 2.4 and 2.5.

Table 2.3: Properties for the structures in the prostate cancer Bioheat model used to solve for the temperature distribution induced by electroporation

Structure	Thermal Conductivity (k) [W/mK]	Specific Heat (c) [J/kgK]	Density (ρ) [kg/m^3]	Reference
Prostate tissue	0.56	3600	1045	(Feng et al. 2009)
Nerve (axon and myelin)	0.5	3600	1043	(DeMarco 2003)

Table 2.4: Properties for the structures in the breast cancer Bioheat model used to solve for the temperature distribution induced by electroporation

Structure	Thermal Conductivity (k) [W/mK]	Specific Heat (c) [J/kgK]	Density (ρ) [kg/m^3]	References
Fatty breast tissue	0.25	2522	900	(Howorka 1996),(Robinson et al. 1991), (Findanza 2003)
Breast gland	0.41	3492	1030	(Dosekun 1961), (Kolka et al. 1984), (Moreira et al. 2006)
Breast tumor	0.48	2926	1186	(Kwok & Krzyspiak 2007), (P. Prakash et al. 2006), (Roth & Wikswo 1985)

Table 2.5: Human blood properties for the prostate and breast cancer Bioheat models accounting for the convective effects of blood flow used to solve for the temperature distribution

Structure	Perfusion Rate [1/s]	Thermal Conductivity (k) [W/mK]	Specific Heat (c) [J/kgK]	Density (ρ) [kg/m^3]	References
Blood	0.002	0.39	3640	1000	(L. Sun et al. 2003), (Valvano & Chitsabesan 1987), (Belov 1978), (Maor, Ivorra & Rubinsky 2008a)

2.3 Models

Five models were used to demonstrate the differences between heterogeneous and homogeneous tissues treated with electroporation. The models mimic techniques implemented in live animal studies (Al-Sakere et al. 2007),(Davalos et al. 2003). The electrodes were taken to have a diameter of one mm (18 gauge) (Rubinsky et al. 2007). The electrodes were placed one cm apart. For boundary conditions in each case, a uniform voltage was imposed on each electrode and a voltage difference of 2000V was imposed between the electrodes.

Case 1a: Prostate tissue (2cm x 2cm) with two electrodes separated by 1cm

Case 1b: A nerve (axon with myelin sheath) in the center of prostate tissue (2cm x 2cm) with two electrodes separated by 1cm. The nerve is modeled as a circular axon surrounded by a uniform layer of myelin. The axon radius was 0.1mm (Takenaka & Murakami 2005) and the thickness of the myelin surrounding it was 0.02mm (Schröder 1972). The axon and myelin structure was centered within the cross section of prostate tissue.

Case 1c: A blood vessel in the center of prostate tissue (2cm x 2cm) with two electrodes separated by 1cm. The blood vessel was 5E-5m in radius and was placed in the center of a cross section of prostate tissue.

Case 2: Fatty breast tissue (2cm x 2cm) with two electrodes separated by 1cm

Case 2b: A duct in the center of fatty breast tissue (2cm x 2cm) with two electrodes separated by 1cm. In the model a duct was surrounded by myoepithelial cells. The breast duct was 0.7mm in radius (Rubinsky et al. 2008) and the surrounding layer of myoepithelial cells were 0.13mm in thickness. The duct and myoepithelial cells were centered within a cross section of breast tissue.

Each model includes a square cross section of tissue ($4cm^2$ for the prostate and the breast), large enough to account for fringe effects of the electric field. Electrodes conductive only at the tips are utilized in vivo, so they were represented as circles in the models. All models were evaluated at a voltage potential difference between the electrodes of 1000V/cm. This voltage potential was chosen because it falls within the range of electric fields that will ablate a cancerous tumor: 250-2000V/cm (Rubinsky et al. 2008). Each model simulated a single voltage pulse of length 0.1ms, and the temperature was evaluated at time steps of 0.1E-4s.

There were two sets of boundary conditions generated; one set for the Laplace equation and another for the Pennes bioheat equation. For the Laplace equation, the edges of the tissue sample were treated as electrically insulating:

$$\frac{\partial \emptyset}{\partial n} = 0 \tag{2.3}$$

where $\emptyset$ is potential. The remaining structures were prescribed continuity boundary conditions:

$$n \cdot (J_1 - J_2) = 0 \tag{2.4}$$

where *n* is the normal vector and *J* is the current density. For the Bioheat equation, the edges of the tissue were set to body temperature:

$$T = 37°C \tag{2.5}$$

The remaining structures were prescribed continuity boundary conditions.

2.4 Results and Discussion

Figure 2.1 illustrates the geometry and mesh that was used for the homogeneous and the heterogeneous models. It is important to note that the mesh becomes more refined around the boundaries of the electrodes in both cases. This ensures accurate results in the vicinity of the electrodes and captures even the smallest temperature difference on the micron scale. The mesh is also extra fine around the boundaries of the heterogeneity.

Figure 2.2 shows the temperature distribution at the end of a single pulse in the homogeneous and heterogeneous models of prostate tissue with two electrodes of voltage potential difference 2000V. The figure depicts isothermal lines and the details of the temperature distribution can be found in Figure 2.3. The elevated temperature reaches a maximum of 40.25°C in the homogeneous case. However, the temperature is only elevated within nanometers of the electrode.

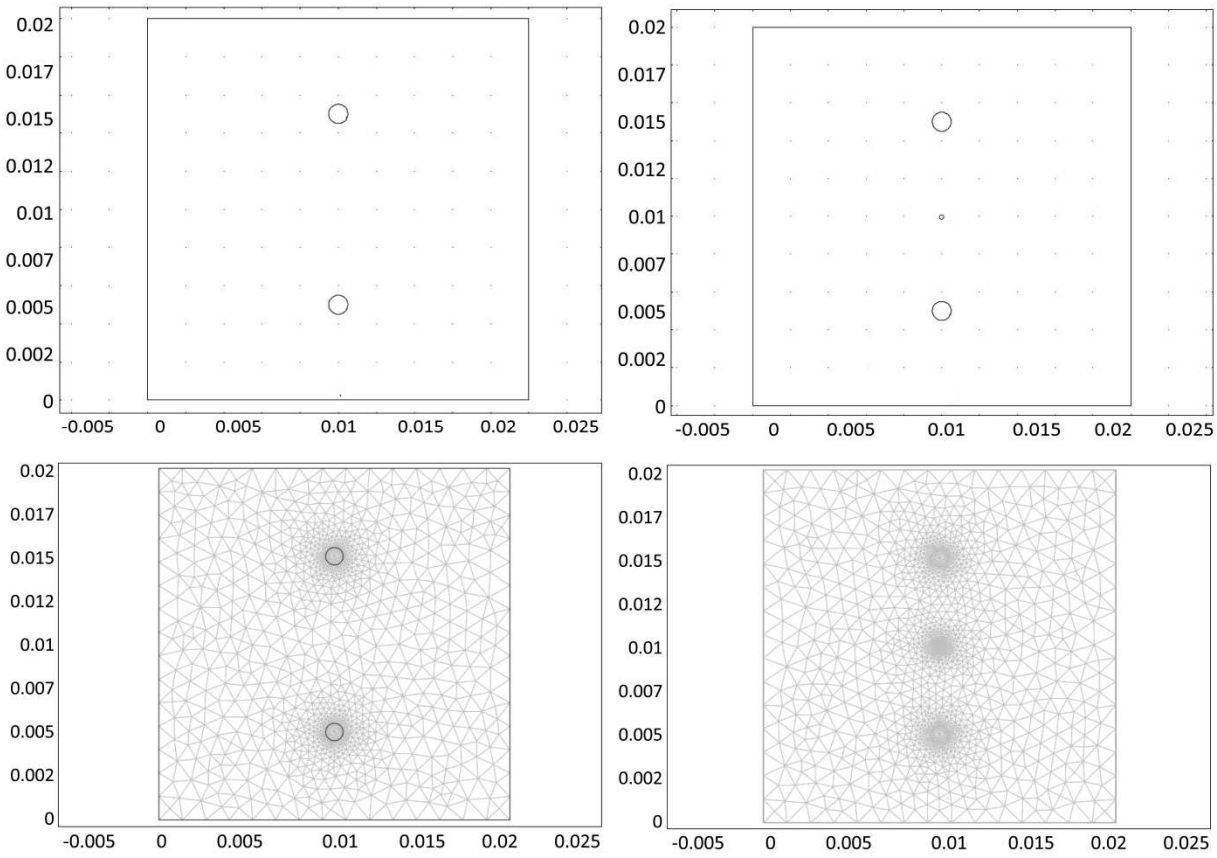

Figure 2.1: Top row, geometry of homogeneous prostate model and electrodes (left) and geometry of heterogeneous prostate model, nerve and electrodes (right) in a cross section of prostate tissue. Bottom row, mesh utilized for homogeneous prostate models that includes two circular electrodes (left). Right, mesh utilized for heterogeneous prostate models that includes a cross section of a nerve between two circular electrodes. Note that the mesh is extra fine in the vicinity of the heterogeneities in order to capture the change in electric field and temperature over such a small distance.

The heterogeneous plot in Figure 2.2 includes a nerve (axon and myelin) within the prostate tissue. The axon radius was 0.1mm (Takenaka & Murakami 2005) and the thickness of the myelin surrounding it was 0.02mm (Schröder 1972). The axon and myelin structure was centered within the square cross section of prostate tissue. The difference between the heterogeneous and homogeneous cases can be seen in the temperature range. The homogeneous model ranges from nearly body temperature, 37.08°C, to 40.28°C. However, the heterogeneous model has a slightly lower temperature, ranging from 37.08C to 40.13°C. Note that the main difference between the homogeneous and heterogeneous cases is the dip in the temperature at the center of the plot in the heterogeneous case, where the nerve is located. This dip does not exist in the homogeneous graphs (two left panels of Figure 2.3). The difference in the temperature distribution between these two plots shows the importance of taking heterogeneous models into account for an accurate portrayal of IRE.

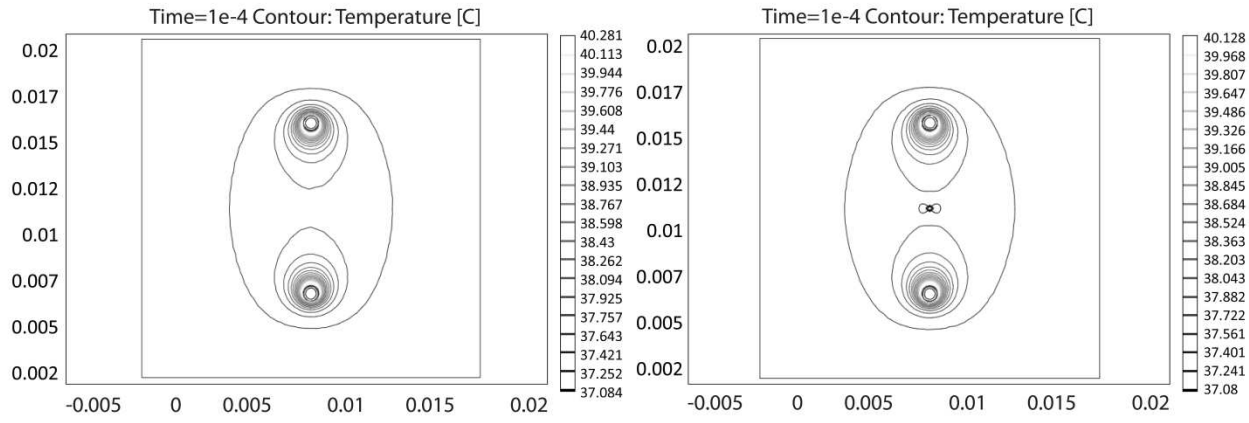

Figure 2.2: Plots illustrating the temperature distribution in the prostate after the application of a single pulse at V=2000V. The figure on the left illustrates the homogeneous case with two electrodes within a square of prostate tissue. The figure on the right illustrates the heterogeneous case with a nerve between two electrodes within a square of prostate tissue.

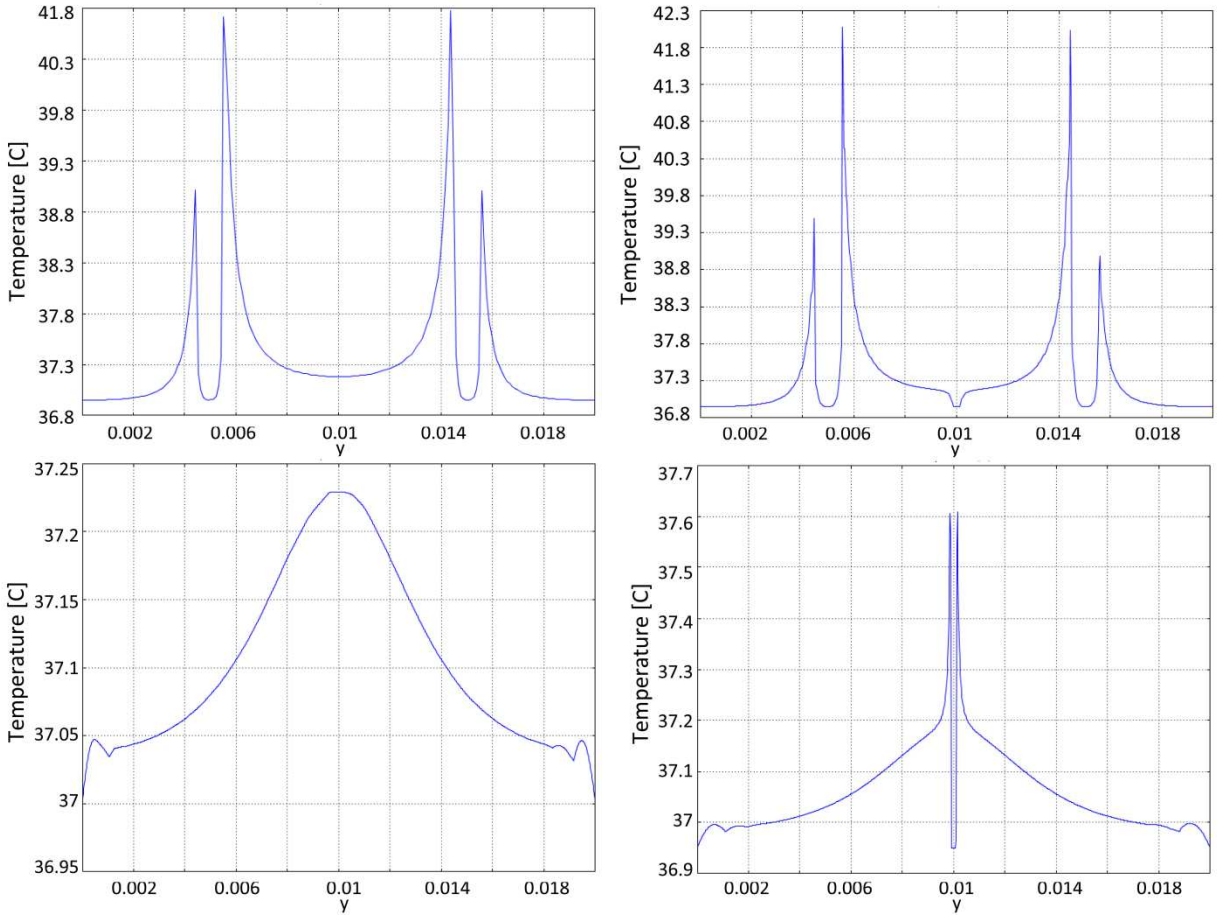

Figure 2.3: The graphs above illustrate vertical and horizontal transects of the temperature distribution in the two cases from figure 2.2. Top left, vertical homogeneous; top right, vertical heterogeneous. Bottom left, horizontal homogeneous; bottom right, horizontal heterogeneous. Note that in both heterogeneous cases the temperature drops drastically at the location of the nerve.

In order to determine the thermal damage experienced by the electroporated tissue a kinetic model based on the Arrhenius equation can be implemented (Wright 2003). The Arrhenius equation is the principal method for determining such damage:

$$\Omega = \int_0^\tau \left(A e^{-E/RT} \right) dt \tag{2.6}$$

where Ω is a dimensionless parameter indicating the level of thermal damage, A is a measure of molecular collision frequency, E is an energy barrier that must be overcome, R is the gas constant, T is temperature, and t is time. Both A and E are dependent upon tissue type and determined experimentally. In order to determine if thermal damage occurs in prostate tissue during the application of the pulse, values from Table 2.6 were used.

Table 2.6: Values for the Arrhenius Equation for both prostate and breast tissues used to calculate the parameter of thermal damage, Ω.

Tissue	A [1/s]	E [J/mole]	t [s]	Reference
Prostate	3.12×10^{20}	1.28×10^{5}	4.5E-5	(Pop et al. 2003)
Breast	4.43×10^{16}	1.29×10^{5}	4.5E-5	(Blakemore 1975)

Values of Ω that are below 1 indicate negligible thermal damage. Although the study only includes a pulse of length 1E-4s, it is important to allow the system time to drop back to body temperature. The time necessary to return to approximately body temperature was determined in Comsol to be 5E-5 seconds. For this reason, τ = 4.5E-4 seconds was used. The maximum temperature experienced by the prostate tissue in the simulation, 40.28°C (313.43K) was applied to the equation. Utilizing Equation 2.6, Ω can be calculated for prostate tissue:

$$\Omega = \int_0^{4.5E-4} \left(3.12 \times 10^{20} e^{-1.28\times10^5/R\times313.43}\right) dt$$

$$\Omega_{prostate} = 6.53E-5$$

Because the value for Ω is well below 1, the Arrhenius equation indicates that the prostate treated with IRE receives negligible thermal damage.

The plot in Figure 2.4 displays lines of constant electrical field in prostate tissue. The plot in Figure 2.5 is a detail of the nerve from Figure 2.4. The maximum electric field, $6.96E5\,\frac{V}{m}$, occurs at the electrodes. The remaining tissue in the square sample above and below the electrodes receives a reduced effect, with the electric field reaching nearly $0\,\frac{V}{m}$ at the edge of the tissue sample. However, in the location between the electrodes, where the nerve would be in the heterogeneous model, that the electric field in the homogeneous model does not reach zero. At this location the electric field only reaches a minimum of $1.45E5\,\frac{V}{m}$. This can be seen in the plot of the electric field along a vertical transect of the homogeneous model (top left panel of Figure 2.6).

The electric field in the heterogeneous prostate (Figure 2.4) is exceptionally different than in the homogeneous prostate. The maximum electric field in the heterogeneous case is $1.85E6\,\frac{V}{m}$, which is more than in the homogeneous model. In the heterogeneous model, the highest levels of electric field occur in the myelin. At $1.7E6\,\frac{V}{m}$, the electric field in the myelin is almost an order of magnitude more than the maximum in the homogeneous model. Elsewhere in the heterogeneous model the electric field is low, except in the immediate vicinity of the

electrodes. The plot of the heterogeneous model (two right panels of Figure 2.6) also shows that the axon receives the lowest levels of electric field, reaching zero. This implies that the myelin insulates the axon from the effect of the electric field. Because axons are able to remyelinate themselves (Rusby et al. 2007) , these results suggest that the nerve structure should be able to fully recover even if the myelin is damaged. This plot demonstrates the importance of heterogeneous models to understand the effect of irreversible electroporation on the nervous system.

These results explain the outcome in clinical trials utilizing IRE to treat prostate cancer (G Onik et al. 2007), in which nerves surrounding the prostate remained unharmed. It is now understood why the nerves near the prostate survived: the myelin insulates the axons from the electric field. Even if damaged, the axons remyelinate via Schwann cells and all neurological functionality is retained.

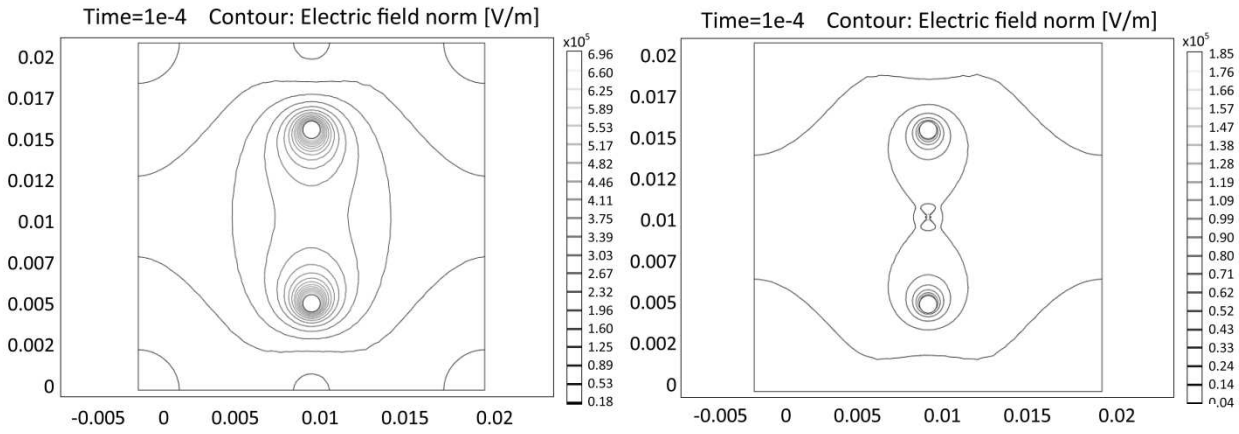

Figure 2.4: Electric field distribution in the prostate from a single pulse of V=2000V. The left figure depicts homogeneous prostate tissue with two electrodes. The right figure depicts the heterogeneous case with a nerve between to electrodes in prostate tissue. Note that in the heterogeneous case the electric field reaches near zero at the location of the nerve, whereas in the same location for the homogeneous model it is $\mathbf{1.45E5\frac{V}{m}}$.

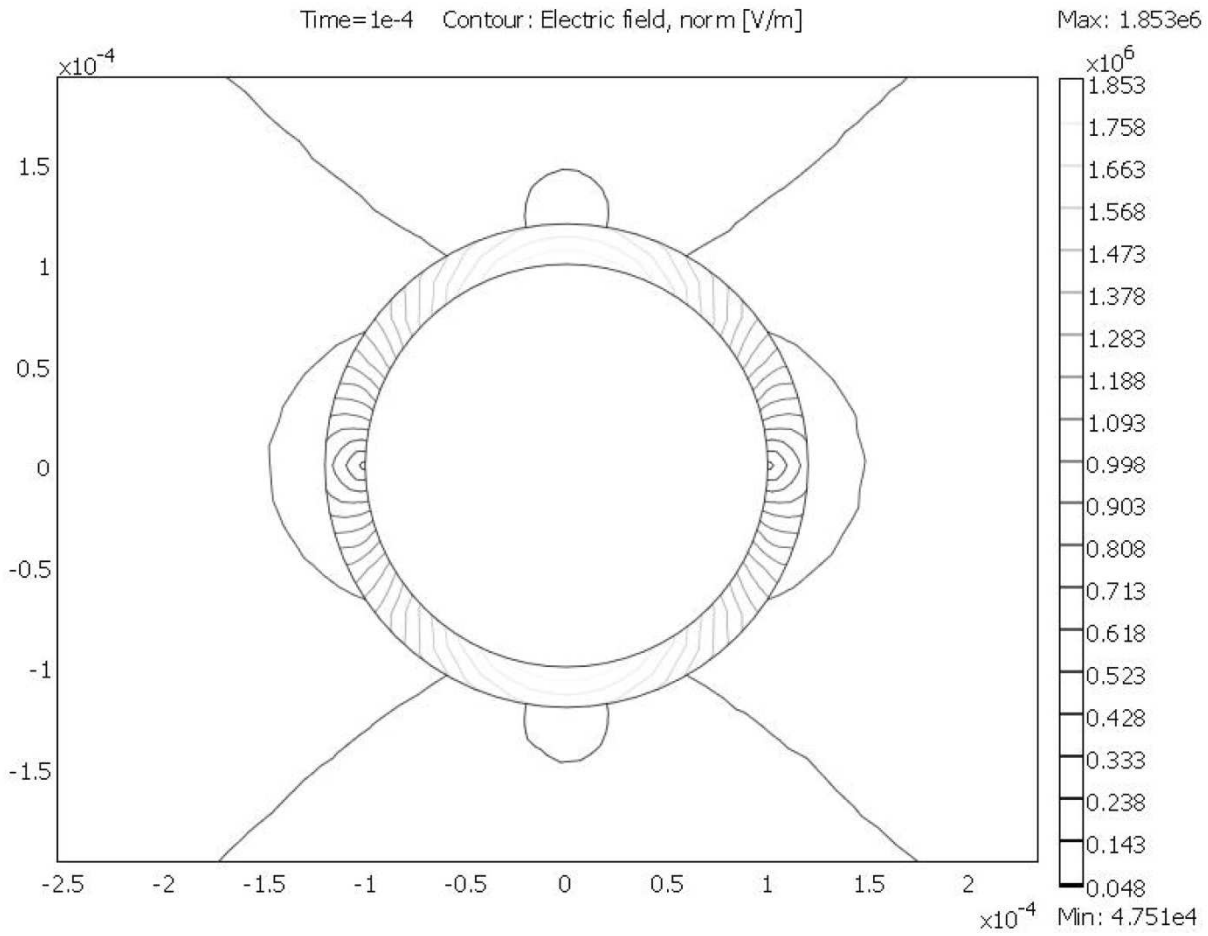

Figure 2.5: A close up of the electric field distribution in the axon and myelin structure in the prostate as a result of a single pulse of V=2000V at 0.1ms. Note that the electric field lines are concentrated inside the myelin and that there are no field lines inside the axon.

Figure 2.5 depicts the electric field in both the axon and the surrounding myelin. This close up of the nerve structure clearly illustrates that the electric field is concentrated in the thin layer of myelin, shown by the densely packed electric field lines. Figure 2.5 also clarifies that there is absolutely no effect of the electric field inside the axon, shown by the lack of electric field lines. Such a result is very promising for IRE as a treatment for cancerous tumors. It suggests that a tumor adjacent to nerves can be eliminated with IRE, while preserving the surrounding nerves.

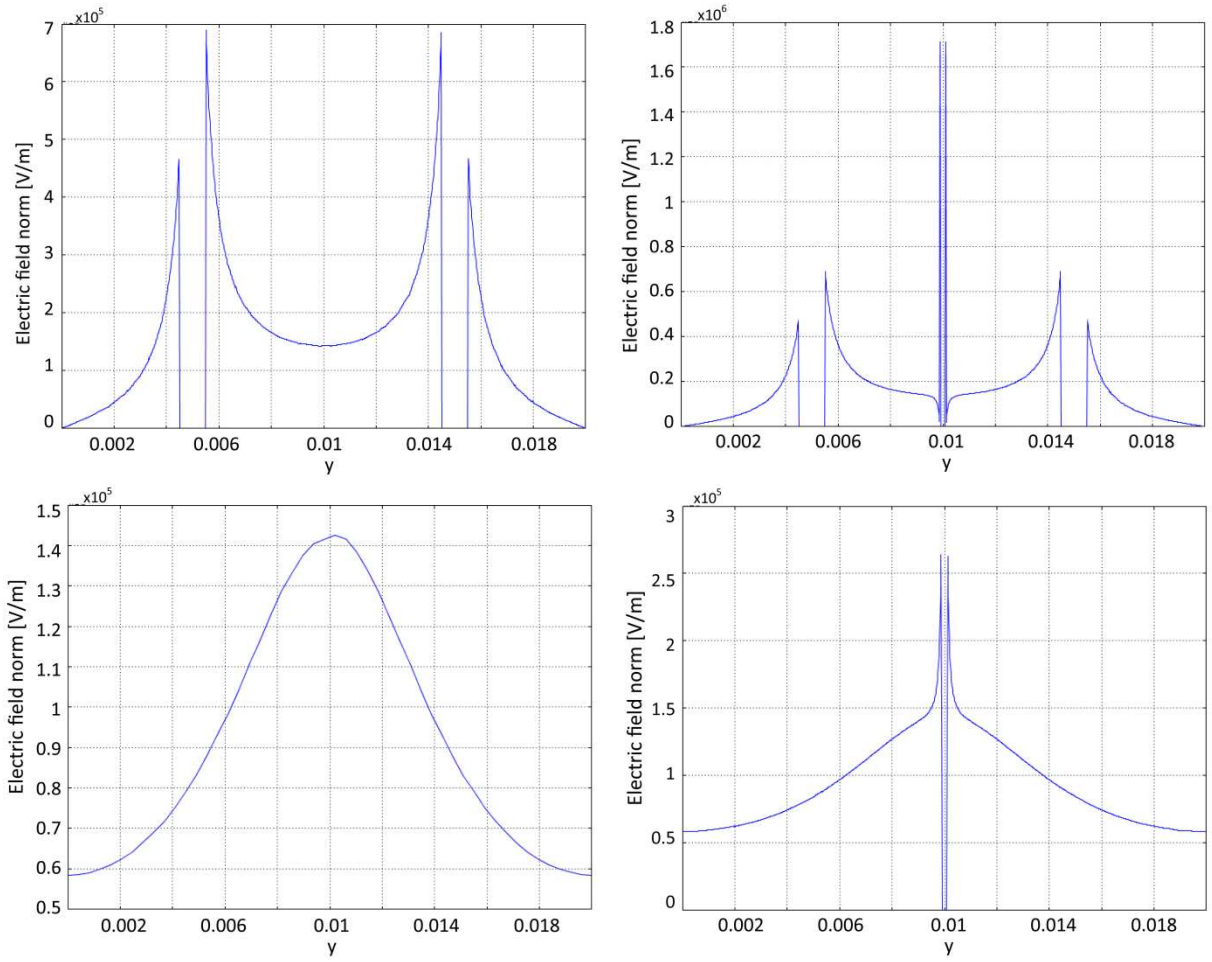

Figure 2.6: The graphs above illustrate vertical and horizontal transects of the electric field distribution in the two cases from figure 2.4. Top left, vertical homogeneous; top right, vertical heterogeneous. Bottom left, horizontal homogeneous; bottom right, horizontal heterogeneous. Note that the highest electric field in the heterogeneous cases (two right hand graphs) occurs in the location of the myelin, and the lowest electric field (0V) at the axon.

The next structure analyzed was the prostate with a blood vessel included. The blood vessel was 5E-5m in radius and was placed in the center of a square cross section of prostate tissue. Figures 2.7 and 2.9 show the temperature distributions in the same manner as Figure 2.2 and 2.3. The maximum temperature reached was 40.43°C for the homogeneous case, while it was 40.28°C for the homogeneous case. The blood vessel model has a temperature distribution between 37.09°C and 40.43°C and temperatures peak in the immediate vicinity of the electrodes (Top left panel of Figure 2.9).

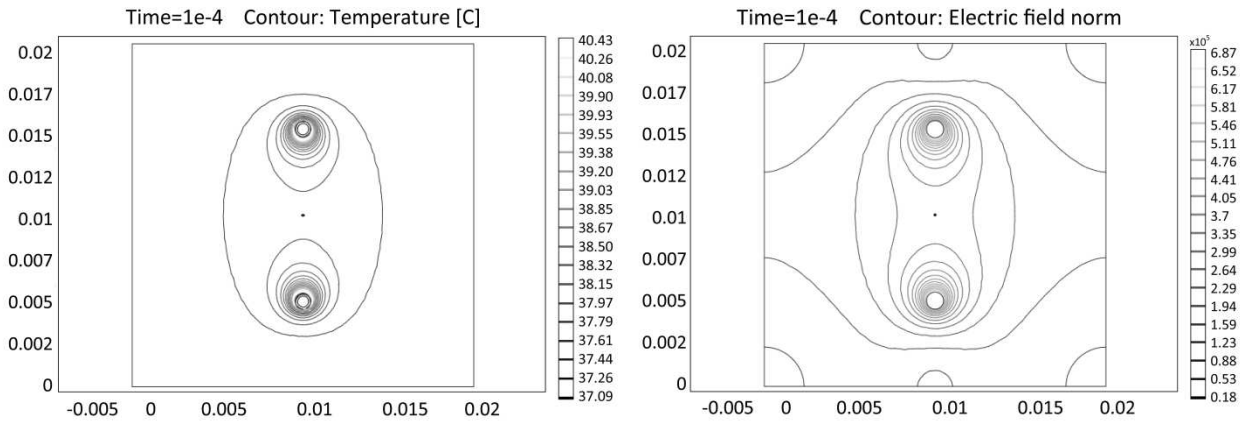

Figure 2.7: Temperature and electric field distribution in the prostate with a blood vessel after a single pulse at 2000V. The left figure illustrates the temperature distribution in the heterogeneous case with a blood vessel between two electrodes in a square of prostate tissue. The right figure illustrates the electric field distribution for the same case.

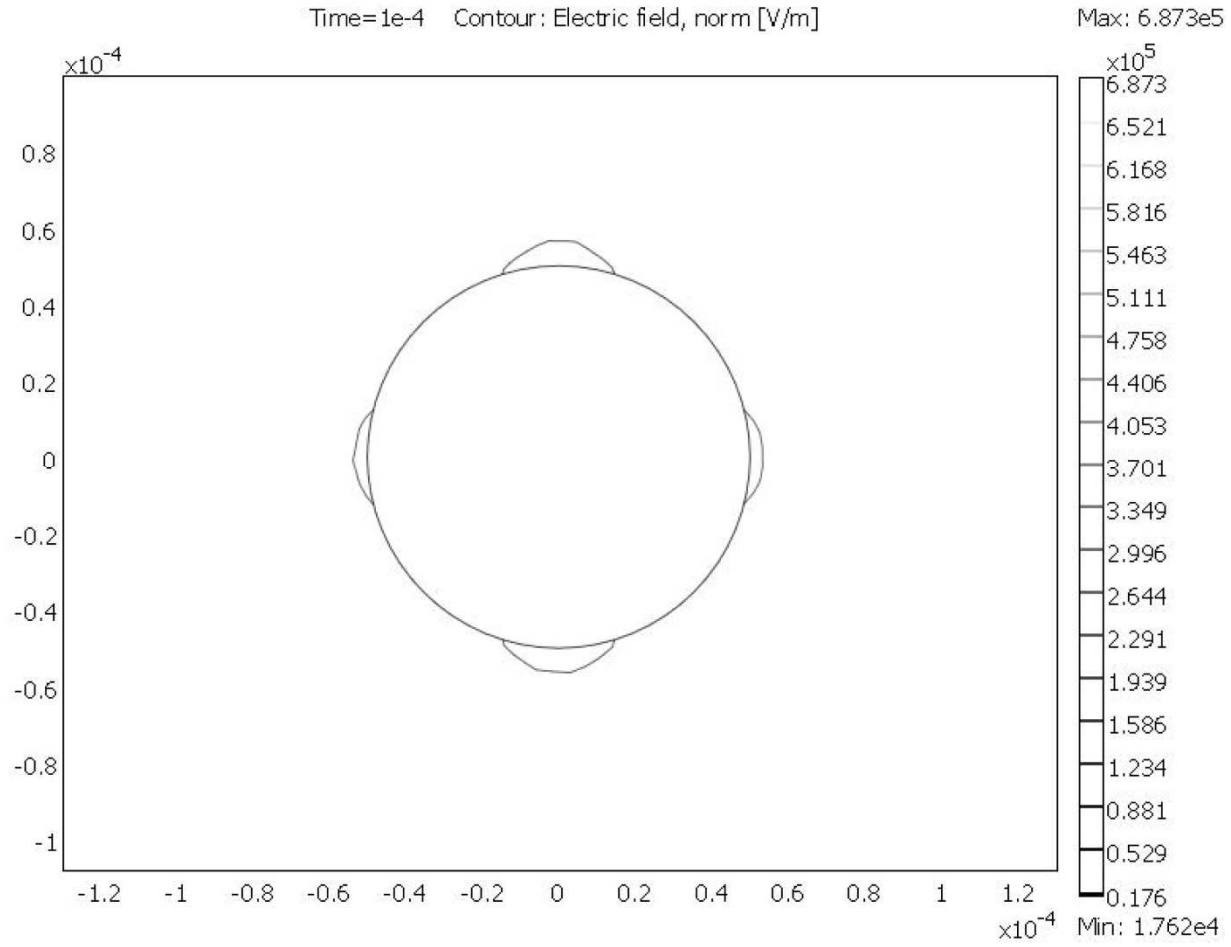

Figure 2.8: Close up of the electric field distribution around the blood vessel in the prostate after a single pulse at 2000V. Note that there are no electric field lines inside the blood vessel.

The electrical fields in this case are depicted in Figure 2.7 and 2.9 in the same manner as Figure 2.4 and 2.6. The maximum electric field in the heterogeneous case with the blood vessel (Figure 2.7) is lower than the homogeneous case. The homogeneous prostate reached $6.96E5\,\frac{V}{m}$, while the prostate with a blood vessel reached $6.87E5\,\frac{V}{m}$. Additionally, there is a slight rise in the electric field in the vicinity of the blood vessel. This occurs because the electrical conductivity of the blood vessel is slightly lower than that of prostate tissue. Nevertheless it receives a low level of electric field, indicating that during clinical trials, blood vessels in the vicinity of a tumor would be unharmed by the effects of the electroporation.

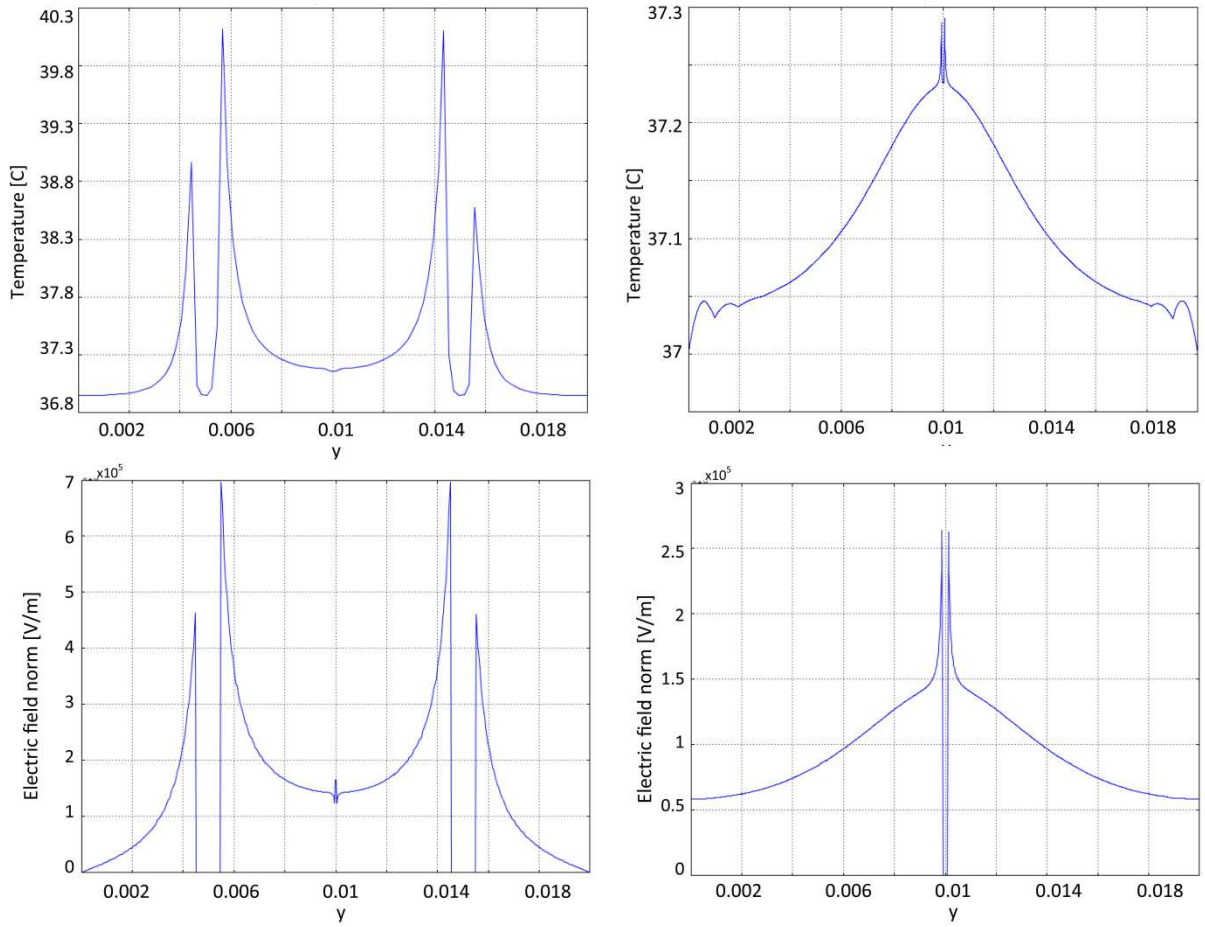

Figure 2.9: The graphs above illustrate vertical and horizontal transect of the temperature and electric field distribution in the two heterogeneous cases from figure 2.7. Top: temperature in prostate with blood vessel; Left, vertical; right, horizontal. Bottom: heterogeneous electric field in prostate with blood vessel; left, vertical; right horizontal.

The highest temperature experienced by the prostate model with a blood vessel included is 40.43°C. With this information, and the values from Table 2.6, the Arrhenius equation can be used to determine if the tissue experienced any thermal damage:

$$\Omega = \int_0^{4.5E-4} \left(3.12 \times 10^{20} e^{-1.28\times10^5/R\times313.58}\right) dt$$

$$\Omega_{prostate}^{b} = 6.68E - 5$$

$\Omega_{prostate}^{b}$ indicates the level of thermal damage for the prostate model with a blood vessel. This value is slightly larger than the level of thermal damage for the prostate model with a nerve, $\Omega_{prostate} = 6.53E - 5$. Nevertheless, it is far below one, which means that the prostate tissue in this model receives negligible thermal damage.

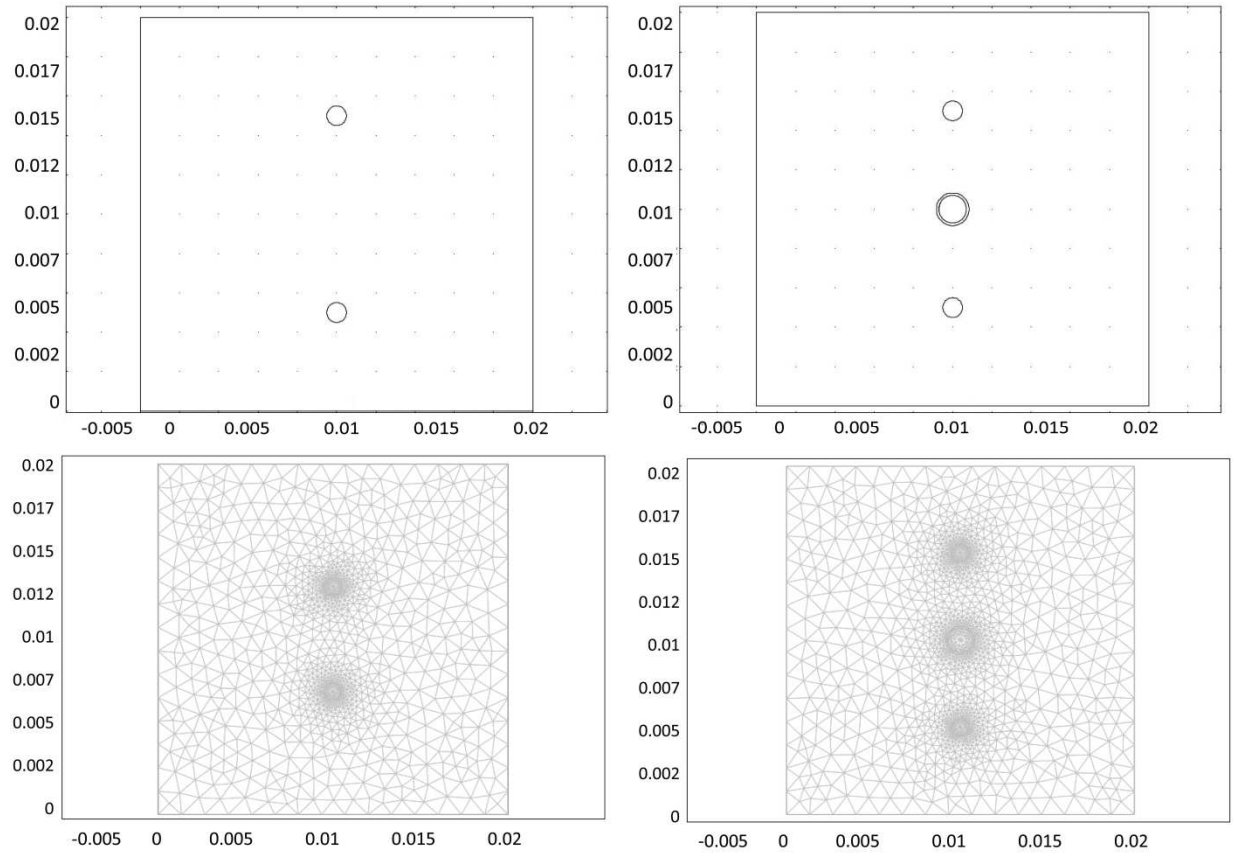

Figure 2.10: Top row, geometry of homogeneous breast model and electrodes (left) and heterogeneous breast model, lactiferous ducts and electrodes (right) in a cross section of breast tissue. Bottom row, mesh utilized for homogeneous breast model that includes two circular electrodes (left). Right, mesh utilized for heterogeneous breast models that includes a cross section of a lactiferous duct between two circular electrodes. Note that the mesh is extra fine in the vicinity of the heterogeneities in order to capture the change in electric field and temperature over the small distance.

The second study investigated the effects of electroporation on breast tissue. The model included a cross section of fatty breast tissue in the homogeneous model. In the heterogeneous model a duct surrounded by myoepithelial cells was included in the breast tissue (Figure 2.10). The breast duct was 0.7mm in radius (Rubinsky et al. 2008) and the surrounding layer of myoepithelial cells were 0.13mm in thickness. The duct and myoepithelial cells were centered within a square cross section of breast tissue. Again, Figure 2.11 and 2.12 are presented in the same manner as Figure 2.2 and 2.3; Figure 2.13 and 2.15 are presented in the same manner as Figure 2.4 and 2.6.

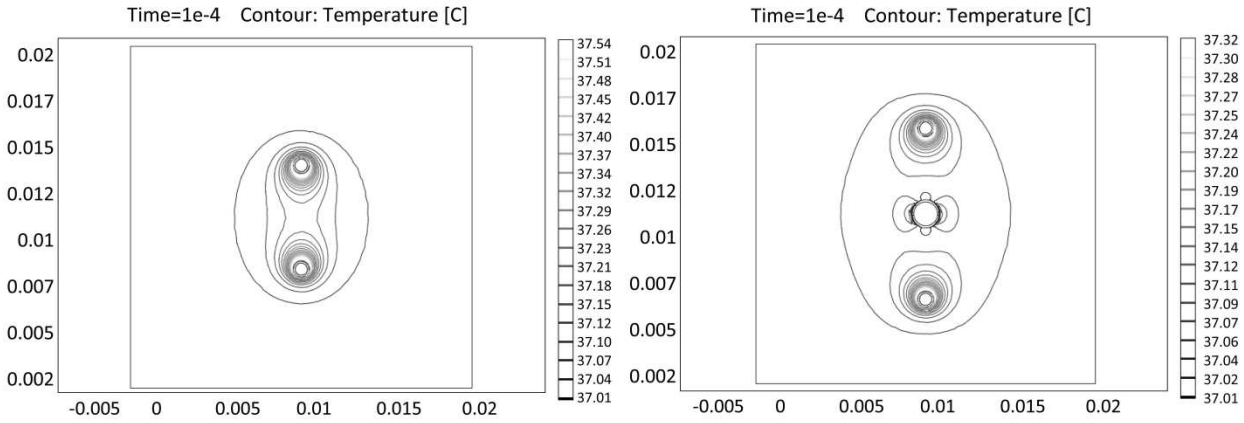

Figure 2.11: Plots illustrating the temperature distribution in the breast after the application of a single pulse at V=2000V. The figure on the left illustrates the homogeneous case with two electrodes in a square of breast tissue. The figure on the right illustrates the heterogeneous case with a duct between two electrodes in a square of breast tissue.

Figure 2.12 shows that in the vertical plane the highest temperature reached in the homogeneous model is 37.55°C, only 0.55 degrees higher than body temperature. In the heterogeneous case, however, the maximum temperature, 37.32°C, is even lower. The temperature distribution is vastly different between the homogeneous and heterogeneous horizontal transects. The homogeneous model reaches a maximum halfway between the electrodes, but the heterogeneous model dips to a minimum in that location.

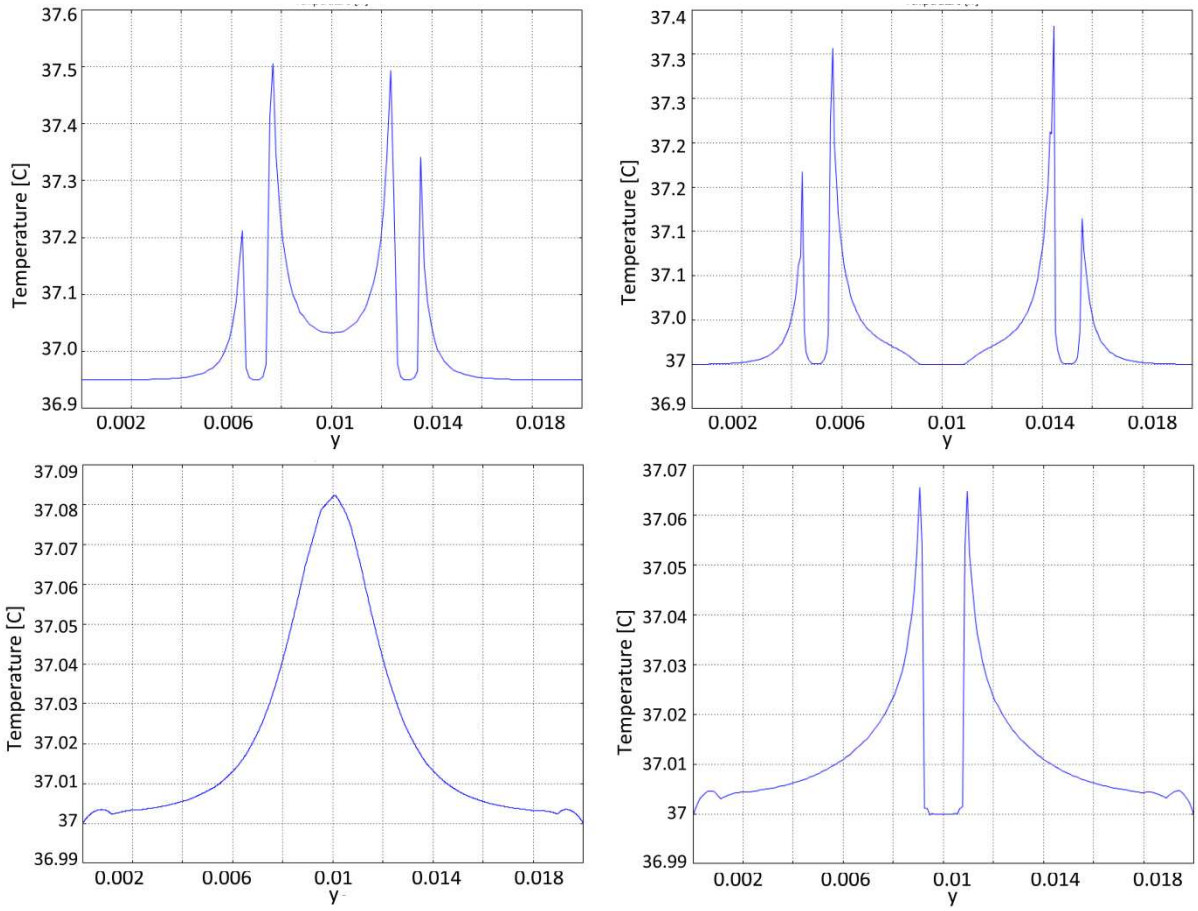

Figure 2.12: The graphs above illustrate vertical and horizontal transects of the temperature distribution in the two cases from figure 2.11. Top left, vertical homogeneous; top right, vertical heterogeneous. Bottom left, horizontal homogeneous; bottom right, horizontal heterogeneous. Note that in both heterogeneous cases the temperature drops at the location of the duct.

Because the breast tissue does not exceed a temperature of 0.55°C above body temperature, the probability that the tissue receives any thermal damage is low. To verify this at the maximum temperature, 37.55°C, the Arrhenius equation can be used to calculate the parameter for thermal damage.

$$\Omega = \int_0^{4.5E-4} \left(4.43 \times 10^{16} e^{-1.29\times10^5/R\times310.7}\right) dt$$

$$\Omega_{breast} = 4.08E - 9$$

Because this value is well below one, the breast tissue experiences negligible thermal damage.

In the homogeneous model the maximum electric field reaches $9.3E5\,\frac{V}{m}$. The maximum electric field in the heterogeneous model, $1.9E6\,\frac{V}{m}$, is slightly higher. However, the electric field between the electrodes is very different in the two models. In the heterogeneous model the electric field reaches zero at the center of the duct (Figure 2.15). However, in the homogeneous model, the electric field only goes down to $2.9E5\,\frac{V}{m}$. Additionally, in the homogeneous model, the highest electric field occurs at the electrodes. But in the heterogeneous model, the highest electric field is within the myoepithelial cells and the next highest electric field is near the electrodes. This, however, does not pose a threat to the physiological function of the ducts because myoepithelial cells are known to regenerate (Takahashi et al. 1997).

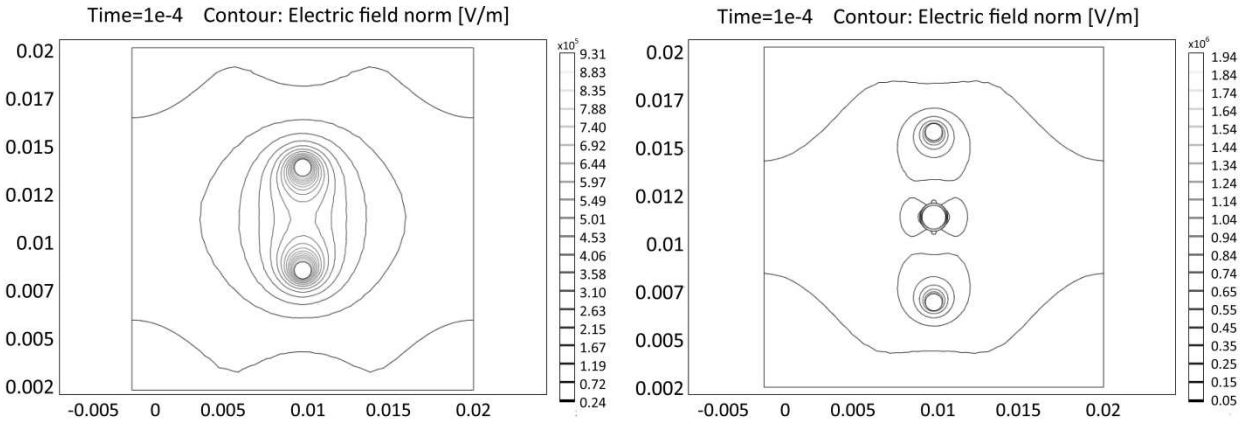

Figure 2.13: Plots illustrating the electric field distribution in breast tissue after a single pulse at 2000V. The left figure depicts the homogeneous case with two electrodes in a square of breast tissue. The right figure illustrates the heterogeneous case, with a duct between two electrodes.

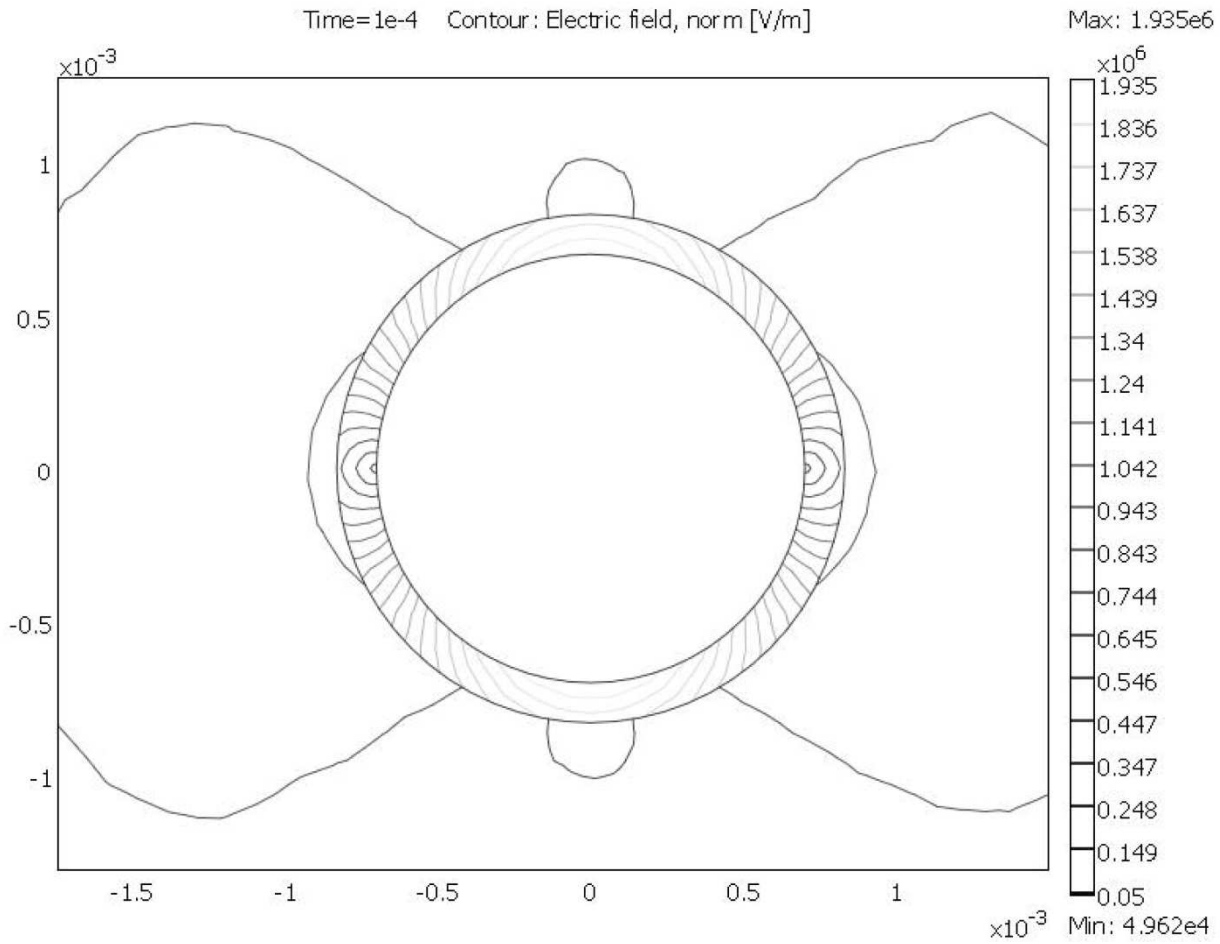

Figure 2.14: Close up of the electric field distribution around the duct in the breast after a single pulse at 2000V. Note that electric field lines are concentrated inside the layer of myoepithelial cells, but that there are absolutely none inside the duct.

Figure 2.14 demonstrates visually that there are no electric field lines inside the duct, and therefore this structure receives no effect from the electrical pulse. Additionally, Figure 2.14 also illustrates that electric field lines are concentrated inside the myoepithelial cells surrounding the duct. Therefore, just as the myelin insulated the nerves from the electrical pulses, the myoepithelial cells insulate the duct from the electrical pulses. In parallel, Figure 2.14 closely resembles Figure 2.5. This suggests that a tumor in close proximity to lactiferous ducts can be eliminated with IRE, while leaving the ducts unharmed.

Figure 2.15 illustrates the trend demonstrated consistently in this study. In the homogeneous breast tissue in the top left quadrant of Figure 2.15, the highest electric field occurs adjacent to the electrodes. However, in the heterogeneous breast tissue, which includes lactiferous ducts, the highest electric field occurs inside the myoepithelial cells and the electric field adjacent to the electrodes is lower. This occurs because the low electrical conductivity of the myoepithial cells causes the electric field to increase in that region. The most important difference between the two cases, however, is that the electric field inside the lactiferous duct is

zero. Whereas in the homogeneous case, in the same location the electric field is approximately 3E5V/m. This is a considerable contrast between the homogeneous and heterogeneous cases. In the lower left quadrant of Figure 2.15, the difference between the homogeneous and heterogeneous cases is also demonstrated clearly. The homogeneous case electric field peaks at the location of the lactiferous duct and the heterogeneous case electric field reaches zero at the location of the duct. This indicates that a lactiferous duct in breast tissue may remain unaffected by the application of electric fields during IRE.

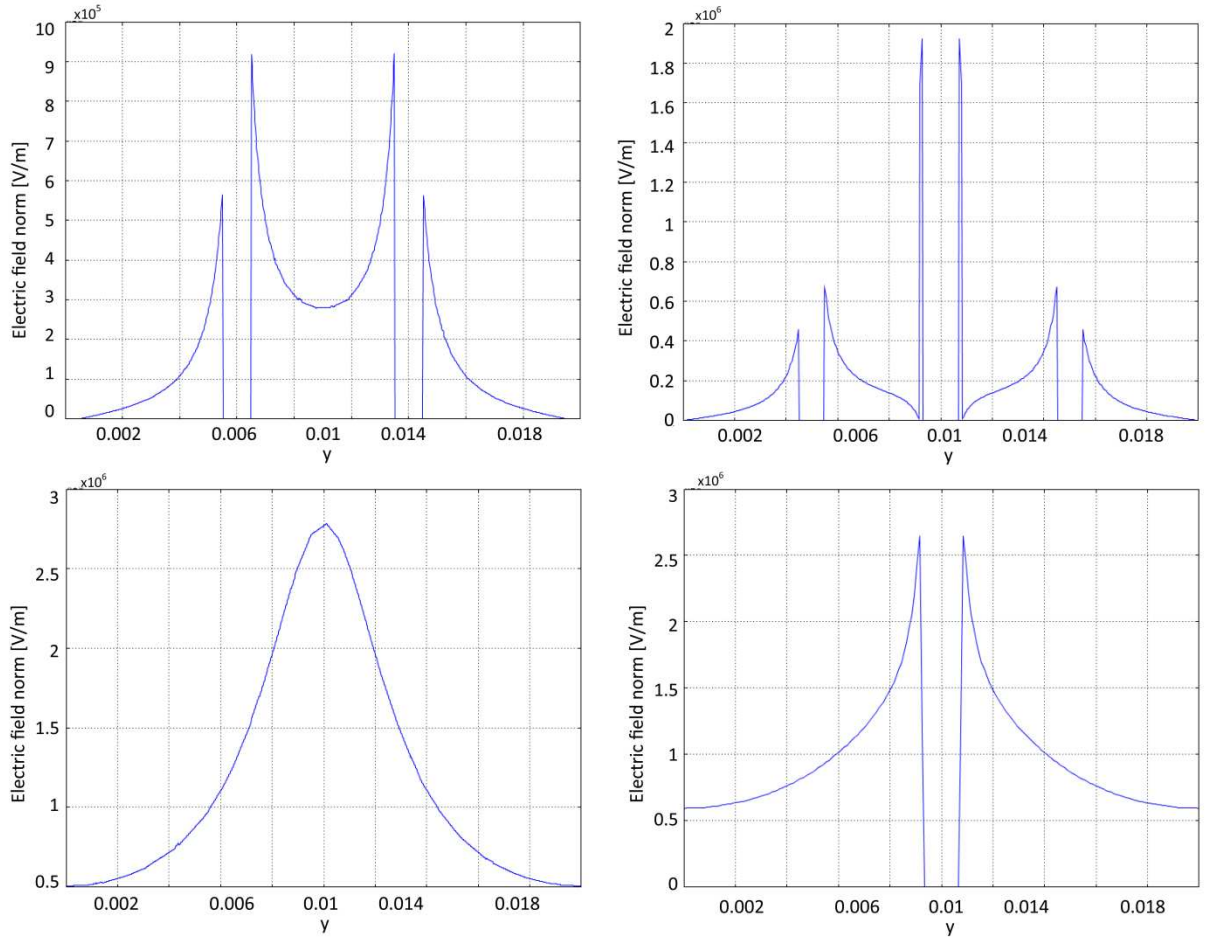

Figure 2.15: The graphs above illustrate vertical and horizontal transects of the electric field distribution in the two cases from figure 2.13.Top: breast tissue vertical electric field. Left, homogeneous; right heterogeneous. Bottom: breast tissue horizontal electric field. Left, homogeneous; right, heterogeneous. Note that the electric field reaches zero at the location of the duct.

2.5 Conclusion

The goal of this study was to prove the importance of investigating heterogeneous models with IRE and to show that when IRE treatment methods are developed they must consider the heterogeneous nature of the tissue. Both the model of the prostate and the breast demonstrated

the substantial difference between homogeneous and heterogeneous cases. Furthermore, unanticipated information about the effects of IRE was also discovered. The impact IRE has on biological structures such as nerves, ducts and blood vessels was previously unknown. This investigation has made clear that nerves can be preserved in treated tissue because of the insulating effect of surrounding myelin layers. Additionally, this study has suggested that lactiferous ducts will remain undamaged because myoepithelial cells have the ability to regenerate. Therefore, heterogeneous models are not only important to consider in order to generate an accurate simulation, but also to understand the effects of electroporation on all included biological structures to improve clinical applications.

Chapter 3: Irreversible Electroporation Modulated with Cryosurgery

3.1 Introduction

During the last 20 years the development and implementation of minimally and non-invasive surgeries have flourished. In comparison to traditional surgery, minimally and non-invasive surgeries are positioned to transform the field of medicine with shorter hospital stays, reduced surgical trauma, improved immune response and greater precision (Fuch 2002). These benefits are primarily due to less intrusive procedures and more targeted tissue ablation. This study deals with a combination of two minimally invasive surgical techniques; cryosurgery and irreversible electroporation (IRE).

Cryosurgery is a minimally invasive surgical technique with a 150 year history (Gage 1998). Cryosurgery uses freezing temperatures to ablate undesirable tissue (Rubinsky 2000). Freezing is induced with cryosurgical probes, usually cooled by an internally circulated cryogen, inserted into or placed in close vicinity to the undesirable tissue. Some applications for cryosurgery include treating skin, liver and prostate cancers. Cryosurgery has several advantages in addition to its ability to ablate tissue. One major advantage is that freezing has a profound effect on the physical properties of tissue and therefore cryosurgery can be monitored with any type of imaging modality. This includes ultrasound, which is one of the most economical and widely available imaging techniques (J. Gilbert et al. 1984), (G Onik et al. 1984). In cryosurgery, freezing is applied to the cryoprobe for a period of time on the order of minutes (Rubinsky & Shitzer 1976), (Rossi et al. n.d.). Because of cryosurgery's time scale, simultaneous imaging with ultrasound allows the physician real time control over the extent of freezing with excellent clinical results (G Onik et al. 1991).

Cryosurgery, however, has its limitations. Perhaps the major disadvantage is related to the mechanism of cell death during cryosurgery. It has been found that cells can survive freezing between -40ºC and -0.56ºC (K Tatsutani et al. 1996),(Gage & J Baust 1998),(J Baust & Gage 2005),(Hoffmann & Bischof 2002),(Xiaoming & Bischof 2003). This means that on the outer rim of the frozen lesion, cells in this temperature range can survive (Gage et al. 2009). Ultrasound, as well as other imaging modalities, can only discriminate between frozen and unfrozen tissue. This is problematic because the region seen as frozen under imaging contains a substantial number of surviving cells, especially on the outer rim. Therefore, the accuracy of targeting pathogenic tissue and the reliability of ablation are compromised. Finding ways to overcome this limitation in cryosurgery is the subject of intensive investigation, e.g. (Koushafar & Rubinsky 1997),(Mir & Rubinsky 2002),(Jiang et al. 2010),(Jiang et al. 2008),(Gage et al. 2009).

Electroporation utilizes pulsed electric fields that target the cellular membrane, increasing membrane permeability through the formation of nanoscale defects. The electric field is delivered through two electrodes that usually delineate the volume of treated tissue. Typical electroporation parameters currently utilized in medicine and biotechnology employ 0.1 to

10^7V/m electric fields, nanosecond to millisecond pulse lengths and one to several hundred pulses. Electroporation can have two different effects on the cell membrane as a function of the electric parameters: reversible and irreversible electroporation. In reversible electroporation the permeabilization of the cell membrane is transient. Reversible electroporation is used in genetic engineering for the introduction of genes into targeted cells (Neumann et al. 1982),(M Jaroszeski et al. 1999)**,**(Somiari et al. 2000). It is also used for tissue ablation in electrochemotherapy, which introduces drugs such as bleomycin into electroporated cells (Okino & Mohri 1987),(Mir et al. 1991),(Mir et al. 1998). In irreversible electroporation (IRE), the effect of membrane permeabilization is permanent and leads to cell death. During the last four decades, IRE was used primarily in the food industry for sterilization of micro-organisms (AJ Sale & WA Hamilton 1968),(WA Hamilton & AJH Sale 1967). Recently IRE has emerged as an important minimally invasive technique for tissue ablation because of its molecular selectivity (Davalos et al. 2004),(Edd et al. 2006). IRE has been found to spare the extracellular matrix and therefore it can leave blood vessels and nerves in the treated area intact (Rubinsky et al. 2007),(G Onik et al. 2007). However, the procedure has also disadvantages. There is no good way to determine the extent of tissue ablation in real time. Furthermore, the time scale is so rapid that it precludes real time control. Therefore, careful treatment planning must be conducted pre-surgery and the success of the procedure depends on the tissue planning.

The biophysical phenomena on which we focus in this chapter are related to the process of freezing at the outer edge of the frozen lesion during cryosurgery. It has been established that the process of freezing at the outer edge of the frozen lesion, where cooling rates are low, is characterized by extracellular freezing and shrinking of the cell to accommodate for the difference in osmotic pressure between the interior of the unfrozen cell and the increased osmolality of the exterior frozen milieu (Meryman 1966),(Mazur et al. 1970),(Mazur 1970),(Rubinsky & Pegg 1988),(Gage & J Baust 1998),(J Baust & Gage 2005),(Hoffmann & Bischof 2002),(Xiaoming & Bischof 2003). During typical cryosurgical protocols, the cells on the outer rim of the frozen region, where cells survive freezing, are: a) unfrozen, b) at below freezing temperatures and c) in a hyperosmotic solution. It should be emphasized that these cells experience additional molecular effects, such as apoptosis (Gage et al. 2009), or in certain procedures, exposure to tumor necrosis factors (Jiang et al. 2010). However, only the fact that the cells at the rim are: a) unfrozen, b) at below freezing temperatures and c) in a hyperosmotic solution is relevant to the time scale investigated in this study. This investigation was motivated by our recent paper in which we show that cold can change electrical properties of tissue and focus electric fields (Daniels & Rubinsky 2011). From this previous study, we expanded our hypothesis to investigate whether freezing can produce a similar effect, and if there is an advantage to using electroporation during cryosurgery. To the best of our knowledge, there are currently no studies on the application of pulsed electric fields on frozen biological tissues. However, there are studies on the effects of temperature on electroporation and on the effects of hyperosmolality on electroporation. We believe that these studies should provide us with some guidelines on what to expect during the electroporation of frozen tissue at the outer rim of the frozen lesion during cryosurgery.

Several studies have investigated the effects of temperature on electroporation. For instance, Diaz investigated the effect of low temperatures on electroporation efficacy. He accomplished electroporation on kidney epithelial cells at temperatures as low as -2°C (Diaz-

Rivera & Rubinsky 2006). Additionally, Gallo demonstrated the trend between temperature and electroporation; as temperature decreases, initial permeabilizing pulse voltage increases (Gallo et al. 2002). Gallo's study operated on the stratum corneum in the range 0-80°C. The same relationship between temperature and electroporation was found in *alga Valonia*, rye leaf protoplast and mammalian cell lines (Kanduser & Miklavcic 2009). From the studies discussed here, we anticipate that: a) electroporation occurs at temperatures that are lower than the lipid phase transition temperature of cells, and b) the strength of the electric field required for electroporation increases with a decrease in temperature of the electroporated cells.

Electroporation was found to be affected by electroporation buffer osmolarity. When electroporation is carried out in a hypertonic media, cells are permeabilized at a lower voltage than cells maintained in isotonic media and exposed to the same electric pulse parameters (Kanduser & Miklavcic 2009). Osmolarity of the media affects the cell size and shape changes caused by electroporation. The electroporation of cells in suspension results in an increase in cell diameter up to 30%, which corresponds to 100% of volume increase in isotonic medium, while the increase is significantly lower in hypertonic medium.

These studies motivated the foundation of this chapter: the introduction of a novel method to ablate the entire frozen region during cryosurgery, including the temperature zone of -40ºC to -0.56ºC of the frozen lesion outer rim. Electrical conductivity in ionic solutions is a function of temperature, exhibiting a positive correlation. Consequently, the electrical conductivity of frozen and cooled tissue is substantially lower than those at physiological temperatures. As a result of the temperature dependency of electrical parameters we hypothesized that applying pulsed electric fields through a cryoprobe during freezing and thawing will concentrate the entire electric field to the low temperature region. Additionally, we hypothesize that cells on the margin of the frozen lesion, which are unfrozen, unaffected by cryosurgery, at high subzero freezing temperatures and are hyperosmotic solutions, will experience electroporation induced cell death. As a consequence, the entire frozen lesion will contain cells ablated by the combined mechanisms of cryosurgery and electroporation, improving the accuracy of cryosurgical procedures. Furthermore, the extent of the frozen region can be monitored in real time by basic imaging modalities, such as ultrasound. Because the time scale of combined cryosurgery and electroporation (cryoIRE) is dominated by that of cryosurgery, the treatment can be controlled by physicians in real time.

The minimally invasive surgery, cryoIRE, was investigated utilizing a numerical mathematical analysis of temperature and electric fields produced by the application of pulsed electric fields during cryosurgery. The focus of this study is to examine the effect of changes in temperature and freezing on electric fields and the subsequent implications for ablating cryosurgery treated tissue with electroporation.

3.2 Methods

3.2.1 Theoretical Model

The models were generated using numerical analysis executed by Comsol Multiphysics (version 4.1). To extract the most salient biophysical aspects of the analysis, we investigate

simple one and two-dimensional configurations in Cartesian and cylindrical coordinates. Each case utilized a coupled thermal and electrical model to simultaneously determine temperature and potential distributions during cryoIRE, respectively. Two equations were solved simultaneously in Comsol. One was the Laplace equation for potential distribution associated with an electric pulse:

$$-\nabla \cdot d\left(\sigma\nabla - J^{e}\right) = dQ_{j} \tag{3.1}$$

where σ is electrical conductivity, V is voltage, J^e is external current density, d is thickness and Q_j is the current source. For all cases, the thickness was set to one.

Physiological saline was used as a first order simulation of biological tissue. The electrical conductivity for saline was derived analytically for subzero temperatures using composite theory and the thermodynamic phase diagram for saline. The equation for freezing point depression was used to calculate the volume of solution as a function of temperature. Data from J.J. Arps (Arps 1953) was curve fitted to calculate the electrical conductivity of the composite medium. The derived electrical conductivity for subzero temperatures was combined with experimental data for higher temperatures (Mazzoleni et al. 1986), resulting in the following piecewise function:

$$\sigma(T) = \begin{cases} \dfrac{4.556}{T-273.15} \times \exp\left(\dfrac{T-273.15}{4.99962}\right) - \dfrac{4.5559}{T-273.15} + 2.365e-8, T \le 272.59 \\ 0.03(T-273.15) + 0.7, T > 272.59 \end{cases} \tag{3.2}$$

Equation 3.2 describes the behavior of electrical conductivity in [S/m] as a function of temperature [K], both above and below freezing. The correlation coefficient of this equation relative to experimental data was tabulated to be *r=0.99989.*

In addition to electrical conductivity, electrical permittivity is also a function of temperature. The following equation (Kaatze 1989) was utilized to take into account the temperature dependence of electrical permittivity:

$$\varepsilon(T) = 10^{\left(1.94404 - 1.99\times10^{-3}(T-273.15)\right)}, \tag{3.3}$$

where ε is electrical permittivity and T is temperature. This equation is valid for low frequency permittivity, experienced by typical electroporation pulse parameters, which are in the range of 0.1-20E-3 seconds (Granot & Rubinsky 2007), (Ivorra & Rubinsky 2007).

The thermal models were generated using numerical analysis executed by COMSOL MULTIPHYSICS (version 4.0). The temperature distribution was obtained from the solution of a modified Pennes bioheat equation, which was solved simultaneously as the electrical potential equation. The general bioheat equation has the following form:

$$\nabla \cdot (k\nabla T) + \rho_b w_b c_b (T_a - T) + q''' = \rho c_p \frac{\partial T}{\partial t}, \qquad (3.4)$$

where k is thermal conductivity, T is temperature, w_b is blood perfusion, c_b is the heat capacity of blood, T_a is arterial temperature, ρ is the tissue density, c_p is the tissue heat capacity and $q''' = Q_{met} + Q_{ext}$. Where Q_{met} is the metabolic heat generation and $Q_{ext} = \sigma|\nabla\phi|^2$ is a term that accounts for Joule heating, where ϕ is electrical potential calculated from Equation 3.1 and σ is electrical conductivity of the tissue. In this study, it was assumed that there is blood flow and metabolism in the unfrozen tissue while the blood flow and metabolism in the frozen region was set to zero. The effect of Joule heating on the temperature distribution was considered in both the frozen and unfrozen tissues. The values for biological tissue utilized in the Pennes bioheat equation are listed in Table 3.1 (Davalos et al. 2004) and the thermal properties used are listed in Table 3.2.

Table 3.1. Temperature dependent properties used in the Pennes bioheat equation for the purpose of solving the temperature distribution due to the application of the cooling probe.

Thermal Conductivity	Blood Perfusion	Blood Heat Capacity	Metabolic Heat	Tissue Density	Tissue Heat Capacity
0.5 [W/mK]	0.5[kg/m^{3}s]	3640 [J/kgK]	33800[W/m^3]	1000 [kg/m^3]	3750 [J/kgK]

Table 3.2. Temperature dependent properties used in the heat conduction equation for the purpose of solving the temperature distribution due to the application of the cryosurgical probe.

	Density (ρ) [kg/m^3]	Specific Heat (C_p) [J/kg K]	Thermal Conductivity (k) [W/m K]	Reference
Frozen	918	2052	2.31	(Ingebritsen & Sanford 1998)
Unfrozen	997	4179	0.613	(Ingebritsen & Sanford 1998)

The enthalpy method was utilized to account for the effects of freezing and thawing during cryosurgery. The enthalpy method is a well established numerical analysis of the phase transition phenomenon and is outlined in (Voller & C. Prakash 1987). Additionally, the enthalpy method for phase change is both utilized, evaluated and validated in several finite element studies (Dantzig 1989), (Rubinsky & Cravalho 1981), (Srinivas & Ananthasuresh 2006), (Marin 2006), (Lamberg et al. 2004). A heat transfer with phase change model, without electrical parameters, was compared to benchmark problems of this kind and validated the approach and results of this chapter. The values utilized in the heat conduction equation for frozen and unfrozen regions are shown in Table 3.1. For consistency with the electric field analysis, properties for physiological saline solution were also used to model the thermal behavior of biological tissue. All three values for frozen media in Table 3.2 were defined at temperatures below freezing, when *T<272.59*. The models defined values for unfrozen media in Table 3.2 at temperatures above freezing, when *T>273.59*. The transition region between the frozen and unfrozen media was defined using a smoothed Heaviside function. Therefore, the Heaviside function represented a volume fraction of liquid in the frozen media. The term for specific heat was modified to account for latent heat of fusion in order to model the phase transition:

$$C_{\text{mod}} = \sum_i C_p + D\lambda \,, \tag{3.5}$$

where λ is the latent heat of fusion (333E3 J/kg (Ingebritsen & Sanford 1998)) and $D = \frac{dH}{dT_{trans}}$.
Where H is the Heaviside function and T_{trans} represents the phase transition temperature.

Studies on the effect of temperature on electroporation protocols have revealed a negative correlation between temperature and fields. The electric fields required for producing electroporation increase as temperature decreases. The goal of this study is to investigate the ultimate effects of temperature modulation on electroporation protocols, such as the fields necessary to induce reversible and irreversible electroporation. To accomplish this, data has been extracted from existing literature to produce a correlation between temperature and the fields at transition values between reversible and irreversible electroporation (Miklavcic et al. 2000). The equation used in this study was derived from the experimental data acquired in (Diaz-Rivera 2000) and is given by:

$$E(T) = \frac{-39}{3200}T + 63700.45 \,, \tag{3.6}$$

where T is temperature [˚C] and E is electric field [V/m]. This equation was used as an approximate correlation for this study. It was used primarily to demonstrate an accurate methodology, but a substantial amount of additional research is needed to generate precise

correlations, which currently have not yet been developed. It should be emphasized that we expect that the hyperosmolarity of the extracellular solution in the high subzero temperature range should reduce the field required for electroporation, (Kanduser & Miklavcic 2009). Therefore we anticipate that Equation 3.6 is an upper limit of the electric field required for electroporation at the conditions on the outer rim of the frozen lesion during cryosurgery.

3.3 Models

In this study we employ three geometries: a) Case 1, a one dimensional Cartesian geometry; b) Case 2, a one dimensional cylindrical geometry with a single cryoprobe; and c) Case 3, a two dimensional cylindrical geometry with two cryoprobes. In all cases the analysis is performed prior to freezing (control at physiological temperature, 310.15K), during freezing, and during thawing. In the freezing case a freezing temperature of 268.15K was applied to the cryoprobe. A temperature of 268.15K (-5°C), was implemented because in very conservative estimates cell survival occurs at temperatures above 258.15K in cryosurgery (K Tatsutani et al. 1996), (Rui et al. 1999), (Pham et al. 1999), (J. Smith & Fraser 1974). Therefore, this thermal condition represents the outer margin of a frozen cryosurgical lesion where cells survive freezing (K Tatsutani et al. 1996); which is a range of temperatures where phenomena related to the CryoIRE concept occur. This range enables a test of the conditions in which IRE can ablate cells on the margin of the frozen lesion where frozen cells survive. Furthermore, this is a subzero temperature at which electroporation was observed to occur (Kanduser & Miklavcic 2009), (Diaz-Rivera & Rubinsky 2006). The duration of freezing was 90 seconds, after which the cold surface is thermally insulated and natural thawing was induced by constant deep body physiological temperature. The duration of the analyzed thawing period was also 90 seconds. While these periods of time for freezing and thawing are short relative to conventional cryosurgery, they are relevant to the relatively high subfreezing range of temperatures which is the focus of this analysis. A voltage difference of 1V was used in the electric field analysis to facilitate a general normalized analysis of the electric fields.

3.3.1 Case 1.

The first study consists of a simple one dimensional 6cm slab of tissue (Davalos et al. 2004) between two parallel plates in Cartesian coordinates. This study is used to demonstrate the fundamental aspects of the cryoIRE concept. The schematic of this geometry is depicted in Figure 3.1. Two resistors in series, representing the frozen and unfrozen portions of the tissue, characterize the electrical configuration of this problem. This was done because at sub-MHz frequencies, such as in this electroporation analysis, capacitance can be neglected (Kotnik & Miklavcic 2000), (Yao et al. 2009). It was assumed that one plate is at constant deep body temperature and the other, the freezing (cryoprobe) plate, was set to 268.15K. The duration of freezing was 90 seconds, after which the cold surface is thermally insulated and natural thawing was induced by constant deep body physiological temperature. The duration of the analyzed thawing period was also 90 seconds. A voltage difference of 1V was imposed between the plates to facilitate a general normalized analysis of the electric fields.

An evenly distributed finite element mesh was incorporated into the model. The mesh size was varied in order to validate the accuracy of the solution. The mesh size was refined until the solution was no longer affected by the quality of the mesh. The mesh for Case 1 consisted of roughly 1500 elements.

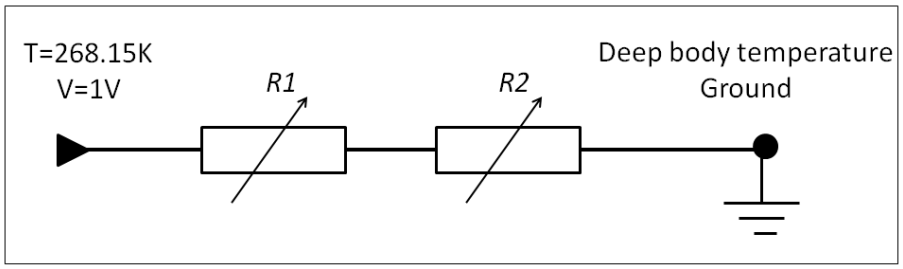

Figure 3.6. Electric current schematic for the one dimensional Case 1 in a slab-like geometry. Variable resistances *R1* and *R2* represent electric and thermal resistance (in the thermal and electrical equivalent circuits). Boundary conditions utilized in the model are specified at the nodes. The initial temperature was set to physiological temperature, 310.15K.

3.3.2 Case 2.

The second geometry included a typical cryoprobe 3.4mm in diameter (Edd et al. 2008), inserted into the center of an infinitely long cylinder of tissue, 6cm in radius. The outer edge of the cylinder was set to a constant deep body temperature and the temperature of the cryosurgical probe was set to 268.15K for 90 seconds of freezing. After freezing, the cryoprobe was modeled as thermally insulating to simulate tissue induced thawing for 90 seconds. The cryoprobe was modeled as thermally insulating when the flow of the cryogen is stopped because in a two dimensional configuration there is no axial heat flow and because typical cryoprobes are made of an insulated hollow thin walled tube, (Rubinsky et al. 1994) which gives them a negligible thermal mass relative to that of the frozen tissue and energy content in phase transition. The outer surface temperature of the tissue cylinder was maintained at a constant deep body temperature, which is what induces the thawing. A voltage difference of 1V was applied between the cryoprobe and the uniform outer edge of the tissue cylinder. This geometry models a cryosurgical procedure during which a cryoprobe is used in tissue and an IRE voltage difference is applied between the cryoprobe and a ground electrode at a distance.

The finite element mesh utilized for this case incorporated triangular elements, as shown in Figure 3.2a. The element size was smallest adjacent to the cryoprobe, and increased in size as it radiated towards the outer boundary. This was done in order to accurately capture the steep temperature gradient adjacent to the cryoprobe. The mesh was refined until the solution was no longer affected by mesh size. Approximately 3000 elements were utilized to cover a 113mm^2 surface area.

3.3.3 Case 3.

The third geometry was an infinite cylinder of tissue 6cm in radius represented in two dimensions. The outer margin of the cylinder was set to a constant deep body temperature and electrically insulated. In typical cryosurgical protocols, developed after the early 1980's when imaging monitored cryosurgery was introduced (J. Gilbert et al. 1984), the procedure was performed using several cryosurgical probes simultaneously inserted into the tissue (G Onik et al. 1991). In many applications of multiple probe cryosurgeries, the cryoprobes are operated sequentially after the insertion (Rubinsky & G Onik 1991). Analyzed here is a simulation of a possible cryoIRE treatment protocol. In this simulation, one 3.4mm cryoprobe was inserted into the center of the tissue and a second 3.4 mm cryoprobe was inserted 3cm away. Typical cryoprobes, which are made of metal, can be used as both cryosurgical probes when connected to the cryogen supply tank, and as electrodes when connected to a voltage supply. In this simulation, the first cryoprobe was set to 268.15K for 90 seconds of freezing. It was assumed that during this period the second cryosurgical probe is not thermally activated, and therefore can be considered thermally insulated as discussed in the Models Section. Following the 90 seconds of freezing, the first cryosurgical probe also ceased being thermally activated, and both cryosurgical probes became thermally insulating. This allowed the frozen tissue to thaw, which continued for 90 seconds. During both the freezing and thawing sequences described above, both cryoprobes were connected to the electroporation power generation system and a voltage difference of 1V was imposed between them to facilitate a general normalized analysis of the electric field.

The finite element mesh in case 3 utilized triangular elements, demonstrated by Figure 3.2b. The element size was smallest in the region surrounding both probes. This was done in order to accurately capture the temperature gradients adjacent to both of the probes. The mesh was refined until the solution was no longer affected by mesh size. Approximately 4000 elements were utilized to cover a 113mm^2 surface area.

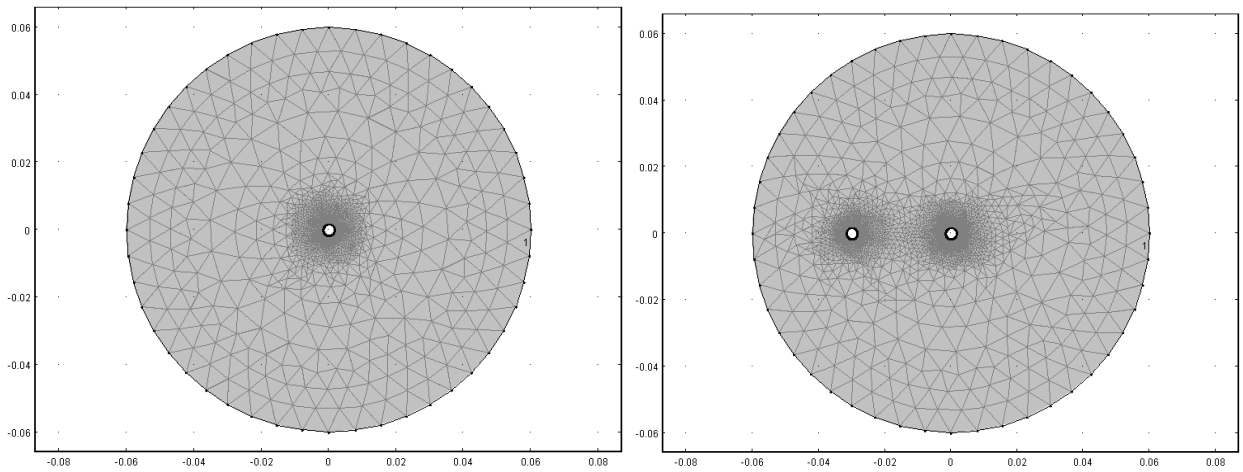

Figure 3.7: a) Mesh for Case 2 with one cryoprobe in the center of tissue cylinder. b) Mesh utilized for Case 3 in which two probes are utilized. Note that the mesh is extra fine in the vicinity of the probes in order to capture the changes in electric field and temperature that occur due to the effect of the probes.

3.4 Results and Discussion

3.4.1 Case 1.

The first case investigated was the most basic. It consisted of a 1D model with the boundary conditions previously specified. The electric circuit and analog thermal circuit are shown in Figure 3.1. While this model is simple, the purpose was to illustrate the fundamental aspects of cryoIRE.

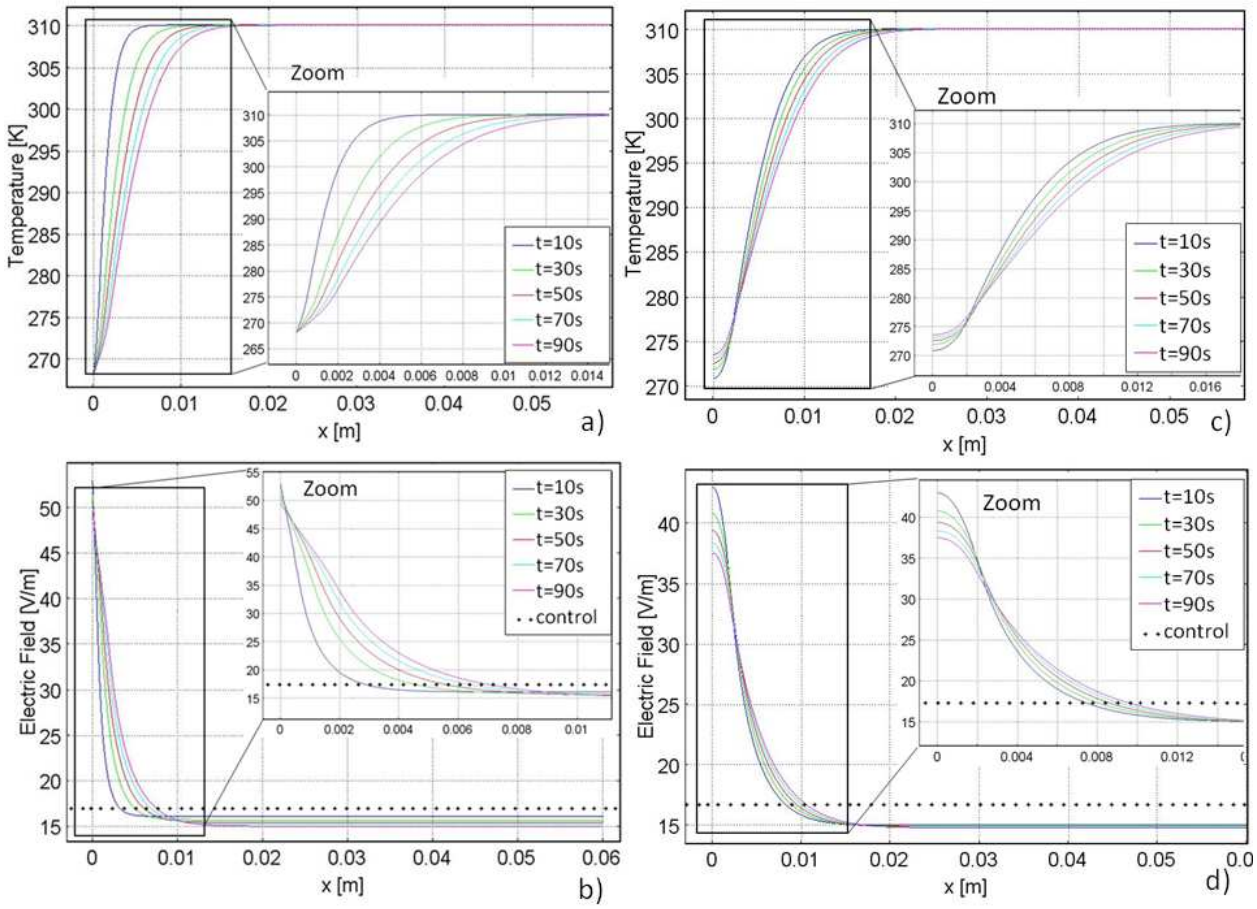

Figure 3.8. Graphs for Case 1. Left column: temperature and electric field distribution during 90 seconds of freezing. Right column: temperature and electric field distribution during 90 seconds of thawing. Each line represents a 20 second time increment. The dotted line shows the electric field in tissue held constant at body temperature for the same voltage boundary conditions.

3.4.1.1 Freezing

The temperature distribution during freezing is shown in Figure 3.3a. The temperature distribution is as expected, increasing from the low temperature at the cryoprobe surface to body temperature. As time progresses, the low temperatures penetrate further into the tissue due to thermal diffusion. Note that at 272.59K, the nonlinear behavior indicates the region of phase change. Figures 3.3a and 3.3b demonstrate the inversely proportional relationship between temperature and electrical conductivity, as described by Equation 3.3. Lower temperatures yield a lower ionic conductivity and subfreezing temperatures yield a dramatic decrease in electrical conductivity. As Figure 3.1 suggests, from continuity of ionic current, the electric field will be higher in the regions of lower electrical conductivity. Indeed, Figure 3.3 illustrates the most important feature of the cryoIRE combination; because of the increased electrical resistance in the frozen and cooled regions of tissue, the highest electric fields are confined to those regions. Figure 3.3b also shows that the fields beyond the frozen and cooled regions in the normal tissue

are substantially lower than those in the frozen/cooled regions. This suggests that the freezing/cooling has the effect of confining the high electric fields to those regions.

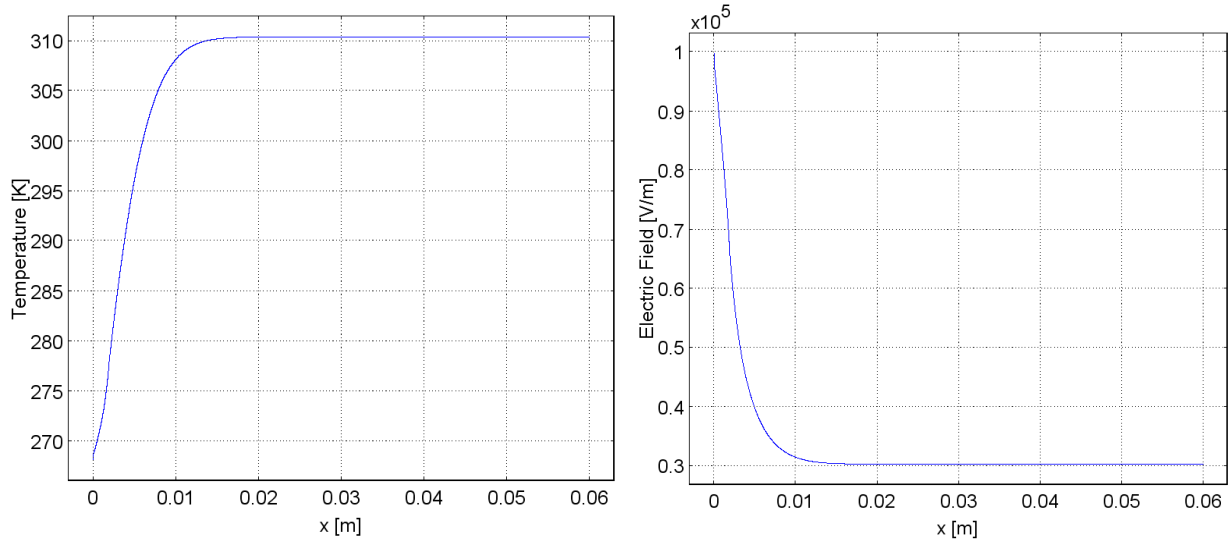

Figure 3.9: Left plot demonstrates the temperature distribution and right plot demonstrates the electric field distribution, both after 90 seconds of freezing with an applied voltage of 2000V for 90 pulses. The trends are similar to those seen in the 1V cases, however, the electric field reaches a maximum of 100000V/m and the temperature rises more quickly at the leftmost plate due to Joule heating.

The plots in Figure 3.3 were obtained for a normalized voltage of 1V. Combining Figures 3.3 and Equation 3.6 suggests that a voltage of about 2000V on the cryoprobe is sufficient to ablate the analyzed frozen tissue, by IRE. Such voltages are typical to those used for tissue ablation with irreversible electroporation. The result of applying 2000V after 90 seconds of freezing to the model in Figure 3.3 can be seen in Figure 3.4. As can be seen by this graph, the temperature distribution in the tissue is similar to that in Figure 3.3, where 1V was applied. However, the one difference is that temperature rises to a higher value over a shorter distance adjacent to the leftmost plate because Joule heating occurs at higher voltages. The electric field distribution in Figure 3.4 demonstrates the same trend as that of the 1V freezing model in Figure 3.3. However, the maximum electric field reached is now 100000V/m. This results in an electric field distribution above 67000V/m, the threshold for irreversible electroporation, in the frozen region.

It should be emphasized that in this study the range of subfreezing temperatures used are relatively high, above -5°C. In this temperature range cells survive freezing (K Tatsutani et al. 1996). Adding IRE during freezing will ablate the cells in the frozen region that survive freezing and thereby making the cryoIRE treatment produce tissue ablation to the edge of the frozen lesion. This also suggests that the cryoIRE technique may not require the cryogenic temperatures used in conventional cryosurgery and cryosurgical systems. Therefore, cooling systems using Joule Thomson, solid state thermoelectric systems or conventional refrigeration cycles may be

sufficient for tissue ablation with this method. Figure 3.3 and this analysis corroborate the initial hypothesis of this study: the effect of freezing and low temperatures on electrical conductivity can actually concentrate the electric field to the cooled/frozen region as well as amplify the electric field in that region, which would require substantial lower voltages on the cryoIRE probes than on conventional electroporation probes.

3.4.1.2 Thawing

Figures 3.3c and 3.3d illustrate the temperature distribution and the electric field during thawing. Figure 3.3c shows that adjacent to the cryoprobe, the temperature inches upwards, because no freezing temperature is applied by the probe during thawing. If thawing were extended beyond 90 seconds, the temperature graph would continue to equilibrate toward the phase transition temperature. The temperature distribution has a point of inversion, which appears to be stationary in time at about 0.2cm from the outer surface. This point of inversion corresponds to the position of the change of phase interface.

The temperature history during thawing of frozen media has a peculiarity caused by the effects of the phase transition, which has been studied extensively in the past (Rubinsky & Cravalho 1979). This effect appears in Figure 3.3c and is of significance to the use of electroporation during thawing. Previous studies have shown that during thawing of frozen lesions, the temperature of the frozen region increases first to the phase transition temperature, before the frozen tissue begins to thaw, and then remains at this value throughout the thawing process (Rubinsky & Cravalho 1979), (Hong & Rubinsky 1995). The explanation for this phenomenon, evident from Figure 3.3, is complex, has been previously discussed in heat transfer papers on cryosurgery, and is not directly relevant to this work.

Figure 3.3d shows that the relationship between temperature and electrical conductivity produces an electric field that also has a point of inversion around 0.2cm, which is the outer edge of the frozen lesion. Figure 3.3d shows that the electric field in the frozen region drops precipitously during thawing to a constant value of 32V/m (for the 1V potential on the cryoprobe). Figure 3.3d and Equation 3.6 suggest that applying an electric potential above 2000V is sufficient to cause irreversible electroporation in the thawing region, in this example. Such voltages are typical to those used for tissue ablation with irreversible electroporation. Figure 3.5 illustrates the temperature and electric field distributions when 2000V is applied after 90 seconds of thawing. The temperature distribution is similar to that seen in Figure 3.3c (when 1V is applied). However, the temperature rises to a higher value over a shorter distance when 2000V is applied due to Joule heating. The lowest temperature is at 275K in the 2000V case rather than 274K as in the 1V case. The electric field in the 2000V case has a similar distribution to the 1V case, except the highest electric field reached in this case is 75000V/m.

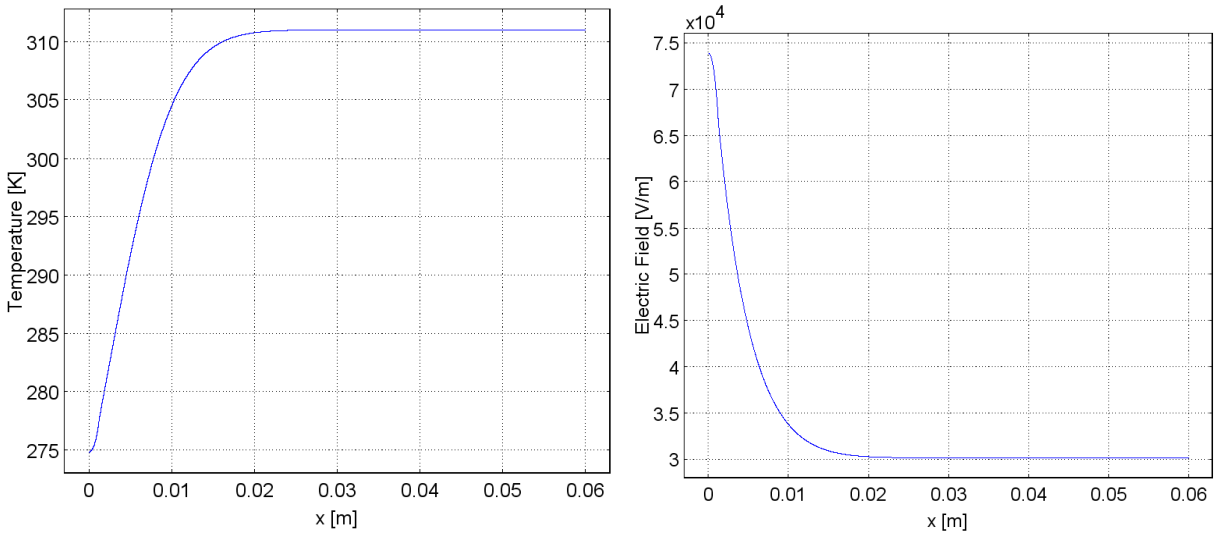

Figure 3.10: Left plot demonstrates the temperature distribution and right plot demonstrates the electric field distribution, both after 90 seconds of thawing with an applied voltage of 2000V for 90 pulses. The trends are similar to those seen in the 1V cases, however, the electric field reaches a maximum of 75000V/m and the temperature rises more quickly at the leftmost plate due to Joule heating.

It is apparent that if the temperature in the frozen region during thawing stays at the phase transition temperature, the electrical conductivity in the frozen region will remain constant throughout thawing and (in Cartesian coordinates) the electric field in the frozen region will remain constant as well. This suggests that if IRE is applied during thawing the fields will be confined and delivered in the frozen region across cells that are all at the highest possible subfreezing temperature. This could allow for precise design of the IRE electrical parameters to take values that affect only cells in the thawing frozen tissue at the phase transition temperature.

3.4.1.3 Control

It is pertinent that the electric field produced during freezing is compared to a control study. The control study applied the same electrical boundary conditions to tissue held at body temperature. This control study is represented by the dotted horizontal line in Figures 3.3b (freezing study) and 3.3d (thawing study). It is evident that the electric field in the frozen/cooled regions is substantially higher than the field produced in the control study in the same region in both freezing and thawing. However, at a distance from the frozen region, in the location of normal body temperatures, the fields are lower than those in the control. This suggests that it should be possible to design cryoIRE protocols in which the IRE induced cell damage is confined to the frozen/cooled regions and the damage does not extend beyond the cooled regions.

CryoIRE protocols can also be designed to induce cell damage via reversible electroporation for the purpose of gene therapy and drug delivery. For example, Figure 3.3b shows that the field produced by 1V potential difference at the cryosurgical probe ranges from

about 50V/m to about 40V/m between the -5°C and +5°C isotherms. If an attempt were made to combine cryosurgery with electrochemotherapy, the fields required for reversible electroporation in the liver are about 36,000 V/m (Miklavcic et al. 2000). Therefore a pulse of about 700V will produce reversible electroporation in the region from -5°C to +5°C. However, Figure 3.3b shows that the same pulse will produce a field of approximately 10,000V/m in the body temperature region, which should have no effect on the tissue in that location. In contrast, in the control case (at constant body temperature), Figure 3.3b shows that a pulse of about 1800V would be needed to produce the fields required for electrochemotherapy and the fields would affect the entire region between the electrodes.

3.4.2 Case 2.

The purpose of this second study was to examine a more realistic cryosurgical configuration. In Case 2 the geometry consists of a single cryoprobe in a cylindrical section of tissue 6cm in radius. Geometric details and boundary conditions were previously mentioned in the Models section.

3.4.2.1 Freezing

Figure 3.6a illustrates the temperature distribution at a transection along the diameter. Note that in Figure 3.6a the gap in the plot is the location of the cryoprobe. As in the 1D Cartesian case, due to thermal diffusion, freezing temperatures penetrate further into the tissue with time. And again, nonlinear behavior at 272.59K indicates the region of phase change.

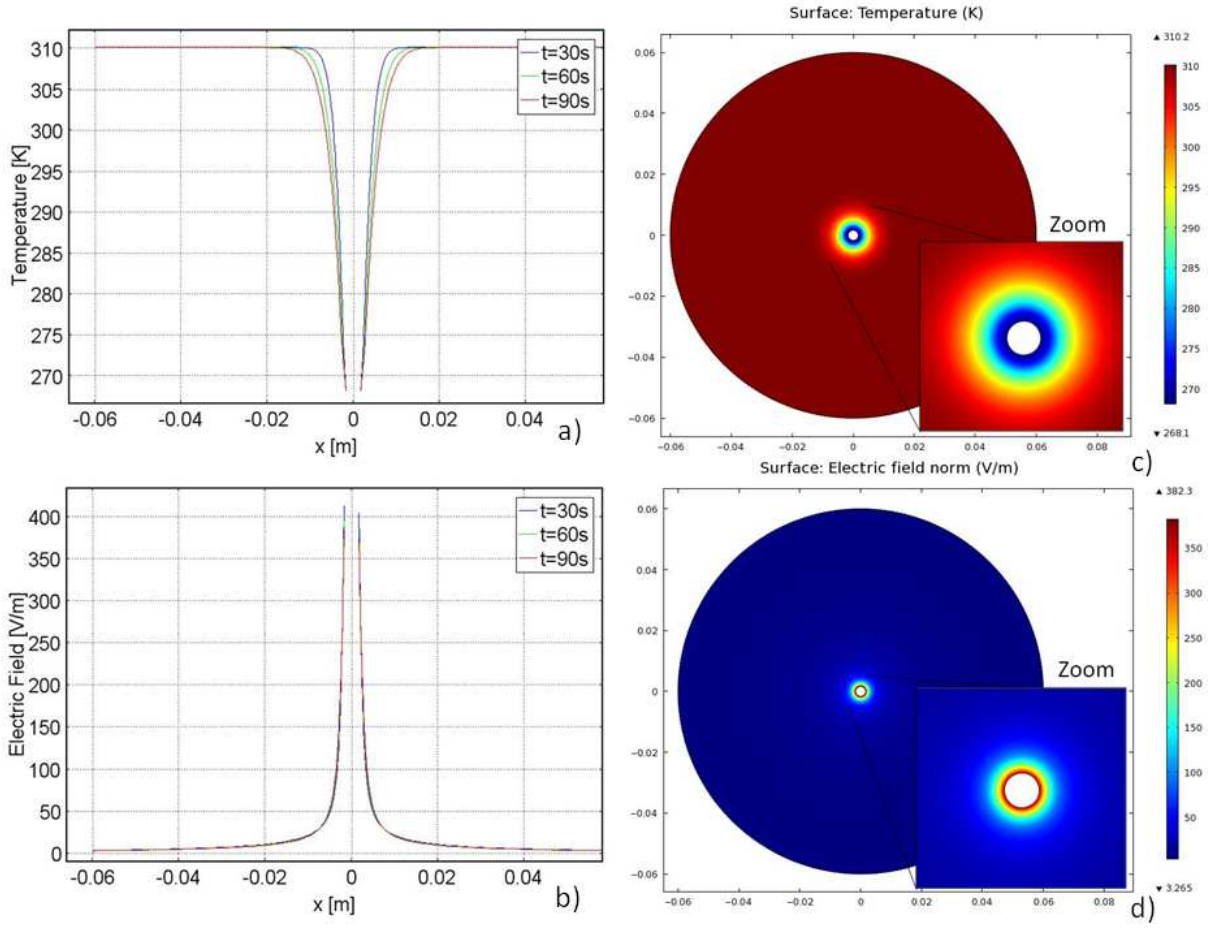

Figure 3.11. Data for Case 2. Temperature and electric field distribution during 90 seconds of freezing. Left column: graph, right column: surface plot.

The relationship between temperature and electric field is discernable from Figures 3.6a and 3.6b. As in the 1D Cartesian study, temperature and electric field are inversely proportional due to the dependence of electrical conductivity on temperature. For this reason, the electric field is highest in the frozen and cooled regions. This result corroborates both the hypothesis of this chapter and the results in the 1D Cartesian study. Because of decreased electrical conductivity in the frozen and cooled tissue, the highest electric fields are confined to those regions. Figure 3.6b shows that the fields beyond the frozen and cooled regions are orders of magnitude lower than those in the frozen/cooled regions. This suggests that freezing/cooling temperatures have the effect of magnifying the high electric fields in those regions. The effect of low temperature on confining the electric field is effectively demonstrated in Figures 3.6c and 3.6d. The zoom panel demonstrates that the electric field is confined within the cooled region, which again validates the original hypothesis of this study. Figure 3.6 shows that the electric field in the frozen region is higher than about 150V/m for a voltage of 1V on the cryoprobe. Equation 3.6 suggests that a voltage of about 400V imposed on the cryosurgical probe is sufficient to ablate the cells with IRE in the analyzed frozen region. A graph of the electric field and temperature distributions

with 400V applied after 90 seconds of freezing can be seen in Figure 3.7. When 400V are applied, the temperature rises to a higher value over a shorter distance than when 1V was applied (Figure 3.6a) due to the effect of Joule heating. The electric field with 400V applied demonstrates the same trend as the case with 1V applied, but reaches a maximum of 160000V/m rather than the peak of 400V/m seen in the 1V case.

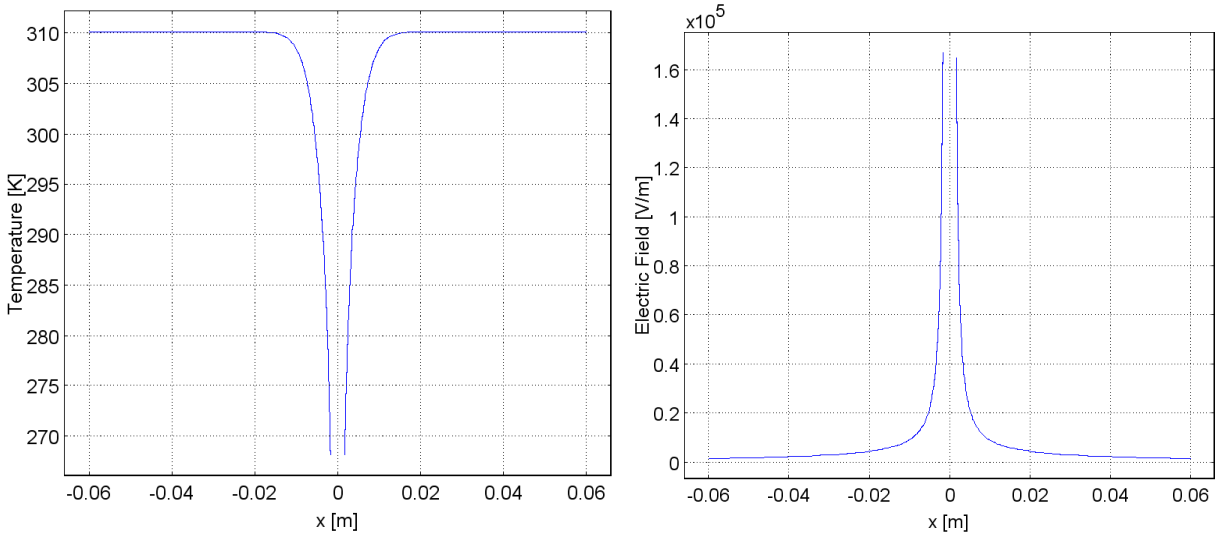

Figure 3.12: Left plot demonstrates the temperature distribution and right plot demonstrates the electric field distribution, both after 90 seconds of freezing with an applied voltage of 400V for 90 pulses. The trends are similar to those seen in the 1V cases, however, the electric field reaches a maximum of 160000V/m.

3.4.2.2 Thawing

Figures 3.8a and 3.8b illustrate the temperature distribution and the electric field during thawing. The temperature distribution during thawing with 1D cylindrical symmetry behaves very similarly to the previously discussed temperature distribution in the 1D Cartesian case. Figure 3.8a shows that temperatures adjacent to the cryoprobe inch upwards as a result of its insulated boundary conditions. The temperature distribution has a stationary point of inversion at 0.6cm. Figure 3.8b shows that the electric field also has a point of inversion around 0.6cm. Figure 3.5b also demonstrates that the electric field in the frozen/cooled region during thawing drops dramatically, effectively confining the field. Because of the transient nature of the temperature distribution, the electric field also changes with time. For instance, 30 seconds into thawing the highest electric field near the cryoprobe has dropped from 400 V/m at the end of freezing to 300V/m.

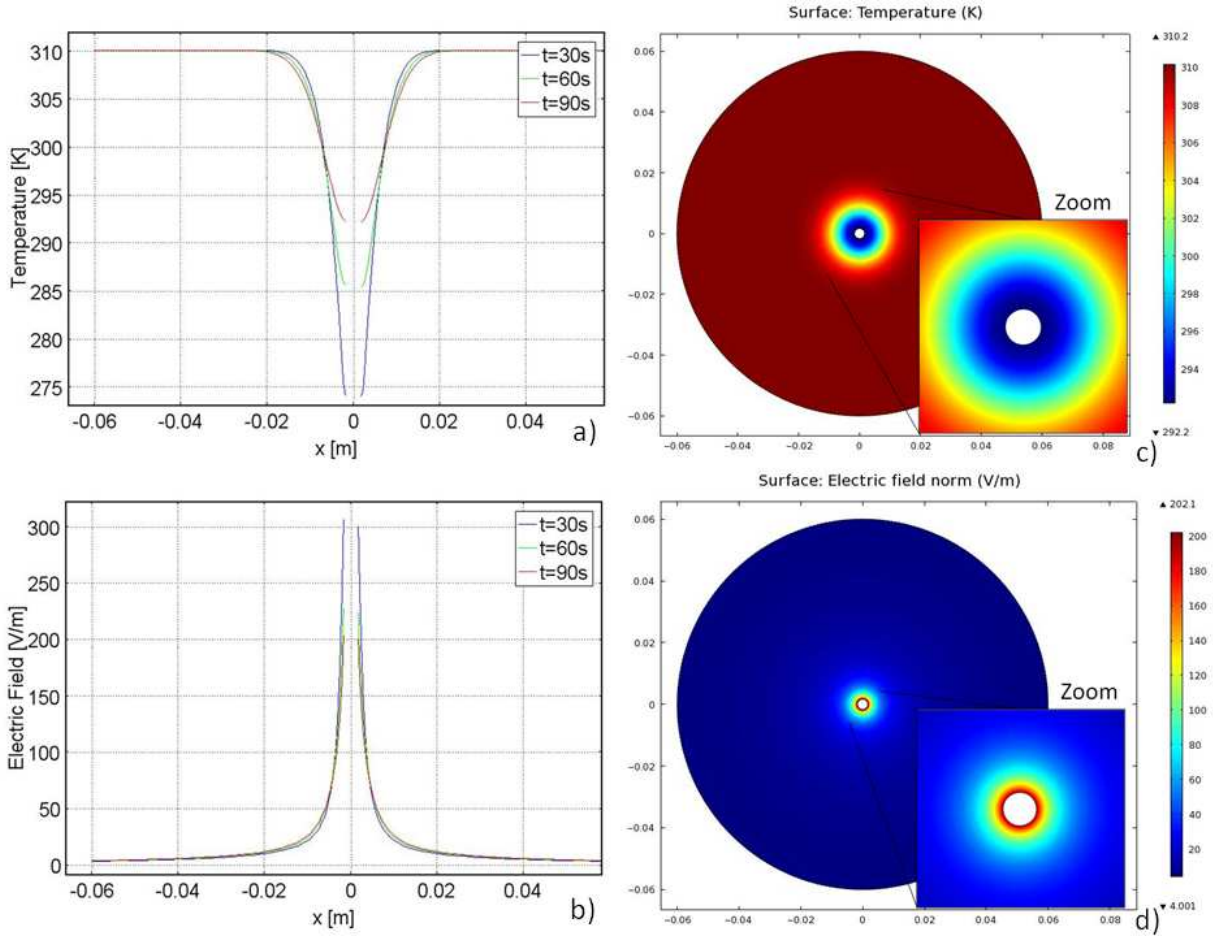

Figure 3.13. Data for Case 2. Temperature and electric field distribution during 90 seconds of thawing. Left column: graph, right column: surface plot.

The location of the highest electric field is the same point in space and time as the lowest temperature, which is consistent with Equation 3.2. Additionally, the electric field decreases in time as thawing progresses and temperatures rise throughout the domain. The slope of the electric field also follows that of the temperature. The slope of the electric field is steepest at the onset of thawing, when temperatures are lowest. But as thawing progresses, and temperatures begin to rise, the slope of the electric field lessens. This indicates the strong relationship between electric field and temperature in the cryoIRE procedure and the ability of freezing/cold temperatures to confine the electric field. This observation is most evident from Figures 3.8c and 3.8d, which depict surface plots of the temperature and electric field distribution, respectively, during the thawing stage of the cryoIRE procedure. The zoom panels clearly illustrate that the electric field is confined inside the lower temperature regions during thawing. Figure 3.8 also suggests that here also, similarly to the Cartesian one dimensional case, the field produced by 1V potential at the cryoIRE probe in the thawing frozen lesion will be higher than about 75V/m. Therefore, Equation 3.6 suggests that a voltage of about 850V on the cryoIRE probe will be sufficient to ablate with IRE, the frozen cells during thawing. Figure 3.9 illustrates the electric field and temperature distributions after 90 seconds of thawing with an applied voltage of 850V.

Due to the higher voltage, Joule heating affects the temperature distribution. In the case of 850V, the lowest temperature in the domain is 301K, whereas with an applied voltage of 1V the lowest temperature is 293K. The electric field achieved due to 850V is also much higher, it reaches a peak of 140000V/m, whereas the peak in the 1V case is 300V/m.

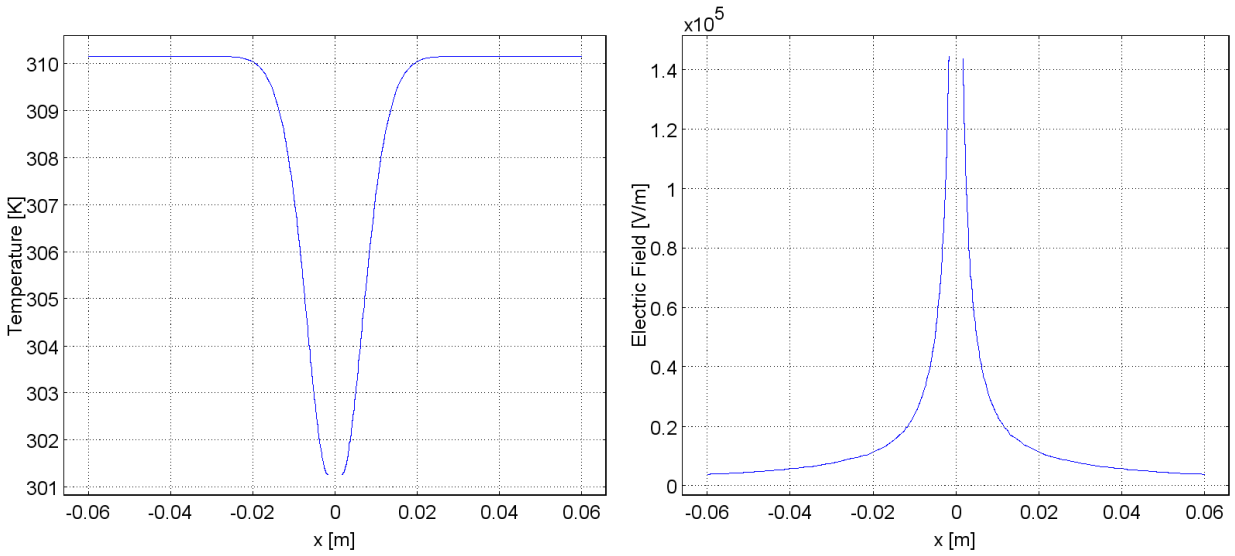

Figure 3.14: Left plot demonstrates the temperature distribution and right plot demonstrates the electric field distribution, both after 90 seconds of thawing with an applied voltage of 400V for 90 pulses. The trends are similar to those seen in the 1V cases, however, the electric field reaches a maximum of 140000V/m and the temperature rises higher on the probe due to Joule heating.

3.4.2.3 Control

The significance of the findings in Figures 3.6 and 3.8 is emphasized by a comparison to the control study. The control study applies the same electrical conditions on the cryoprobe as freezing and thawing, but holds the probe and tissue at constant body temperature. The control case represents conventional IRE delivered by a monopolar probe, which in this case is the cryoprobe. The comparison of the resulting electric fields can be seen in Figure 3.10. It is clear that the electric field in the frozen/cooled regions during freezing (Figure 3.10b) and thawing (Figure 3.10c) are substantially higher than the field produced in the control study in the same region (Figure 3.10a). The magnitudes of the peak electric field in the freezing and thawing cases are more than double the magnitude of the peak electric field in the control case. However, at a distance from the frozen/cooled tissue, in the region of normal body temperatures, the fields during freezing and thawing are lower than those in the control. This indicates that not only do freezing/cold temperatures amplify the electric field; they also exhibit an effect of targeting the electric field to the cold region. In fact, once the electric field has decayed and reached a constant value, it is zero in the cryoIRE case, and above zero in the control IRE case.

Figures 3.10a, 3.10b and 3.10c show that the highest electric field occurs, in descending order: freezing, thawing and control. Figures 3.10a, 3.10b and 3.10c also illustrate the ability of cold/freezing temperatures to concentrate the electric field because the most narrowly spread electric field occurs in the freezing case, followed by thawing and then control. This Figure most clearly demonstrates the ability of freezing/cold temperatures to both amplify and direct the electric fields of IRE.

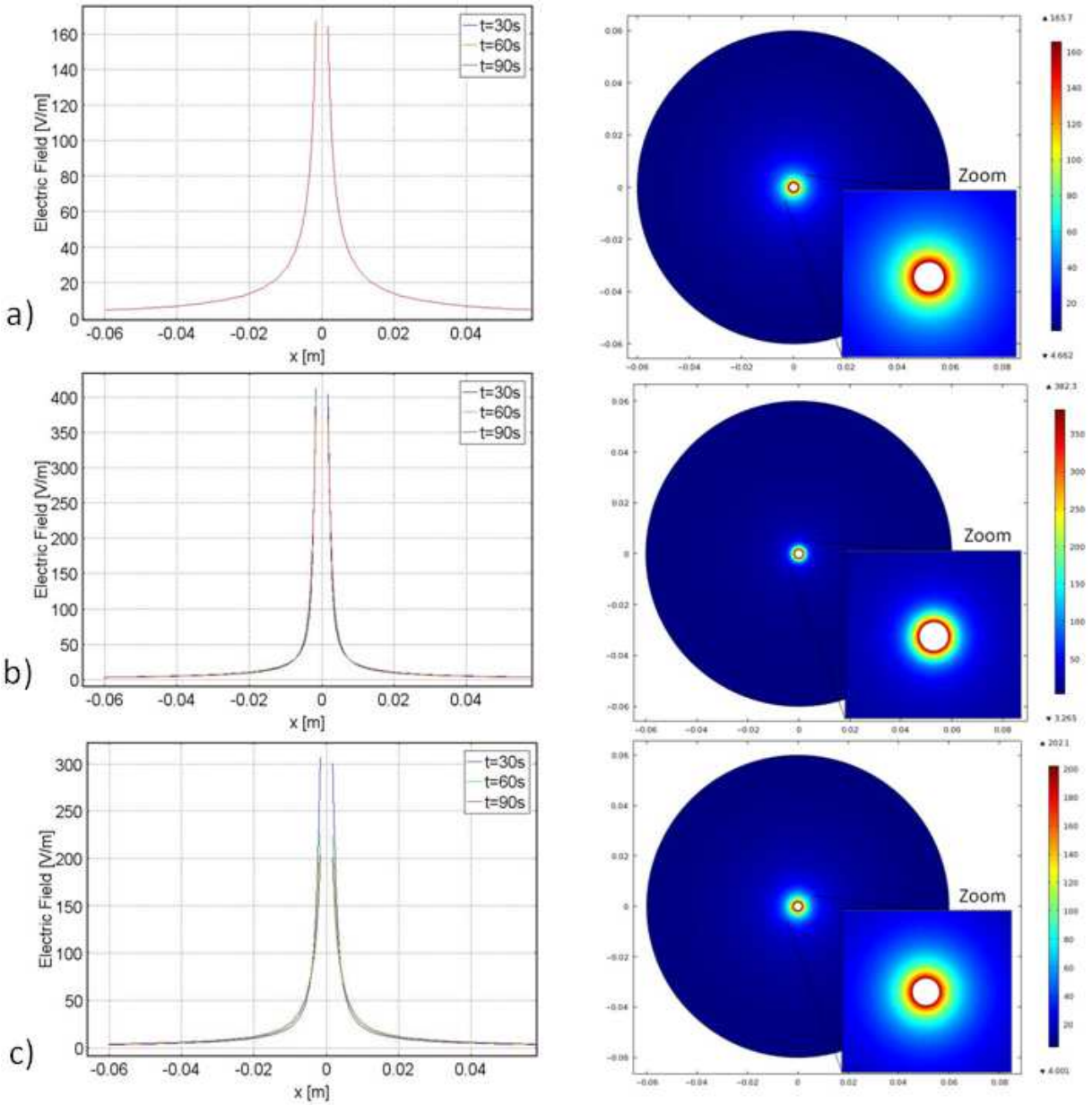

Figure 3.15. Electric field distribution for Case 2. From top to bottom row: control, freezing and thawing. Aligned for the purpose of comparison.

These results suggest that it will be possible to design a cryoIRE treatment in which the IRE induced cell damage is confined to the frozen/cooled regions and the damage does not extend beyond these regions. The possibility of designing electrical parameters which concentrate the electric field in the frozen/cooled region suggests that utilizing cryosurgical imaging techniques could possibly image cells ablated due to IRE. Ultrasound is capable of differentiating between frozen and unfrozen media during cryosurgical procedures (J. Gilbert et al. 1985). Therefore, by concentrating the electric field to the frozen tissue, imaging frozen tissue with ultrasound will also show cells ablated by IRE in real time during the procedure. This first order theoretical result indicates the potential feasibility of this technology. As in Case 1, most temperatures in Case 2 are above -5°C. This suggests that the cryoIRE technique may not require temperatures as low as those utilized in conventional cryosurgery.

Several additional advantages of the cryoIRE procedure can be theorized as a result of these two studies. Because cells survive these high subzero freezing temperatures, cryoIRE would retain electroporations ability to selectively ablate only cellular membranes without affecting the extracellular matrix. Furthermore, the cold induced electric field targeting effect may produce an additional advantage related to a major problem in IRE: electric field induced muscle contractions. The electric field in Figure 3.6a has spread beyond the area in which it is effective for electroporation, while in Figure 3.10b and 3.10c it has not. Therefore, the targeting effect during cryoIRE holds the potential to reduce electric field induced contractions beyond the treated area.

The field enhancement in regions of lower conductivity is explained by the potential-divider circuit in Figure 3.1. This is because the electric field vector is normal to the boundary of the two regions of different conductivity. If the electric field is parallel to this boundary, then the equivalent circuit will be two resistors in parallel, rather than in series, and there will be negligible field enhancement or possible field decrease, depending on the relative electrical conductivity of the tissues. The particular configuration developed in this study is a direct consequence of the fact that the cryoprobes serve both as the heat sink and as the electric source. Obviously, the configurations used in this study were chosen to accomplish this effect.

3.4.3 Case 3.

The purpose of this third analysis was to model a scenario in which the electroporation potential is applied between two cryosurgical probes, in which one serves as a cryoIRE probe and the other as the ground IRE electrode. This ground electrode was placed 3cm from the center cryoprobe with boundary conditions as specified in the Models section.

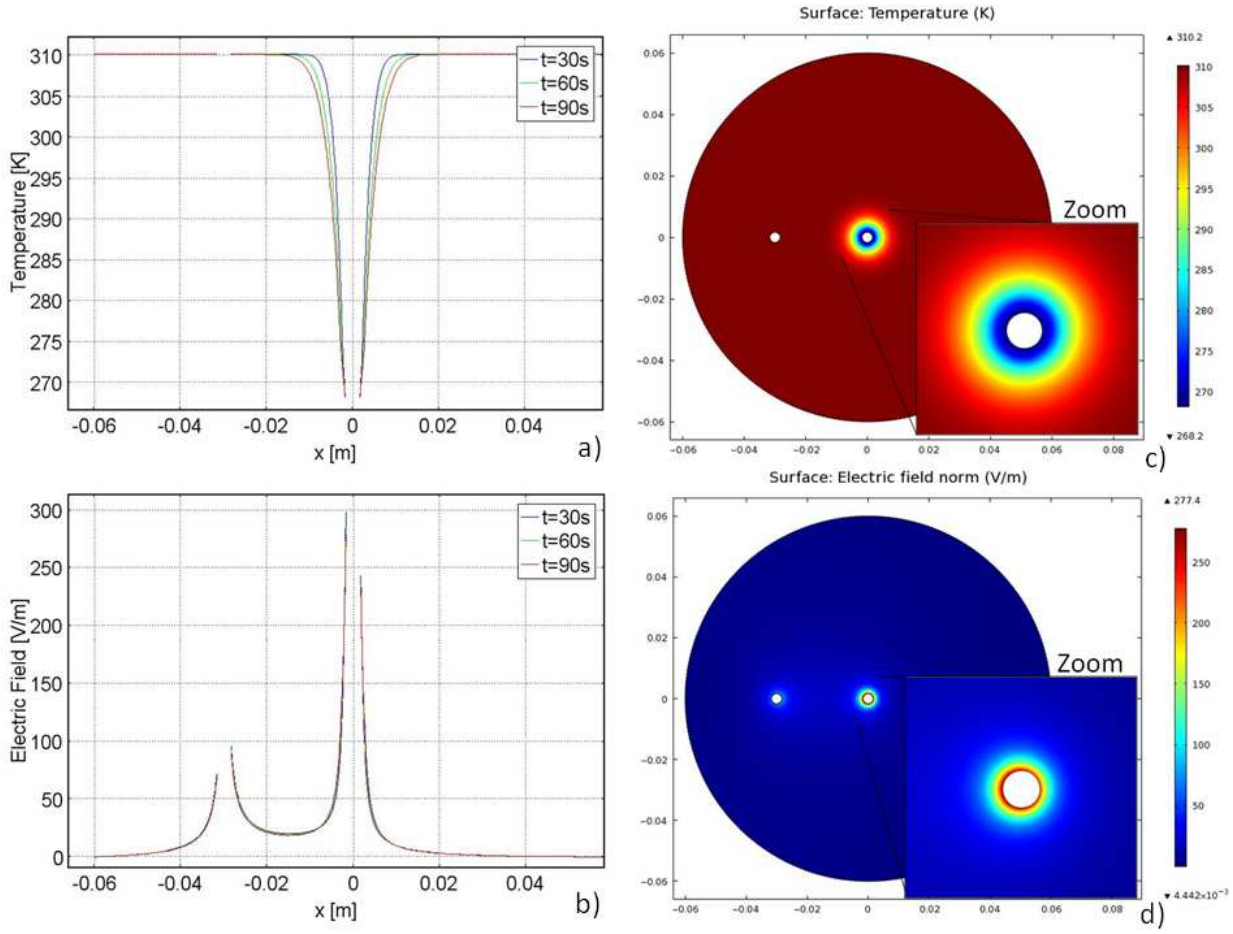

Figure 3.16. Data for Case 3. Temperature and electric field distribution during 90 seconds of freezing. Left column: graph, right column: surface plot.

3.4.3.1 Freezing

Figures 3.11a and 3.11c illustrate the temperature distribution which, as expected, is identical to Case 2. The electric field is plotted in Figures 3.11b and 3.11d. The two peaks in electric field occur adjacent to each probe. The most notable aspect of Figure 3.11b is the asymmetry between these two peaks. It is shown later that in the case of the control study (Figure 3.14a) the two peaks have identical magnitudes. Therefore, the asymmetry of the electric field peaks in the freezing case can be attributed to the freezing temperature applied to the rightmost probe. In this case, the application of freezing temperatures results in an electric field tripled in magnitude when only 1V is applied. Figure 3.11d clearly demonstrates how the freezing/cooling concentrates the electric field to the thermally treated area. The electric field in the frozen region of the tissue is higher than 150V/m for a 1V potential on the cryoIRE probe. This field is higher than the electric field around the unfrozen probe. Therefore, according to Equation 3.6, if a potential of about 400V is set on the cryoIRE probe, only the cells in the frozen lesion will be ablated by IRE. It should be re-emphasized that under the freezing conditions studied here, the cells in the frozen lesion would have survived freezing. In Figure 3.12, the temperature and

electric field distribution due to an applied voltage of 400V after 90 seconds of freezing are depicted. It is clear that the higher voltage results in higher temperatures on the leftmost probe due to Joule heating, as well as higher electric fields throughout the domain.

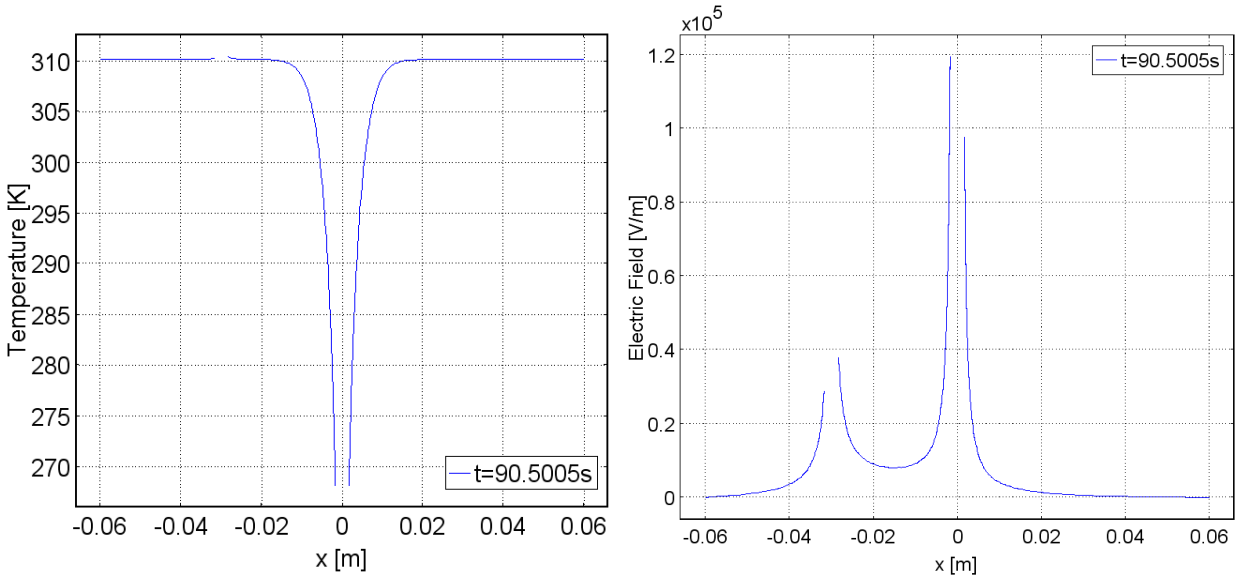

Figure 3.17: Left plot demonstrates the temperature distribution and right plot demonstrates the electric field distribution, both after 90 seconds of freezing with an applied voltage of 400V for 90 pulses. The trends are similar to those seen in the 1V cases, however, the electric field reaches a maximum of 120000V/m and the temperature rises higher on the probe due to Joule heating.

3.4.3.2 Thawing

The second half of this case investigated thawing. Figures 3.13a and 3.13c plot the temperature during thawing. The temperature distribution during thawing is also similar to that of Case 2. The temperature distribution has a stationary point of inversion at 0.6cm. Figure 3.13b shows that the electric field also has a point of inversion around 0.6cm, after which it drops dramatically to a constant value. The elevated temperatures in the frozen region during thawing have an effect on the electric field. As a result of higher temperatures experienced during thawing, an electric field lower than in the freezing case results. On both sides adjacent to the cryoprobe the electric field is lower in the thawing case than in the freezing case. After 90 seconds of thawing the peak electric field is 140V/m, while after 90 seconds of freezing the peak electric field was 275V/m. This significant decrease in resulting electric field was expected from Equation 3.9. Figure 3.13d is similar to Figure 3.11d and clearly shows how the freezing/cooling amplifies the electric field in the thermally treated area. However, during thawing in this configuration, the electric fields in the thawing frozen region around the cryoIRE probe become comparable to those around the ground IRE probe, and irreversible electroporation pulses applied in this case may affect both the frozen and the unfrozen region. Therefore, care needs to be exercised in designing optimal cryoIRE protocols.

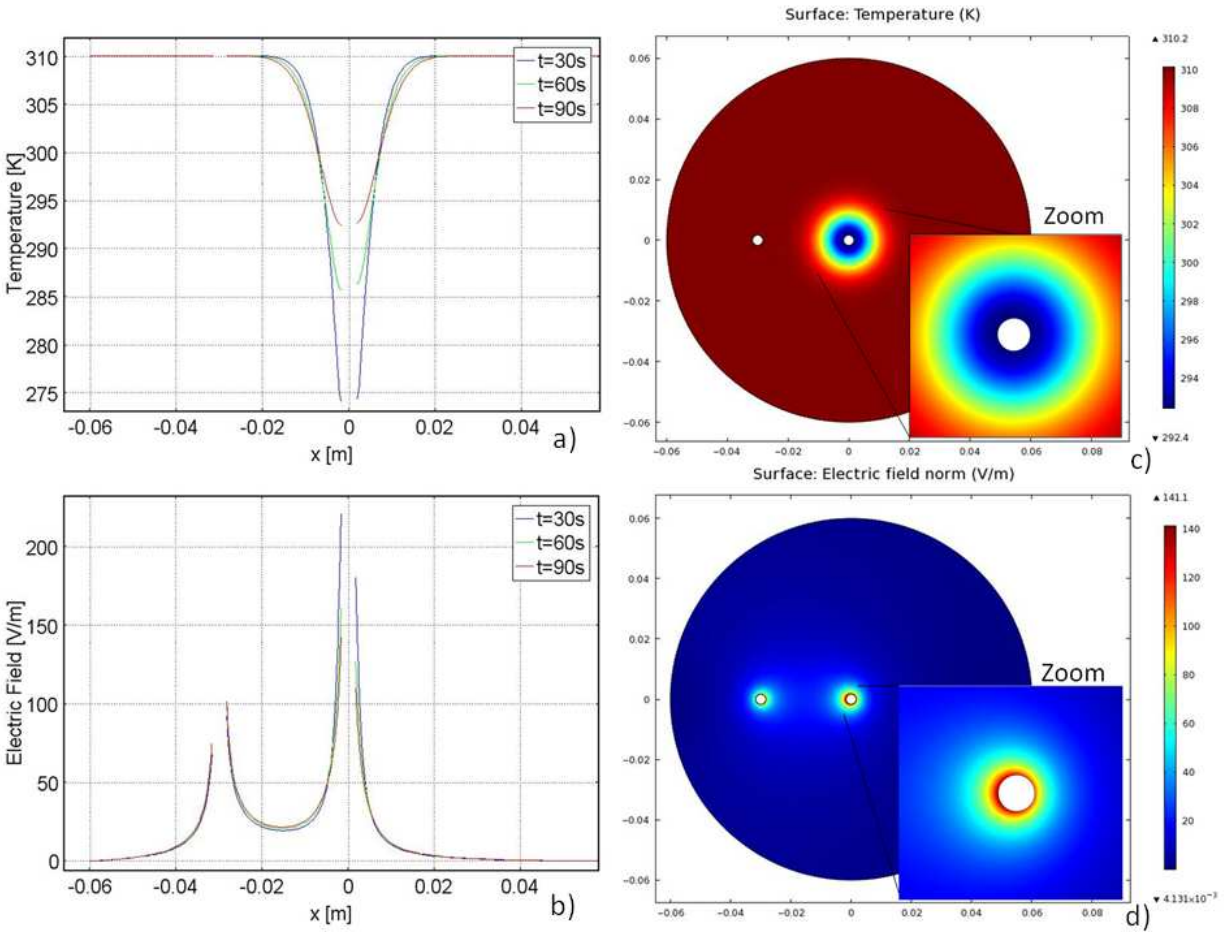

Figure 3.18. Data for Case 3. Temperature and electric field distribution during 90 seconds of thawing. Left column: graph, right column: surface plot.

3.4.3.3 Control

It is especially interesting to compare the electric field during freezing and thawing to those of the control (Figure 3.14). In the control, a conventional electroporation procedure was simulated, in which the electric pulse was delivered between two electrodes (probes in this case), while the temperature of the tissue and the probes were kept constant at body temperature. In the control case, (Figure 3.14a) the electric field around both probes is identical, as expected. In the case of thawing (Figure 3.14c), the electric field is higher at the freezing probe than at the leftmost probe. And in the case of freezing (Figure 3.14b), the electric field rises further on the freezing probe and decreases more on the leftmost probe. This is indicative of several facts. First of all, the drastic increase in electric field on the rightmost probe during freezing in comparison to the control study indicates that in this case, as well as Cases 1 and 2, the electric field is amplified in the frozen/cooled region. Second, the fact that the electric field is higher in the control than in the freezing case on the leftmost probe (the one without freezing applied)

indicates that not only does the freezing temperature concentrate the electric field; it decreases the electric field elsewhere in the domain. This could be beneficial during treatment because it could protect surrounding structures.

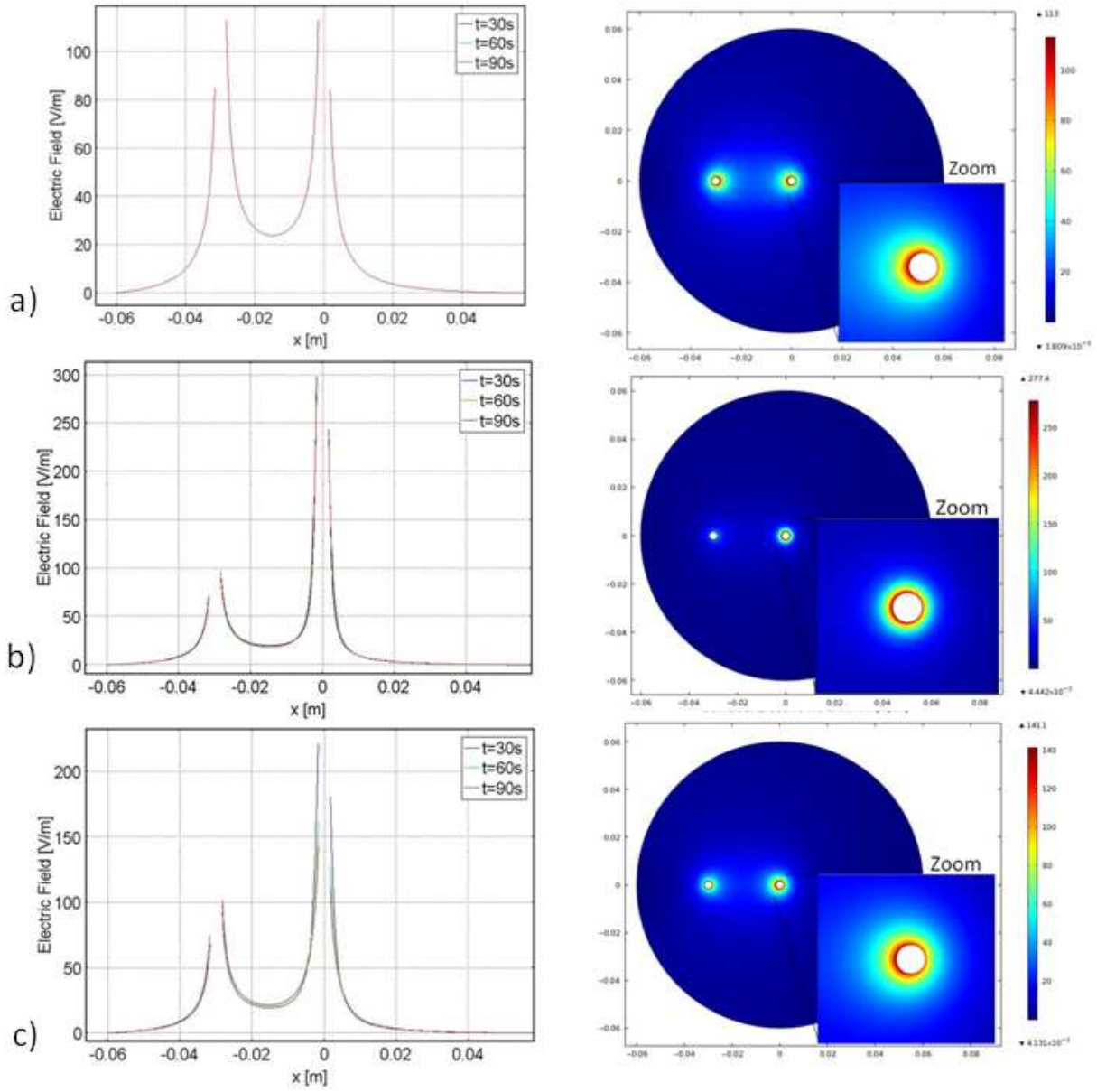

Figure 3.19. Electric field distribution for Case 3. From top to bottom row: control, freezing and thawing. Aligned for the purpose of comparison.

During the last three decades, cryosurgery has become widely accepted as a minimally invasive surgical technique and is currently used to ablate undesirable tissues in a large number

of clinical applications, such as treatment of cancer and arrhythmias. This suggests that the new concept of cryosurgery enhanced by IRE could be more readily accepted among practitioners of cryosurgery. Cryosurgical probes and apparatuses can easily be modified for a cryoIRE application. The shaft of any cryoprobe is metal and electrically conductive, and therefore could also be used as an electrode. In fact, many cryosurgical probes also have an electrical conduit through the shaft, housing a thermocouple for the purpose of measuring temperatures at the tip of the cryoprobe. This could be one possible path for the electric pulses. Another possible path could be through direct connection to the metal shaft. To deliver the electric pulse only at the thermally active tip of the cryoprobe, it would be sufficient to apply a thin layer of electric insulation along the cryoprobe shaft, as in typical electroporation needles (G Onik et al. 2007),(Rubinsky et al. 2007). The pulsed electric field power supply can either be stand alone, or incorporated in the cryosurgery console and connected to the electrically conductive cryoprobe shaft.

There are several ways in which the electric fields could be delivered during cryosurgery. Currently, typical IRE devices operate only between two electrodes at a time, even when multiple electrodes are inserted in the tissue (Rubinsky 2010). Therefore, in a first application modality, one thermally active cryoprobe would be connected to one pole of the power supply. The second pole (or ground) could be connected either to a second cryoprobe inserted into the tissue or at a distance; for instance, on the leg, like during radio frequency ablation. The combined cryoIRE effect takes place primarily in regions of tissue in which there is freezing and thawing. Therefore, we anticipate that in typical procedures, the electric fields will be delivered at the onset of freezing and during freezing and thawing. To take advantage of the ability of medical imaging to detect the extent of freezing, we anticipate that real time imaging with ultrasound or CT will be employed during the cryoIRE procedure and in this way ensure that the electric fields are delivered only in the desired cooled area, with real time control over delivery. In this study we have shown only a few of the possible combinations in which this procedure could be used. It is quite obvious that multiple combinations of cryoprobes or different combinations of cold and heat are possible as a way to increase or reduce the magnitude of the electric fields in desired regions of tissue.

3.5 Conclusion

The goal of this study was to evaluate the feasibility and the characteristics of a minimally invasive surgical procedure in which cryosurgery was modulated with electroporation, in the hope that this will improve the effectiveness of cryosurgery and eliminate the problems related to cell survival on the outer rim of frozen tissue. One and two dimensional models demonstrated that low and freezing temperatures have a substantial effect on IRE produced electric fields. Furthermore, unanticipated information about the effects of subzero temperature on IRE was also discovered. This investigation has made clear that both low and subzero temperatures are capable of concentrating the electric field because of the temperature dependence of electrical conductivity. Additionally, this study has demonstrated the ability of low temperatures to increase the magnitude of the electric field.

These results have far reaching implications in terms of imaging strategy and procedural methodology regarding accuracy of treating tissue with cryosurgery. Utilizing cryoIRE may potentially allow ultrasound to image real time cell death, a previously unachieved endeavor, and in turn increase surgical accuracy. A further inadvertent consequence of targeted electric fields may be the elimination of muscle contractions during surgery due to the substantial reduction in electric field outside the cryoIRE treated zone.

Although this is a first order theoretical analysis and additional theoretical and experimental research is needed to further develop this new concept, these primary results act as a promising foundation for future work. For these reasons, this numerical study has indicated the undeveloped potential and the motivation for pursuing cryoIRE.

Chapter 4: Temperature Modulation of Irreversible Electroporation in Biological Matter

4.1 Introduction

The current direction of surgical technologies is toward a minimally and non-invasive strategy. In comparison to traditional surgery, minimally and non-invasive surgeries are positioned to transform the field of medicine with shorter hospital stays, reduced surgical trauma, improved immune response and greater precision (Fuch 2002). These benefits are primarily due to less intrusive procedures and exceptionally targeted tissue treatment.

Electroporation is becoming commonly used in minimally invasive and non-invasive surgery. Electroporation technologies utilize electric fields which target the cellular membrane, increasing membrane permeability through the formation of nanoscale defects. The electric fields are usually delivered through electrodes in contact with the tissue. Typical electroporation parameters currently used in medicine and biotechnology employ 0.1 to 1E7V/m electric fields, nanosecond to millisecond pulse lengths and one to several hundred pulses. They can be AC or DC. Electroporation can have two different effects on the cellular membrane as a function of the electrical parameters: reversible and irreversible electroporation. Reversible electroporation causes the transient permeabilization of the cell membrane. Reversible electroporation is used in genetic engineering for the introduction of genes into targeted cells (Neumann et al. 1982), (M Jaroszeski et al. 1999), (Somiari et al. 2000). It is also used for tissue ablation in electrochemotherapy, which introduces drugs such as bleomycin into electroporated cells (Okino & Mohri 1987), (Mir et al. 1991), (Mir et al. 1998). In irreversible electroporation (IRE), the effect of membrane permeabilization leads to cell death. In the past, it was thought that IRE was produced by microsecond to millisecond pulses only. However, it was recently found that nanosecond pulses also produce IRE when used with appropriate electric field strength (RP Joshi & K. Schoenbach 2002), (Vernier et al. 2008). During the last four decades, IRE was used primarily in the food industry for sterilization of micro-organisms (AJ Sale & WA Hamilton 1968), (WA Hamilton & AJH Sale 1967). Recently, IRE has emerged as an important minimally invasive technique for tissue ablation, because of its molecular selectivity (Edd et al. 2006),(Rubinsky et al. 2007).

Mathematical studies have shown that naturally occurring local heterogeneities in the electrical properties of tissue affect the applied electric fields during electroporation and thereby affect the outcome of electroporation procedures (Daniels & Rubinsky 2009),(Edd & Davalos 2007). It is well established that temperature affects the electrical properties of tissue (Edd et al. 2005). It occurred to us that temperature could be used to locally modify electrical tissue properties in a desirable and controlled way and thereby produce greater local control over the outcome of minimally invasive electroporation procedures. The goal of this study is, therefore, to explore the hypothesis that local changes in electrical properties of tissue produced by changes in temperature can be used to modulate and control the effect of electroporation on biological matter. This is a mathematical study using the numerical analysis tools described in (Daniels & Rubinsky 2009).

Electrical conductivity of tissue is a function of temperature, exhibiting a positive correlation. Consequently, the electrical conductivity of cooled tissues is substantially lower than those at physiological temperatures. In this study, we will focus on an examination of the effect of lowering the temperature locally on the outcome of the electroporation protocol. While many methods for cooling tissue locally are possible, this study will simulate the use of cooling probes. Such probes are commonly used in minimally invasive surgery at temperatures below freezing (Rubinsky 2000). Here it is assumed that for this particular application, the probes are cooled to above freezing temperatures and used only as a means for changing tissue electrical properties.

The biophysical effect of temperature on the process of electroporation will be also considered and incorporated into the mathematical model. Several studies have investigated the effects of temperature on electroporation. For instance, Diaz investigated the effect of low temperatures on electroporation efficacy (Diaz-Rivera 2000). He accomplished electroporation on kidney epithelial cells at temperatures as low as -2°C (Diaz-Rivera & Rubinsky 2006). Additionally, Gallo demonstrated the trend between temperature and electroporation; as temperature decreases, initial cell membrane permeabilizing pulse voltage increases (Gallo et al. 2002). Gallo's study operated on the stratum corneum in the range 0-80°C. The same relationship between temperature and electroporation was found in *alga Valonia*, rye leaf protoplast and mammalian cell lines (Kanduser & Miklavcic 2009).

As a first order study, the concept introduced here investigated a mathematical analysis of temperature and electric fields produced by the application of IRE in conjunction with local cooling. The focus of this theoretical study is to examine the effect of changes in temperature on electric fields and the subsequent implications for tissue electroporation. For simplicity and to extract the most salient biophysical aspects of the analysis, we investigate simple two dimensional configurations in cylindrical coordinates in which the electrical and thermal effects are produced by electroporation probes and cooling probes with dimensions typical to commercially available devices. This study focuses on the change in electrical parameters as a result of temperature. It is evident that following this first order analysis, much additional theoretical and experimental work remains to be done.

4.2 Methods

The models were generated using numerical analysis executed by Comsol Multiphysics (version 4.1). This initial study utilized 2-dimensional models because these are sufficient to demonstrate the significant effect of temperature induced electrical property heterogeneities. Two equations were solved simultaneously in Comsol. The first of which was the Laplace equation for potential distribution associated with an electric pulse:

$$-\nabla \cdot d\left(\sigma\nabla - J^{e}\right) = dQ_{j}, \qquad (4.1)$$

where σ is electrical conductivity, V is voltage, J^e is external current density, d is thickness and Q_j is the current source. For all boundaries, the external current density and the current source were set to zero, and thickness was set to one. The electric field was solved in the AC/DC Conductive Media module using a transient analysis to account for electrical pulses.

The electrical conductivity, σ, was determined by the local tissue temperature according to data from the literature. Properties for physiological saline solution were used as a first order simulation for biological tissue, since electrical property data for tissues in the entire range of temperatures of interest is not available. Data from J.J. Arps (Arps 1953) was curve fitted to calculate the electrical conductivity of the composite medium. The derived electrical conductivity also employed experimental data from (Mazzoleni et al. 1986), resulting in the following function:

$$\sigma(T) = 0.03(T - 273.15) + 0.7, T > 272.59\,. \tag{4.2}$$

Equation 4.2 describes the behavior of electrical conductivity in [S/m] as a function of temperature T in [K]. The correlation coefficient of this equation relative to experimental data was tabulated to be *r=0.99989*.

In addition to electrical conductivity, electrical permittivity is also a function of temperature. The following equation (Kaatze 1989) was utilized to take into account the temperature dependence of electrical permittivity:

$$\varepsilon(T) = 10^{\left(1.94404 - 1.99\times10^{-3}(T-273.15)\right)}, \tag{4.3}$$

where ε is electrical permittivity and T is temperature in [K]. This equation is valid for low frequency permittivity, experienced by typical electroporation pulse parameters, which are in the range of 0.1-20E-3 seconds (Granot & Rubinsky 2007), (Ivorra & Rubinsky 2007).

The temperature distribution was obtained from the solution of the Pennes Bioheat equation, which was solved simultaneously as the electrical potential equation. The general Pennes Bioheat equation to be solved for this case took the following form:

$$\nabla\cdot(k\nabla T) + \rho_b w_b c_b (T_a - T) + q''' = \rho c_p \frac{\partial T}{\partial t}\,, \tag{4.4}$$

where k is thermal conductivity, T is temperature, w_b is blood perfusion, c_b is the heat capacity of blood, T_a is arterial temperature, ρ is the tissue density, c_p is the tissue heat capacity and $q''' = Q_{met} + Q_{ext}$. Q_{met} is the metabolic heat generation and $Q_{ext} = \sigma|\nabla\phi|^2$, which accounts for Joule heating, where ϕ is electrical potential and σ is electrical conductivity of the tissue. In this study, the effect of Joule heating on the temperature distribution was considered. The values for biological tissue utilized in the Pennes Bioheat equation are listed in Table 4.1 (Davalos et al. 2003).

Table 4.1: Temperature dependent properties used in the Pennes bioheat equation for the purpose of solving the temperature distribution due to the application of the cooling probe.

Thermal Conductivity	Blood Perfusion	Blood Heat Capacity	Metabolic Heat	Tissue Density	Tissue Heat Capacity
0.5 [W/mK]	0.5[kg/m^{3}s]	3640 [J/kgK]	33800[W/m^3]	1000 [kg/m^3]	3750 [J/kgK]

Studies on the effect of temperature on electroporation protocols have revealed a negative correlation between temperature and fields. The electric fields required for producing electroporation increase as temperature decreases. The goal of this study is to investigate the ultimate effects of temperature modulation on electroporation protocols, such as the fields necessary to induce reversible and irreversible electroporation. To accomplish this, data has been extracted from existing literature to produce a correlation between temperature and the fields required for reversible and irreversible electroporation (Miklavcic et al. 2000). The equation used in this study was derived from the experimental data acquired in (Diaz-Rivera 2000) and is given by:

$$E(T) = \frac{-39}{3200}T + 63700.45094, \qquad (4.5)$$

where T is temperature [˚C] and E is electric field [V/m]. Equation 4.5 is plotted in Figure 4.1. It is clear from both the equation and the graph that temperature dependence of the electric field is very low. However, the data available is very limited and cells in tissue may behave differently from cells in solution. For this reason, this equation was used as an approximate correlation for this study. It was used primarily to demonstrate an accurate methodology, but a substantial amount of additional research is needed to generate precise correlations, which currently have not yet been developed.

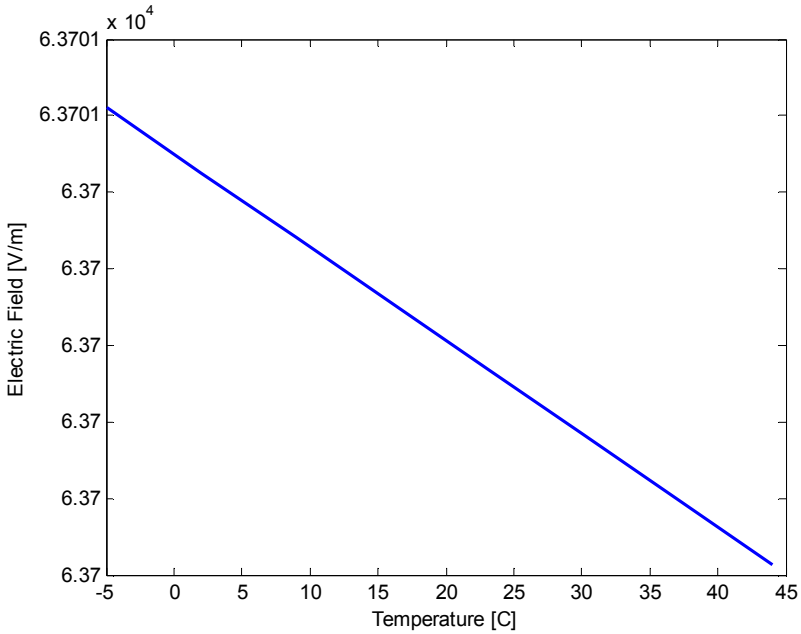

Figure 20: Graph plotting the temperature dependence of threshold irreversible electroporation electric field as a function of temperature. Derived experimentally from cells in solution.

4.3 Models

The primary goal of this study is to examine how local changes in tissue electrical properties due to changes in temperature affect electric fields during electroporation protocols. This study will focus in particular on the effects of cold temperatures. The complex volumetric effect of temperature induced changes in tissue electrical properties can be approximated by voltage divider circuits consisting of elements of resistance in series or in parallel. To capture these effects two models were examined. Case 1 includes temperature induced resistance in series with the original tissue impedance. Case 2 includes temperature induced resistance in parallel. These two cases can also be viewed as the difference between an electrically active cooling probe (resistance in series) and an electrically inactive cooling probe (resistance in parallel). These descriptions are only an approximation of the more complex models investigated in this study, and are described here for clarification of the resulting electrical phenomena.

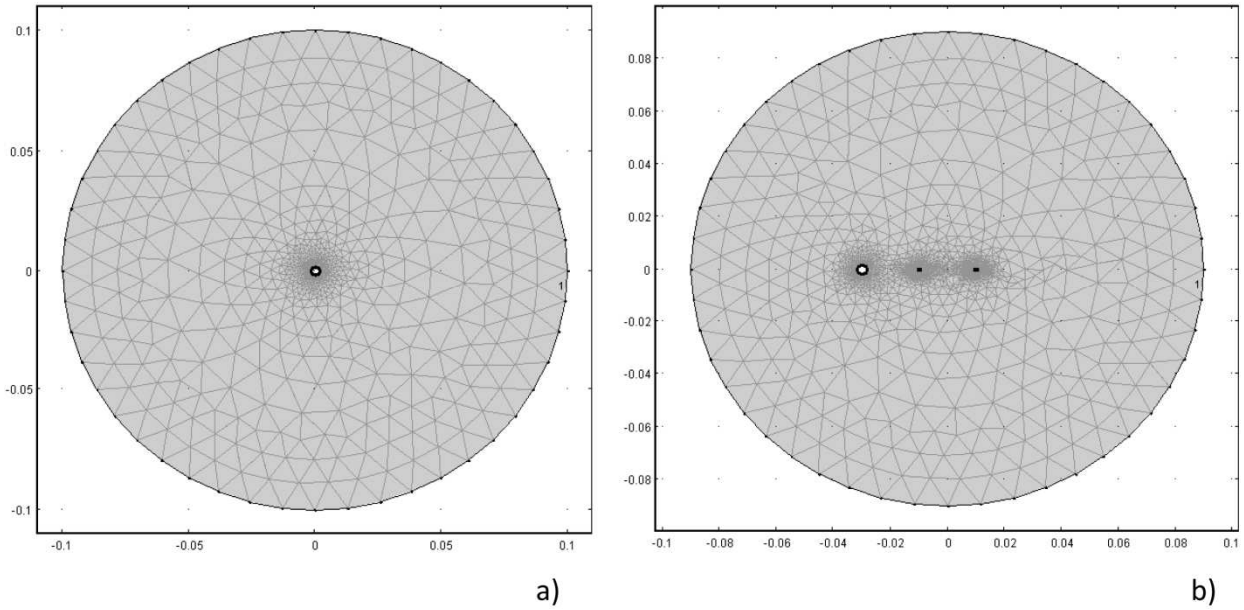

Figure 4.2: a) Mesh for Case 1, in which one cold probe is utilized for both cooling and as a IRE electrode. b) Mesh for Case 2, in which two typical electroporation probes are used to deliver the electric pulses and one cold probe is used to cool the tissue and induce local changes in electric properties. Note that the mesh is extra fine in the vicinity of the probes in order to capture the changes in electric field and temperature that occur due to the effect of the probes.

6.3.1 Case 1: Resistors in Series

The first geometry considered was represented in 2D and consisted of a single cryoprobe inserted into the center of a sample of tissue. The cryoprobe simultaneously applied a cold temperature and voltage pulses. In this case, the cooling of tissue simulates the addition of a resistor in series. The cryoprobe, measuring 3.4mm in diameter (Edd et al. 2008), was inserted into the center of an infinitely long cylinder of tissue, 6cm in radius. The outer edge of the cylinder was set to constant deep body temperature, 37ºC. The initial temperature of the system was also deep body temperature.

Cryoprobes are designed as hollow conduits through which a coolant flows. Because the probes are made of electrically conductive metal, the same probe can be used to both cool the tissue and apply pulses as electrodes when connected to a voltage supply. Therefore, the cold probe was modeled as an IRE electrode. A typical IRE voltage of 2500V was applied between the cold probe and the uniformly grounded outer edge of the tissue cylinder. A typical irreversible electroporation pulse sequence of 50μs pulse length at a frequency of 1Hz was used. This geometry was chosen because it simulates a typical clinical procedure during which a single probe applies a voltage and a grounding pad is placed at a distance, similar to radio-frequency ablation technique.

To understand the implications of temperature induced effects on the electric field, two variations of Case 1 have been modeled. The first applies a temperature of 0 ºC to the cold probe.

The second applies a thermally insulating boundary condition to the probe, which serves as a control.

The finite element mesh for this case utilized triangular elements, as shown in Figure 4.2a. The element size was smallest adjacent to the cryoprobe, and increased in size as it radiated towards the outer boundary. This was done in order to accurately capture the steep temperature gradient adjacent to the cold probe. The mesh was refined until the solution was no longer affected. Approximately 3800 elements were utilized to cover a 314cm^2 surface area.

4.3.2 Case 2: Resistors in Parallel

The second 2D geometry utilized three probes: two electrodes and a cooling probe at a distance. Because a single probe is not acting as an electrode and a cooling probe simultaneously, this configuration approximates two resistors in parallel. An infinitely long cylinder of tissue 6cm in radius was set to constant deep body temperature and electrical insulation at the outer margin. The initial temperature of the system was also deep body temperature. The delivery of electroporation was applied through two typical irreversible electroporation electrodes (Rubinsky et al. 2007) of 1mm in diameter. The leftmost electrode was held at ground and the rightmost probe applied a voltage of 2500V. A typical irreversible electroporation pulse sequence of 50μs pulse length at a frequency of 1Hz was used. As in Case 1, the cold probe was 3.4 mm in diameter. A temperature of 0ºC was applied to the cold probe and it was considered electrically insulated. The cold probe was set at various distances from the electrodes, to study the dependence of temperature induced heterogeneities on geometry. The exact geometries are specified in the Results and Discussion section.

To understand the implications of temperature induced effects on the electric field, two variations of Case 2 have been modeled. The first applies a temperature of 0 ºC to the cold probe. The second applies a thermally insulating boundary condition to the probe, which serves as a control.

The finite element mesh in this study utilized triangular elements, demonstrated by Figure 4.2b. The element size was smallest in the region surrounding both probes. This was done in order to accurately capture the temperature gradients adjacent to both of the probes. The mesh was refined until the solution was no longer affected. Approximately 5100 elements were utilized to cover a 314cm^2 surface area.

4.4 Results and Discussion

4.4.1 Case 1: Resistance in Series

The first case investigated was a 2D model with the boundary conditions previously specified. The purpose of this model was to illustrate the temperature induced effects on electric field due to a probe simultaneously delivering IRE and cold temperatures.

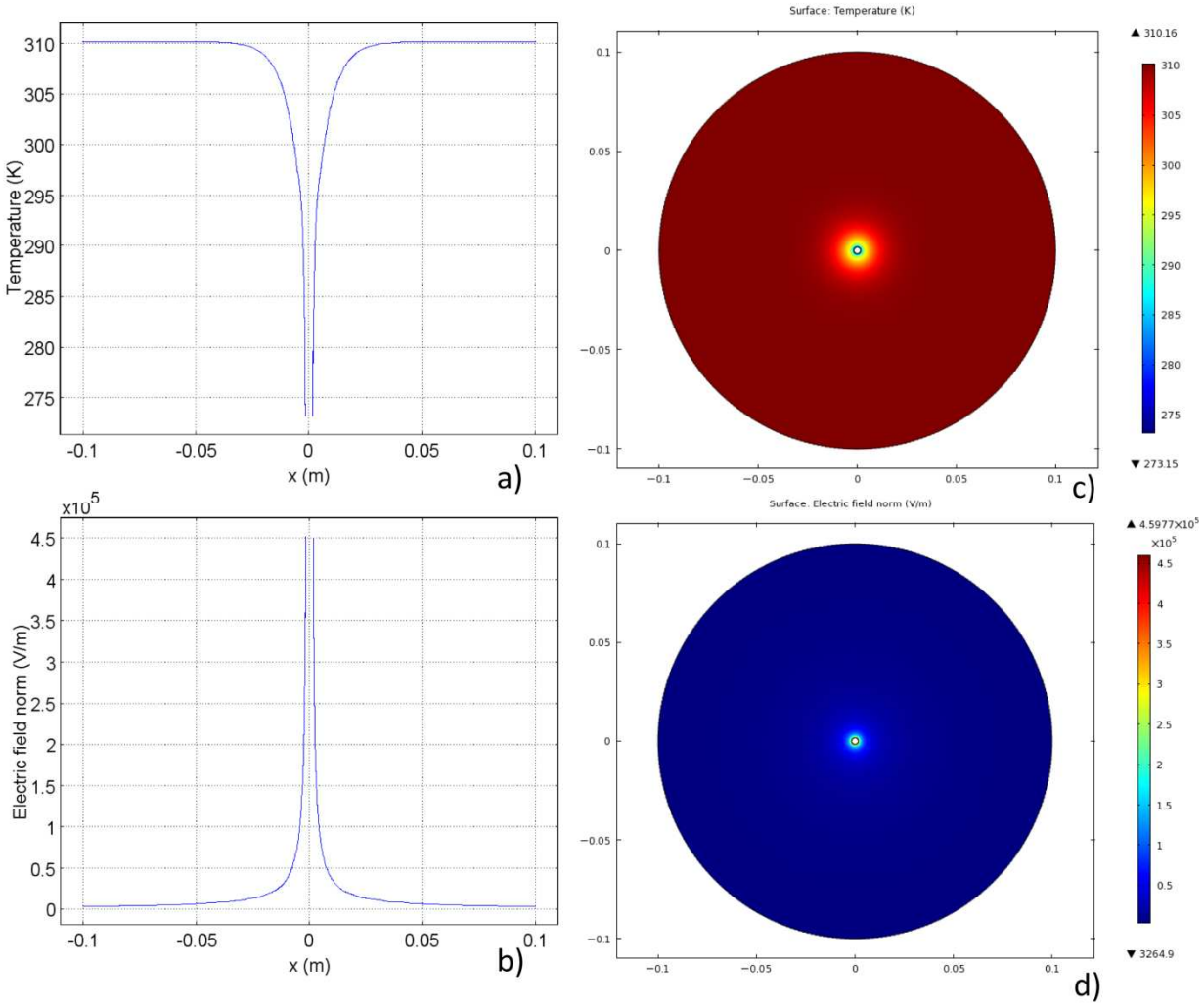

Figure 4.3: Results for Case 1. a) and b) Temperature and electric field distribution, respectively, at a transection along the diameter of the domain. c) and d) Temperature and electric field surface plots, respectively, in the domain. Plots reflect results after 2000 seconds of cooling at 0ºC followed by ten 2500V pulses (1Hz, 50µs) with full bioheat parameters considered.

4.4.1.1 Cooling

The temperature distribution after the cooling and IRE procedure is illustrated in Figure 4.3a. The temperature distribution, as expected, increases from the low temperatures at the cold probe surface to body temperature at the outer boundary. The corresponding electric field is demonstrated in Figure 4.3b. It is clear from these two graphs that the electric field and temperature distribution are inversely proportional. This relationship is a result of the temperature dependence of electrical conductivity, demonstrated by Equation 4.2. As a result, the highest electric fields occur in the regions of lowest temperature. It can be seen clearly that the electric field is confined within the low temperature region, and reaches zero nearly everywhere else.

4.4.1.2 Control

It is pertinent that the electric field produced during cooling be compared to a control study. The control study applied the same electrical boundary conditions as the cooling case to tissue held at body temperature. Figure 4.4 plots the electric field in the control and cooling case on the same axes for comparison purposes. It is evident from this graph that the electric field in the cooled regions is substantially higher than the field produced in the control study in the same region. The peak electric field in the cooling case is, in fact, three times larger than the control case. However, at a distance from the cooled region, in the location of normal body temperatures, the fields for the cooled case are lower than those in the control. This indicates that cold temperatures are capable of both magnifying the electric field and confining it to the cold regions.

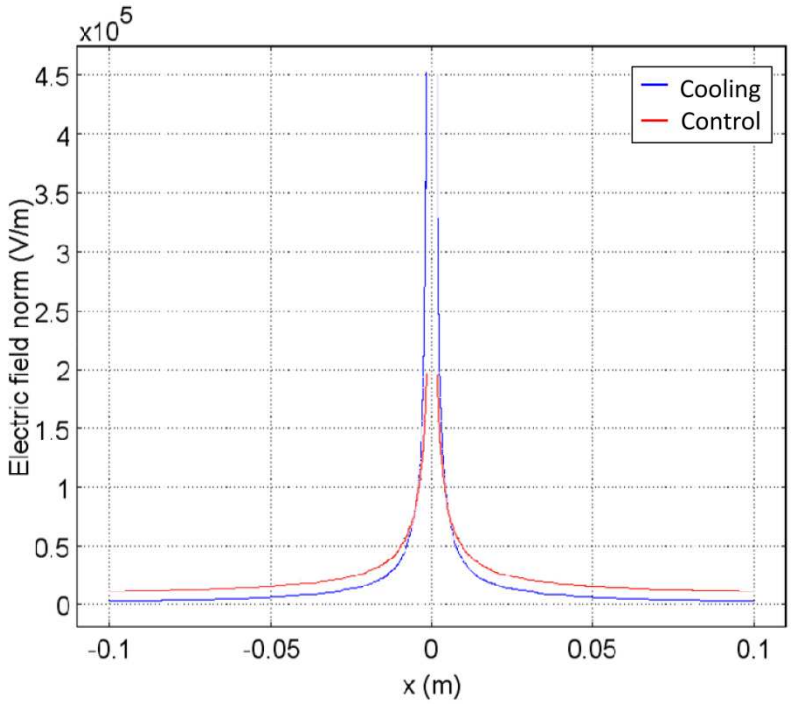

Figure 4.4: Control results for Case 1. Comparison of electric field distributions along a transection at the diameter of the sample. Blue line: electric field after 2000 seconds of cooling at 0˚C followed by ten 2500V pulses (1Hz, 50µs). Red line: control electric field after ten 2500V pulses (1Hz, 5µs), With full bioheat parameters considered.

The effects of cooling found in Figures 4.3 and 4.4 are caused by the change in the electrical properties of tissue due to temperature. Lower temperatures yield a lower ionic conductivity. The electric field distribution (Figure 4.4), demonstrates the inversely proportional relationship between temperature and electrical conductivity, as described by Equation 4.2. For the same voltage boundary conditions, from continuity of ionic current, the electric field will be

higher in the regions of lower electrical conductivity. Because of the increased electrical resistance in the regions of colder tissue, in a situation in which the cold region acts as a resistor in series with the area of tissue that is not affected by cooling, the highest electric fields are confined to the cold regions. The fields beyond the cooled regions, in tissue at normal temperature, are substantially lower than those in the cooled regions.

This effect is seen best in a supplemental analysis, shown in Figure 4.5. It consists of a simple one-dimensional Cartesian study of a 6cm slab of tissue between two parallel plates. The leftmost plate applies a voltage of 2500V and the rightmost plate applies ground. Figure 4.5 compares the electric field at constant temperature with the case in which cooling at 0ºC is applied on the leftmost plate and body temperature, 37ºC, is applied to the rightmost plate for 90 seconds. The effect of temperature induced tissue property heterogeneities is evident. At a constant temperature, the electric field is constant across the slab. For the case of cooling at one plate, the field is substantially higher near the cold surface and it decays to low values away from the cold surface. The difference between the electric field in cold regions and the electric field at body temperature is an order of magnitude. These results, as well as those demonstrated in Figures 4.3 and 4.4, suggest that inducing heterogeneity in tissue electrical properties through local cooling, with an analogue circuit of two resistors in series, has the effect of confining and enhancing the electric fields in the colder regions and reducing the field in the higher temperature regions.

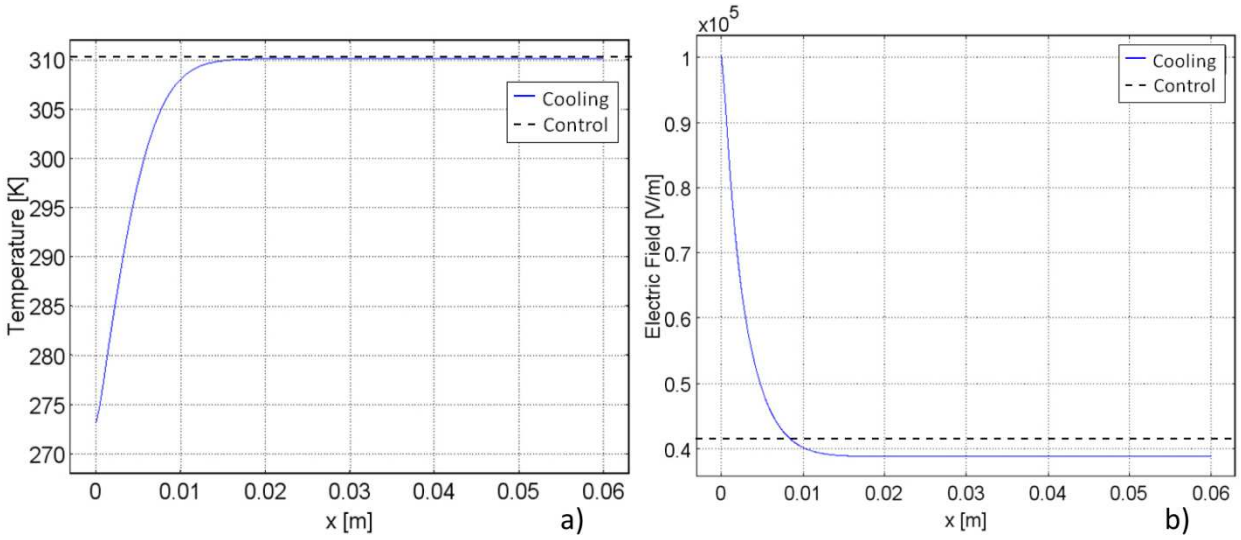

Figure 4.5: Comparison of cooling and control models for a) Temperature and b) electric field. Control models are held at constant body temperature.

The results from Case 1 suggest that it should be possible to design IRE protocols in which the electric field induced effects on cells are confined to the cooled regions of tissue and do not extend beyond the cooled regions. Furthermore, cooling the IRE electrode will yield

higher electric fields in the vicinity of the probe. The complementary effect of this observation is that the electric fields beyond the cooled area will be substantially reduced. Several recent studies have shown that stray electric fields beyond the IRE treated areas could have negative effects on other organs, such as the heart (Deodhar et al. 2011), or create undesirable muscle contractions. Reducing the electric fields beyond the treated area with cold should also reduce these effects. In addition, it is well established that the electric currents in IRE treated tissues are very high, on the order of tens of Amperes. The increased resistance caused by the cooled IRE probes, in a configuration such as the one discussed here, will substantially reduce the currents for the same applied voltage, while, on the other hand increasing the field in the cooled volume.

Note, however, that the effects discussed here, for Case 1, are restricted to situations in which the effect of cooling is that of a resistance in series. The second half of the study will address a situation in which the cooled area is not produced by the IRE probes but rather by a different cooling probe. In that case the effect is that of adding a high resistance in parallel.

4.4.2 Case 2: Resistance in Parallel

The configuration examined in the second half of this study is illustrated schematically in Figure 4.6. In Case 2, the effect of cooling delivered by a probe that is not electrically active on a typical irreversible electroporation protocol is investigated. The electric fields were delivered by two electrodes of 1mm diameter, separated by 2cm. The 3.4mm diameter cold probe was placed at various locations from the center along the axial line connecting the centers of the IRE electrodes. The protocol consisted of 2000 seconds of cooling applied by the cold probe at 0ºC, followed by ten, 2500V pulses (1Hz, 50μs length) applied by the IRE electrodes. The cooling probe was electrically insulated. In the control case, ten 2500V pulses (1Hz, 50μs length) applied by the IRE electrodes without using the cooling probe. Full bioheat parameters were utilized to simulate tissue.

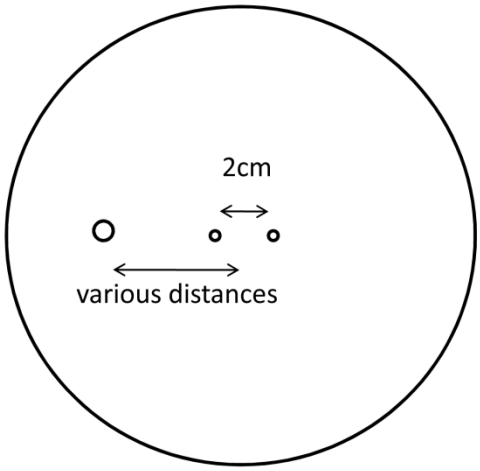

Figure 4.6: Schematic of the positioning of the cooling probe and electrodes in the different variations of Case 2.

Figure 4.7 illustrates the electric field along a transection through the center of the electrodes and cooling probe for various locations of the cooling probe. Figure 4.7a shows the control case and Figure 4.7b shows the cooling case at 4cm from the center of the domain. It is clear that in the configuration described here the increased electrical resistance due to the cold region acts as a current path of high electrical resistance in parallel to the higher temperature path of lower resistance. This configuration, in contrast to the trends identified in Case 1, results in a substantial decrease in the electric field in the cooled region. In fact, the electric field reaches 0V/m in the location of the cold probe.

Figure 4.8 illustrates a potential application of this observation. Equation 4.5 has been utilized to calculate the regions of tissue that undergo irreversible electroporation. The results are presented as surface plots in Figure 4.8. Figure 4.8 demonstrates that a cooling probe can avoid irreversible electroporation damage at a particular location. Figure 4.8b demonstrates that this can be accomplished outside of the treatment region when the cooling probe is placed at a distance from the electrodes. Figure 4.8c demonstrates that a cold probe can protect a region between the two electrodes as well.

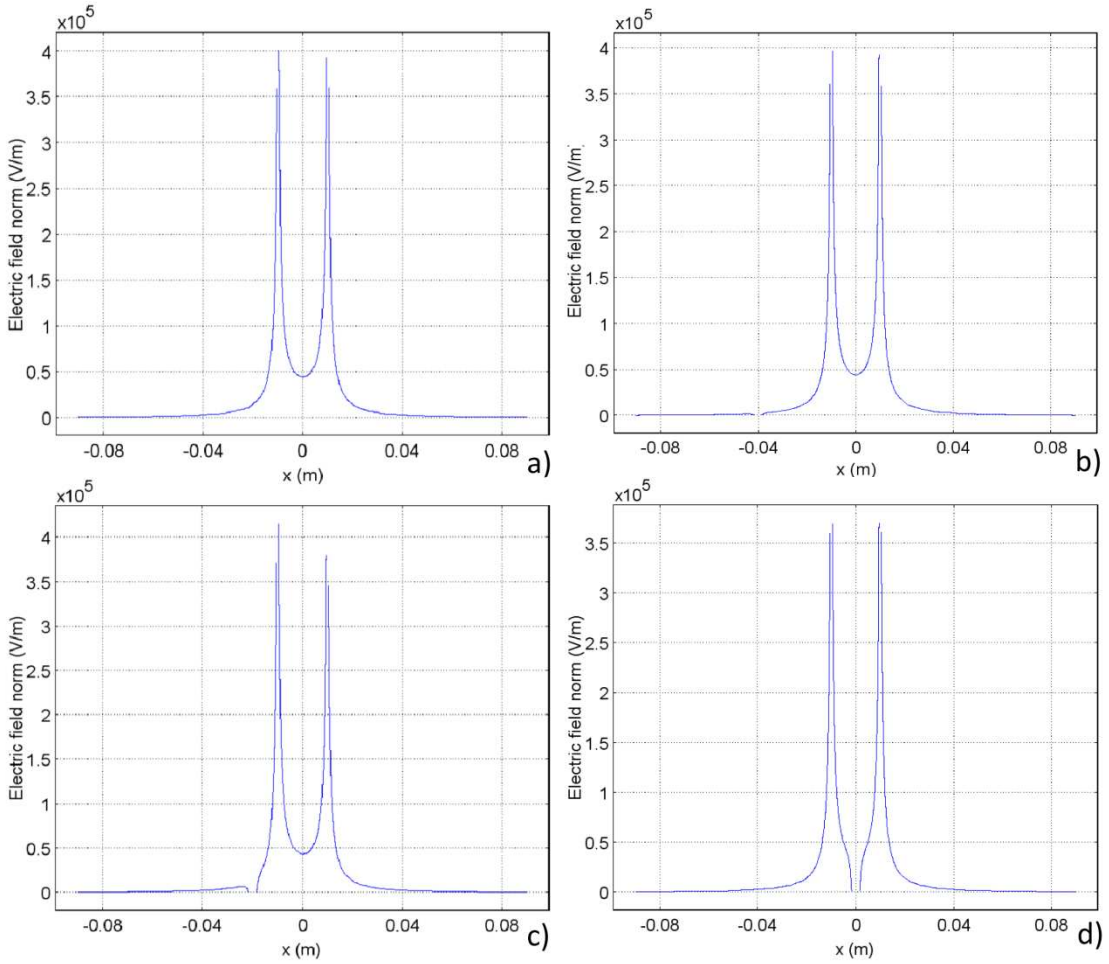

Figure 4.7: Case 2 Results. The electric field distributions along a transection at the diameter of the sample. a) Control, b) cold probe 4cm from center, c) cold probe 2cm from center, and d) cold probe 0cm from center.

These results illustrate a potential important application of the use of cooling with IRE. When comparing Figure 4.8a and 4.8b, it is seen that in 4.8b the temperature induced changes in electrical potential due to the cold probe cause the irreversible electroporation field near the probe to recede (the edge flattens). This suggests that if a sensitive tissue structure is close to the outer edge of the IRE treatment region, the simple application of cold can protect this structure. Figure 4.8c shows that the use of cold can eliminate electric fields even in the center of the treated area. This suggests that critical tissues, which need protection during an IRE protocol, can be protected by cold. One clinically relevant example is the bladder sphincter, which is particularly vulnerable during the IRE treatment of the prostate. Cooling the sphincter, and thereby increasing its electrical resistance, could protect it from damage during minimally invasive treatment of the prostate with IRE. By increasing the local electrical resistance through the placement of cooling instruments, electric fields can be modulated to obtain desired effects.

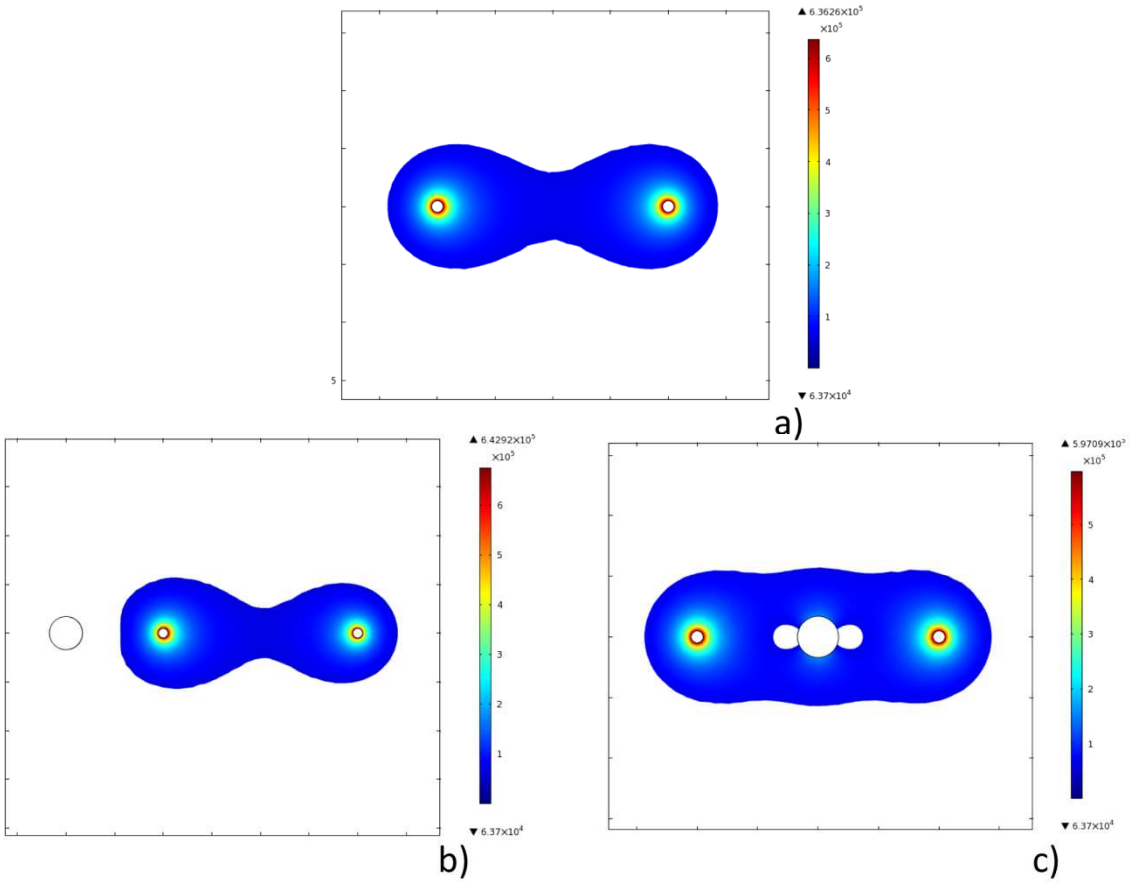

Figure 4.8: Case 2 results. Illustrated in this figure is the area of tissue that undergoes irreversible electroporation. a) Control case without any cooling applied, b) cooling probe located 2cm from the center, c) cooling probe located at the center of the tissue.

4.5 Conclusions

The goal of this study was to evaluate the feasibility and the characteristics of a minimally invasive surgical procedure in which changes in electric properties due to local changes in temperature were used to modulate electric fields during IRE procedures. The hope was that control over the outcome of the procedure will improve as a result. This investigation examined two different possible configurations. The first configuration, Case 1, utilizes the IRE electrode also as a cooling probe, with the resulting electrical effect of a resistance in series. In this configuration, the electric fields are confined to the cold region and magnified in that region while the fields at a distance are reduced. The second configuration, Case 2, applies cold with an element that is not electrically active, with the resulting electrical effect of resistances in parallel. In Case 2, the electric field in the cold region is reduced.

Perhaps the most important conclusion from this study is that temperatures can be used to modulate and control electric fields. Through proper placement of cold, various desirable and

controlled IRE protocols can be accomplished that could not have been achieved otherwise. It is clear that a variety of configurations of cold and heat could be used to achieve various IRE goals.

Although this is a first order theoretical analysis and additional theoretical and experimental research is needed to further develop this new concept, these primary results act as a promising foundation for future work. For these reasons, this numerical study has indicated the undeveloped potential and the motivation for pursuing the use of temperature to modulate and control IRE.

Chapter 5: Dissertation Conclusions and Future Work

5.1 Dissertation Conclusions Overview

Electroporation as a treatment for malignant tissues is still in its infancy. While human studies have been conducted (G Onik & Rubinsky 2010), further investigation and proof of efficacy is still necessary. Despite being in its infancy, electroporation studies have yielded meaningful and promising results. Previous experiments have demonstrated the success of IRE as a treatment method for cancer, exceeding expectations. IRE has proven successful in long term studies involving rat (Edd et al. 2006) and pig (Rubinsky et al. 2007) livers. An experiment performed in a small rodent study illustrated that IRE can treat cancer (Al-Sakere et al. 2007), establishing a strong foundation for electroporation. Another experimental study demonstrated the potential of IRE to achieve focal tissue ablation of the prostate while sparing the urethra and nerves (G Onik et al. 2007). In addition, recent clinical studies have shown electroporation's ability to treat prostate cancer in humans (G Onik & Rubinsky 2010).

These results are promising. As a result, further investigation into the field of electroporation is even more pertinent. Therefore, the purpose of this dissertation was to explore one of the previously uninvestigated domains of electroporation to develop the depth of this field.

5.1.1 Intrinsic Heterogeneous Tissues

The goal of this chapter was to demonstrate the importance of investigating anatomically heterogeneous models with IRE. Current treatment methods do not consider surrounding tissue during pre-surgical planning. The goal of this chapter was also to show that when IRE treatment methods are developed, they must consider the heterogeneous nature of the tissue.

Both the model of the prostate and the breast demonstrated the substantial difference between homogeneous and heterogeneous tissues. The electric field trends varied greatly between the heterogeneous and homogeneous tissues. In fact, the maximums and minimums occurred in different locations. Furthermore, this theoretical study was able to provide an explanation for a previously unexplained phenomenon that occurred during human trials. During treatment of prostate cancer, the pelvis plexus nerve structure went untouched in all patients, a achievement unaccomplished by current techniques (G Onik & Rubinsky 2010). The reason for this, however, was unknown. This was in part due to the fact that the impact IRE has on biological structures such as nerves, ducts and blood vessels was also previously unknown. This investigation has made clear that nerves can be preserved in treated tissue because of the insulating effect of surrounding myelin layers. Additionally, this study has suggested that lactiferous ducts will remain undamaged because surrounding myoepithelial cells also have an insulating, and therefore protective effect on the ducts. Additionally, because myelin and myoepithelial cells have the ability to regenerate, any damage experienced by these structures

can be theoretically reversed. Following the release of these results, animal experiments validated the theory (Schoellnast et al. 2011).

Therefore, anatomically heterogeneous models are not only important to consider in order to generate an accurate simulation, but also to understand the effects of electroporation on all included biological structures to improve clinical applications.

5.1.2 Extrinsic Heterogeneous Tissues: Freezing

The goal of this chapter was to evaluate extrinsic heterogeneous tissues. It specifically investigated how heterogeneities induced by an externally applied subzero temperature effected electric fields. The feasibility and the characteristics of a minimally invasive surgical procedure in which cryosurgery was modulated with IRE were investigated in the hope that it could improve the effectiveness of cryosurgery and eliminate the problems related to cell survival on the outer rim of frozen tissue. As expected, one and two dimensional models demonstrated that freezing temperatures have a substantial effect on IRE produced electric fields. Furthermore, detailed information about the effects of subzero temperature on IRE was also discovered. This investigation has made clear that both low and subzero temperatures are capable of concentrating the electric field as a result of the temperature dependence of electrical conductivity. Additionally, this study has demonstrated the ability of low and subzero temperatures to increase the magnitude of the electric field. This phenomenon is also due to the fact that electrical conductivity is a function of temperature. The low electrical conductivity in frozen regions generates a larger voltage difference because of the high resistance to current, and therefore a higher electric field.

These results have far reaching implications in terms of imaging strategy and procedural methodology regarding accuracy of treating tissue with both cryosurgery and electroporation. Utilizing cryoIRE may potentially allow ultrasound to image real time cell death, a previously unachieved endeavor during electroporation procedures, and in turn increase surgical accuracy. A further inadvertent consequence of targeted electric fields is the elimination of muscle contractions during surgery due to the substantial reduction in electric field outside the cryoIRE treated zone. In fact, in an animal experiment conducted at Sloan-Kettering Cancer Research center in Manhattan, muscle contractions were eliminated. The experiment compared muscle contractions of a pig without muscle relaxant medication during normal IRE treatment to a cryoIRE treatment. The results were persuasive. A participating surgeon ranked the contractions during the normal IRE treatment on a scale of 1-10 (10 being largest contractions) as a 10. During the cryoIRE treatment, they were ranked a 0.

7.1.3 Extrinsic Heterogeneous Tissues: Cooling

The goal of this chapter was to further investigate the effect of temperature on electric fields. This study extended the temperature range of interest into cooling values. The purpose was to evaluate the feasibility and the characteristics of a minimally invasive surgical procedure in which changes in electric properties due to local changes in temperature were used to

modulate electric fields during IRE procedures. The hypothesis was that control over the outcome of the procedure will improve as a result.

The electrode and cryo/cooling probe configuration was found to play an important role in results because of the electrical circuit they create. For this reason, this investigation examined two different possible geometric configurations. The first configuration, Case 1, utilized the IRE electrode simultaneously as a cooling probe; effectively resulting in an electrical equivalent of resistors in series. In this configuration, the electric fields were confined to the cold region and magnified in that region while the fields at a distance are reduced. This finding was consistent with the results achieved in the previous chapter on freezing. Because cooling temperatures have a higher electrical conductivity, the effect of concentrating and increasing the electric field was smaller, which was also expected.

The second configuration, Case 2, applied cold with an element that was not electrically active. This resulted in an electrical effect equivalent to resistors in parallel. In this second case, the electric field in the cold region is reduced, rather than increased. This was a direct result of the effective equivalent circuit. Because a parallel circuit was simulated, current no longer was forced to travel through both resistors. Instead, current traveled the path of least resistance, which is the tissue of higher conductivity: the tissue closer to body temperature. Because current is concentrated in areas closer to body temperature, the cooled regions experience little to no electric field. In this second case, low temperatures can be used to decrease the electric field, rather than increase them.

In combination with the results of freezing temperature on electric fields, cooling results suggest that the most important conclusion from this study may be that temperatures can be used to modulate and control electric fields. Through proper placement of cold and freezing probes, various desirable IRE protocols can be controlled and accomplished, ones that could not have been achieved otherwise. It is clear from these investigations that a variety of configurations of cold and heat could be used to achieve various different surgical goals and IRE protocols.

Because the temperature dependency of electrical fields has not been investigated before, this investigation of temperature on IRE is only a first order analysis. And while the data presented is only a theoretical analysis, both in vitro and in vivo studies are currently being conducted to verify and validate the findings herein. Additional theoretical and experimental research is needed to further develop this new concept. Nevertheless, these primary results act as a promising foundation for future endeavors in this field. For these reasons, the results of these numerical studies have indicated the latent potential and the motivation for pursuing the use of temperature to modulate and control IRE.

5.2 Future Work

This work establishes the field of heterogeneous tissues in electroporation. Because this topic has not been previously explored, much additional research is necessary to optimize IRE protocols while considering heterogeneous tissues. Specifically, in vitro and in vivo work is necessary to validate all theoretical findings.

In vitro work is necessary to quantify the behavior of electric fields in frozen and cooled tissues. The first question that must be probed is if electroporation occurs in frozen and cooled tissue the same manner it does in tissue at body temperature. Because the mechanism of electroporation is still not thoroughly understood, this question is of great importance. Specifically, the efficiency of electroporation in frozen and cooled tissues must be quantified and compared to conventional electroporation.

In vivo work is also necessary. While the first animal experiments (publication pending) on the technology indicate the elimination of muscle contractions when using cryoIRE, further quantification is necessary. Maximum achievable voltage magnitude without muscle relaxants must be determined in various organs and tissues. Efficiency of cryoIRE as compared to electroporation must be understood and compared to in vitro work.

In vivo work must also establish fundamental parameters approximated in this study. The values for electrical conductivity of mammalian tissue at subzero temperatures are currently not available in scientific data. In these studies, values for biological saline solution were used as a first order approximation. However, for comprehensive and accurate analysis, values for electrical conductivity of mammalian tissue must be established.

The potential use of ultrasound as an imaging modality for cryoIRE should be investigated. Specifically, the diameter of the region experiencing tissue necrosis should be rigorously compared to the diameter of the frozen regions viewed by ultrasound. It should be determined f these two regions are of equivalent size and location, or if electroporation protocols can be adjusted to accomplish this. If this can be achieved consistently in different organs and tissues, then it may indicate that a real time imaging modality is possible for electroporation procedures. This holds the potential to vastly improve surgical accuracy and patient outcomes.

References

Abidor, I. et al., 1979. Electric breakdown of bilayer membranes: 1. The main experimental facts and their qualitative discussion. *Bioelectrochemistry and Bioenergetics*, 6, pp.37-52.

Advisory Committee on Immunization Practices, 2006. Prevention and control of influenza: recommendations of the Advisory Committee on Immunization Practices (ACIP). *Mortaility and morbidity report*, 55, pp.1-42.

Agah, R. et al., 1994. Rate Process Model for Arterial Tissue Thermal Damage: Implications on Vessel Photocoagulation. *Lasers in Surgery and Medicine*, 15, pp.176–184.

Al-Sakere, B., Andre, F. & Bernat, C., 2007. Tumor Ablation with Irreversible Electroporation. *PLoS one*, 2(11).

Andersson, K. & Ohlsson, T., 1999. Including environmental aspects in production development: a case study of tomato ketchup. *LWT*, 32(3), pp.134–141.

Andreuccetti, D., Fossi, R. & Petrucci, 1997. Dielectric Properties of Body Tissues: Output data. *Italian National Research Council Institute for Applied Physics IFAC*.

Arps, J., 1953. The Effect of Temperature on the Density and Electrical Resistivity of Sodium Chloride Solutions. *Petroleum Transactions*, 198, pp.327-330.

Bailey, M. et al., 2003. Physical Mechanisms of the Therapeutic Effect of Ultrasound (A Review). *Acoustical Physics*, 49(4), pp.437–464.

Baust, J & Gage, A., 2005. The molecular basis of cryosurgery. *BJU International*, 95, pp.1187–1191.

Belov, S., 1978. Effects of high-frequency current parameters on tissue coagulation. *Biomedical Engineering*, 12(4), pp.209-211.

Benz, R., Beckers, F. & Zimmermann, U., 1979. Reversible electrical breakdown of lipid bilayer membranes: A charge-pulse relaxation study. *Journal of Membrane Biology*, 48, pp.181-204.

Blakemore, W., 1975. Remyelination by Schwann Cells of Axons Demyelinated by Intraspinal Injection of 6-Aminonicotinamide in the Rat. *Journal of Neurocytology*, 4(6), pp.745–757.

Bown, S., 1983. Phototherapy of tumors. *World Journal of Surgery*, 7(6), pp.700-709.

Campbell, A. & Land, D., 1992. Dielectric properties of female human breast tissue measured in vitro at 3.2 GHz. *Physics in Medicine and Biology*, 37, pp.193-210.

Chang, D. & Reese, T., 1990. Changes in membrane structure induced by electroporation as revealed by rapid-freezing electron microscopy. *Biophysical Journal*, 58(1).

Chang, D. et al., 1992. *Guide to Electroporation and Electrofusion*, New York: Academic Press.

Charny, C., 1992. Mathematical models of bioheat transfer. *Advances in Heat Transfer*, 22, pp.19-155.

Crawford, N. & Chronos, N., 1996. Electro-encapsulating drugs within blood platelets: local delivery to injured carotid arteries during angioplasty. *Seminars of Interventional Cardiology*, 1, pp.91-102.

Crowley, J., 1973. Electrical Breakdown of Bimolecular Lipid Membranes as an Electromechanical Instability. *Biophysical Journal*, 13(7), pp.711-724.

Daniels, C. & Rubinsky, B., 2009. Electrical field and temperature model of nonthermal irreversible electroporation in heterogeneous tissues. *Journal of Biomechanical Engineering*, 131(7), pp.071006-12.

Daniels, C. & Rubinsky, B., 2011. Temperature modulation of electric fields in biological matter. *PLoS ONE*, 6(6).

Dantzig, J., 1989. Modelling Liquid-Solid Phase Changes With Melt Convection. *International Journal for Numerical methods in Engineerings*, 28.

Davalos, R. & Rubinsky, B., 2008. Temperature considerations duringirreversible electroporation. *International Journal of Heat and Mass Transfer*, 51, pp.5617–5622.

Davalos, R., Mir, L. & Rubinsky, B., 2004. Tissue Ablation with Irreversible Electroporation. *Annals of Biomedical Engineering*, 33(2), pp.223-231.

Davalos, R., Rubinsky, B. & Mir, L., 2003. Theoretical analysis of the thermal effects during in vivo tissue electroporation. *Bioelectrochemistry*, 61(1-2), pp.99-107.

Davalos, R., Rubinsky, B. & Otten, D., 2002. A feasibility study for electrical impedance tomography as a means to monitor tissue electroporationfor molecular medicine. *IEEE Transactions of Biomedical Engineering*, 49, pp.400-403.

DeMarco, S., 2003. Computed SAR and thermal elevation in a 0.25-mm 2-D model of the human eye and head in response to an implanted retinal stimulator - part I: models and methods. *IEEE Transactions on Antennas and Propagation*, 51, pp.2274-2285.

Deodhar, A. et al., 2011. Irreversible Electroporation Near the Heart: Ventricular Arrhythmias Can Be Prevented With ECG Synchronization. *American journal of roentgenology*, 196.

Deryagin, B. & Gutop, Y., 1962. Theory of the breakdown (rupture) of free films. *Kolloidn. Zh.*, 24, pp.370-374.

Dev, S. et al., 2000. Medical Applications of Electroporation. *IEEE Transactions on Plasma Science*, 28.

Diaz-Rivera, R., 2000. Micro and Nano Scale Bioelectronics in Cell Micro-Electroporation. *Doctoral Dissertation, UC Berkeley*.

Diaz-Rivera, R. & Rubinsky, B., 2006. Electrical and thermal characterization of nanochannels between a cell and a silicon based micro-pore. *Biomedical Microdevices*, 8(1), pp.25-34.

Doevenspeck, H., 1961. Influencing cells and cell walls by electrostatic impulses. *Fleischwirtschaft*, 13, pp.986-987.

Dosekun, F., 1961. The Measurement of Metabolic and Vascular Responses in the Thyroid Gland With Observations on Its Responses to Insulin, Glucose and Adrenaline. *Journal of Physiology*, 157, pp.504-512.

Edd, J. & Davalos, R., 2007. Mathematical Modeling of Irreversible Electroporation for Treatment Planning. *Technology in Cancer Research and Treatment*, 6(4).

Edd, J., Horowitz, L. & Rubinsky, B., 2005. Temperature dependence of tissue electrical properties in electrical impedance tomography of cryosurgery. *IEEE Transactions of Biomedical Engineering*, 52.

Edd, J. et al., 2006. In vivo results of a new focal tissue ablation technique: irreversible electroporation. *IEEE Transactions of Biomedical Engineering*, 53(7), pp.1409-15.

Edd, J. et al., 2008. Imaging cryosurgery with EIT: tracking the ice front and post-thaw tissue viability. *Physiological Measurement*, 29(8).

Feng, Y. et al., 2009. Nanoshell-Mediated Laser Surgery Simulationfor Prostate Cancer Treatment. *Engineering with Computers*, 25, pp.3–13.

Findanza, F., 2003. Body fat in adult man: semicentenary of fat density and skinfolds. *Acta Diabetologica*, 40, p.s242-s245.

Foster, R. et al., 1993. High-intensity focused ultrasound in the treatment of prostatic disease. *European Urology*, 23, pp.29-33.

Frankenhaeuser, B. & Widén, L., 1956. Anode break excitation in desheathed frog nerve. *The Journal of Physiology*, 131, pp.243-247.

Fuch, K., 2002. Minimally Invasive Surgery. *Endoscopy*, 34(2), pp.154-159.

Gabriel, B. & Teissié, J., 1997. Direct observation in the millisecond time range of fluorescent molecule asymmetrical interaction with the electropermeabilized cell membrane. *Biophysical Journal*, 73(5), pp.2630-2637.

Gage, A., 1998. History of cryosurgery. *Seminars in Surgical Oncology, Special Issue: Hepatic Cryotherapy*, 14(2), pp.99-109.

Gage, A. & Baust, J, 1998. Mechanisms of Tissue Injury in Cryosurgery. *Cryobiology*, 37(3), pp.171-186.

Gage, A., Baust, JM & Baust, JG, 2009. Experimental cryosurgery investigations in vivo. *Cryobiology*, 59(3), pp.229-243.

Gallo, S. et al., 2002. Temperature-dependent electrical and ultrastructural characterizations of porcine skin upon electroporation. *Biophysics Journal*, 82, pp.109-119.

Gehl, J. & Mir, L., 1999. Determination of optimal parameters for in vivo gene transfer by electroporation, using a rapid in vivo test for cell permeabilization. *Biochemical and Biophysical Research Communications*, 261(2), pp.377-380.

Geier, D., Sykes, L. & Geier, M., 2007. A review of thimerosal (merthiolate) and its ethylmercury breakdown product: specific historical considerations regarding safety and effectiveness. *Journal of Toxicology and Environmental Health, Part B*, 10, pp.575-596.

Gilbert, J. et al., 1984. The use of ultrasonic imaging for monitoring cryosurgery. *IEEE Transactions of Biomedical Engineering*, 563(8).

Gilbert, J., Rubinsky, B. & Onik, GM, 1985. Solid-Liquid Interface Monitoring with Ultrasound During Cryosurgery. *ASME Paper #85-WA/HT-83*.

Glaser, R. et al., 1988. Reversible electrical breakdown of lipid bilayers: formation and evolution of pores. *Biochimica et Biophysica Acta*, 940, pp.275-287.

Golberg, A., Belkin, M. & Rubinsky, B., 2009. Irreversible electroporation for microbial control of drugs in solution. *AAPS PharmSciTech*, 10(3), pp.881-886.

Goldberg, S. et al., 2000. Treatment of intrahepatic malignancy with radiofrequency ablation. *American Cancer Society*, 88(11).

Granot & Rubinsky, B., 2007. Methods of optimization of electrical impedance tomography. *Physiol. Meas.*, 28(10).

Hamilton, WA & Sale, AJH, 1967. Effects of high electric fields on microorganisms: II. Mechanism of action of the lethal effect. *Biochim Biophys Acta*, 148(3), pp.789-800.

Hassan, N., 2003. Numerical study of induced current perturbations in the vicinity of excitable cells exposed to extremely low frequency magnetic fields. *Physics in Medicine and Biology*, 48, pp.3277-3293.

Higgins, S. & Hafty, B., 1994. Pregnancy and lactation after breast-conserving therapy for early stage breast cancer. *Cancer*, 73, pp.2175-2180.

Hjouj, M. & Rubinsky, B., 2010. Magnetic resonance imaging of irreversible electroporation in tubers. *XII Mediterranean Conference on Medical and Biological Engineering and Computing 2010*, 29, pp.371-375.

Hodgkin, A., 1951. The ionic basis of electrical activity in nerve and muscle. *Biological reviews of the Cambridge Philosophical Society*, 26, pp.339–409.

Hoffmann, N. & Bischof, J., 2002. The cryobiology of cryosurgical injury. *Urology*, 60(2, Supplement 1), pp.40-49.

Hong, J. & Rubinsky, B., 1995. Phase Transformation in Materials With Nonuniform Phase Transition Temperatures. *Journal of Heat Transfer*, 117(3), pp.803-806.

Howorka, K., 1996. Thermal conductivity of minke whale blubber. *Journal of Thermal Biology*, 21, pp.123-128.

Ingebritsen, S. & Sanford, W., 1998. *Groundwater in Geologic Processes*, Cambridge University Press.

Ivorra, A. & Rubinsky, B., 2010. Historical Review of Irreversible Electroporation in Medicine. *Series in Biomedical Engineering*, pp.1-21.

Ivorra, A. & Rubinsky, B., 2007. In vivo electrical impedance measurements during and after electroporation of rat liver. *Bioelectrochemistry*, 70(2).

Jaroszeski, M et al., 1999. In vivo gene delivery by electroporation. *Advanced Drug Delivery Reviews*, 35(1), pp.131-137.

Jiang, J. et al., 2008. Tumor necrosis factor-alpha-induced accentuation in cryoinjury: mechanisms in vitro and in vivo. *Molecular Cancer Therapy*, 8, pp.2547-55.

Jiang, J. et al., 2010. Pre-conditioning cryosurgery: cellular and molecular mechanisms and dynamics of TNF-α enhanced cryotherapy in an in vivo prostate cancer model system. *Cryobiology*, 61(3), pp.280-288.

Jimenez, L., 2007. Microbial diversity in pharmaceutical product recalls and environments. *PDA Journal of Pharmaceutical Science and Technology*, 61(5), pp.383-399.

Joshi, RP & Schoenbach, K., 2002. Mechanism for membrane electroporation irreversibility under high-intensity, ultrashort electrical pulse conditions. *Physical Review E.*, 66(5).

Kaatze, U., 1989. Complex permittivity of water as a function of frequency and temperature. *J. Chem. Eng. Data*, 34(4).

Kanduser, M. & Miklavcic, D., 2009. Electroporation in biological cell and tissue: an overview. *Food Engineering Series*, pp.1-37.

Kinosita, K. & Tsong, K., 1977. Formation and resealing of pores of controlled sizes in human erythrocyte membrane. *Nature*, 268, pp.438-441.

Kinosita, K. et al., 1988. Electroporation of cell membrane visualized under a pulsed-laser fluorescence microscope. *Biophysical Journal*, 53, pp.1015-1019.

Knoell, D. & Yim, I., 1998. Human gene therapy for hereditary diseases: A review of trials. *American Journal of Health-System Pharmacy*, 55, pp.899-904.

Kochanek, K. et al., 2011. National vital statistics report: Deaths, preliminary data for 2009. *U.S. Department of Health and Human Services, Centers for Disease Control and Prevention, National Center for Health Statistics*, 59(4).

Kolka, M., Holden, W. & Gonzalez, R., 1984. Heat Exchange Following Atropine Injection Before and After Heat Acclimation. *Journal of Applied Physiology*, 56, pp.896–899.

Kotnik, T. & Miklavcic, D., 2000. Theoretical evaluation of the distributed power dissipation in biological cells exposed to electric fields. *Bioelectromagnetics*, 21(5).

Koushafar, H. & Rubinsky, B., 1997. Effect of antifreeze proteins on frozen primary prostatic adenocarcinoma cells. *Urology*, 49(3), pp.421-425.

Kwok, J. & Krzyspiak, J., 2007. Thermal Imaging and Analysis for Breast Tumor Detection.

Labbé, A. et al., 2006. Comparison of toxicological profiles of benzalkonium chloride and polyquaternium-1: an experimental study. *Journal of Ocular Pharmacology and Therapeutics*, 22(4), pp.267-278.

Lamberg, P., Lehtiniemi, R. & Henell, A., 2004. Numerical and experimental investigation of melting and freezing processes in phase change material storage. *International Journal of Thermal Sciences*, 43(3).

Lasry, J., 1987. Depression and body image following mastectomy and lumpectomy. *Journal of Chronic Diseases*, 40, pp.529-534.

Lee, R., 2005. Cell injury by electric forces. *Ann N Y Acad Sci*, 1066, pp.85-91.

Leung, E., Medeiros, F. & Weinreb, R., 2008. Prevalence of ocular surface disease in glaucoma patients. *Journal of Glaucoma*, 17(5), pp.350-355.

Lewis, T., 2003. A model for bilayer membrane electroporation based on resultant electromechanical stress. *IEEE Transactions on Dielectrics and Electrical Insulation*, 10.

Love, R. et al., 1989. Side effects and emotional distress during cancer chemotherapy. *Cancer*, 63(3), pp.604-612.

Maldarelli, C. et al., 1980. Stability of symmetric and unsymmetric thin liquid films to short and long wavelength perturbations. *Journal of Colloid and Interface Science*, 78(1), pp.118-143.

Maor, E., Ivorra, A. & Rubinsky, B., 2008a. Intravascular Irreversible Elec-troporation: Theoretical and Experimental Feasibility Study. *Proceedings of the IEEE EMBC 2008 Conference*.

Maor, E., Ivorra, A. & Rubinsky, B., 2008b. Irreversible electroporation attenuates neointimal formation after angioplasty. *IEEE Transactions of Biomedical Engineering*, 55(9).

Maor, E., Ivorra, A. & Rubinsky, B., 2009. Non Thermal Irreversible Electroporation: Novel Technology for Vascular Smooth Muscle Cells Ablation. *PLoS ONE*, 4(3).

Marin, T., 2006. Solidification of a Liquid Metal Droplet Impinging on a Cold Surface. *Excerpt from the Proceedings of the COMSOL Users Conference, Boston*.

Mattson, B. & Sonesson, U., 2003. Introduction. In *Environmentally friendly food processing*. CRC Press: Boca Raton, pp. 1-2.

Mazur, P., 1970. Cryobiology: The Freezing of Biological Systems. *Science*, 68.

Mazur, P. et al., 1970. Interaction of Cooling Rate, Warming Rate and Protective Additives on the survival of Frozen Mammalian Cells. *Churchill, London*.

Mazzoleni, A., Sisken, B. & Kahler, R., 1986. Conductivity values of tissue culture medium from 20°C to 40°C. *Bioelectromagnetics*, 7(1), pp.95-99.

Meryman, H., 1966. Review of Biological Freezing in "Cryobiology." *Academic Press New York/London*.

Michael, D. & O'Neill, M., 1970. Electrohydrodynamic instability in plane layers of fluid. *Journal of Fluid Mechanics*, 41, pp.571-580.

Miklavcic, D. et al., 2000. A validated model of in vivo electric field distribution in tissues for electrochemotherapy and for DNA electrotransfer for gene therapy. *Biochim Biophys Acta*, 1523(1), pp.73-83.

Mir, L. & Rubinsky, B., 2002. Treatment of cancer with cryochemotherapy. *British Journal of Cancer*, 86(10), pp.1658-60.

Mir, L. et al., 2006. Standard operating procedures of the electrochemotherapy: Instructions for the use of bleomycin or cisplatin administered either systemically or locally and electric pulses delivered by the CliniporatorTM by means of invasive or non-invasive electrodes. *European Journal of Cancer Supplements*, 4, pp.14-25.

Mir, L. et al., 1998. Effective treatment of cutaneous and subcutaneous malignant tumours by electrochemotherapy. *British Journal of Cancer*, 77(12), pp.2336-42.

Mir, L. et al., 1991. Electrochemotherapy potentiation of antitumour effect of bleomycin by local electric pulses. *European Jounal of Cancer*, 27(1), pp.68-72.

Montorsi, F., 1997. Recovery of spontaneous erectile function after nerver-sparing radical retropubic prostatectomy with and without early intracavernous injections of alprostadil: resullts of a prospective, randomized trial. *The Journal of Urology*, 158, pp.1408-1410.

Moreira, C. et al., 2006. Quantitative Age-Related Differences in Human Sublingual Gland. *Archives of Oral Biology*, pp.960–966.

Mouneimne, Y. et al., 1990. Stable rightward shifts of the oxyhemoglobin disassociation curveinduced by encapsulation of insitol hexaphostate in red blood cellsusing electroporation. *FEBS Letters*, 275, pp.117-120.

Mouneimne, Y. et al., 1991. Electroinsertion of xeno proteins in red blood cell membranes yields a long lived protein carrier in circulation. *Biochimica et Biophysica Acta*, 1066, pp.83-89.

Narsetti, R. et al., 2006. Microbial inactivation in water using pulsed electric fields and magnetic pulse compressor technology. *IEEE Transactions on Plasma Science*, 34(4).

Neumann, E. et al., 1982. Gene transfer into mouse lyoma cells by electroporation in high electric fields. *EMBO*, 7(1), pp.841-845.

Neumann, E., Sowers, A. & Jordan, C., 1989. *Electroporation and Electrofusion in Cell Biology*, New York: Plenum Press.

Okino, M. & Esato, K., 1990. The effects of a single high voltage electrical stimulation with an anticancer drug on in vivo growing tumors. *Surgery Today*, 20(2), pp.197-204.

Okino, M. & Mohri, H., 1987. Effects of a high-voltage electrical impulse and an anticancer drug on in vivo growing tumors. *Jpn. J Cancer Re.*, 78(12), pp.1319-21.

Onik, G & Rubinsky, B., 2010. Irreversible electroporation: first patient experience focal therapy of prostate cancer. *Series in Biomedical Engineering*, pp.235-247.

Onik, G et al., 1984. Ultrasonic characteristics of frozen liver. *Cryobiology*, 21(3), pp.321-328.

Onik, G, Mikus, P. & Rubinsky, B., 2007. Irreversible electroporation: implications for prostate ablation. *Technology in Cancer Research and Treatment*, 6(4).

Onik, G et al., 1991. Ultrasound-guided hepatic cryosurgery in the treatment of metastiatic colon carcinoma. Preliminary results. *Cancer*, 67(4), pp.901-7.

Organ, L., 1976. Electrophysiologic Principles of Radiofrequency Lesion Making. *Applied Neurophysiology*, 39, pp.69-76.

Petrov, A., 1980. Edge energy and pore stability in bilayer lipid membranes. *Advances in Liquid Crystal Research and Applications*, pp.695-737.

Petrov, A., Seleznev, S. & Derzhanski, A., 1979. Principles and methods of liquid crystal physics applied to the structure and functions of biological membranes. *Acta Physica Polonica*, A55, pp.385-405.

Pham, L., Dahiya, R. & Rubinsky, B., 1999. An in vivo study of antifreeze protein adjuvant cryosurgery. *Cryobiology*, 38(2), pp.169-75.

Phillips, M., Maor, E. & Rubinsky, B., 2011. Principles of tissue engineering with nonthermal irreversible electroporation. *Journal of Heat Transfer*, 133(1).

Pop, M. et al., 2003. Changes in Dielectric Properties at 460 kHz of Kidney and FatDuring Heating: Importance for Radio-Frequency Thermal Therapy. *Physics in Medicine and Biology*, 48(15), pp.2509–2525.

Prakash, P. et al., 2006. Measurement of the Specific Heat Capacity of Liver Phantom. *Physiological Measurement*, 27, p.N41–N46.

Ragde, H. et al., 2008. Modern prostate brachytherapy. *Cancer Journal for Clinicians*, 50(6), pp.380-393.

Reed, J., 1999. Biology of neoplasia: dysregulation of apoptosis in cancer. *Journal of Clinical Oncology*, 17(9).

Robinson, M. et al., 1991. New Materials for Dielectric Simulation of Tissues. *Physics in Medicine and Biology*, 36, pp.1565–1571.

Rossi, M. et al., Computerized planning of cryosurgery using bubble packing: an experimental validation on a phantom material. *The International Journal of Heat and Mass Transfer*, 51, pp.5671-5678.

Roth, B. & Wikswo, J., 1985. The magnetic field of a single axon. A comparison of theory and experiment. *Biophysics Journal*, 48, pp.93-105.

Rubinsky, B., 2000. Cryosurgery. *Annual Review of Biomedical Engineering*, 2, pp.157-187.

Rubinsky, B., 2010. Irreversible Electroporation. *Springer Publications Series in Biomedical Engineering*, XIV.

Rubinsky, B. & Cravalho, E., 1981. A Finite Element Method for the Solution of One-Dimensional Phase Change Problems. *International Journal of Heat and Mass Transfer*, 24(12).

Rubinsky, B. & Cravalho, E., 1979. Analysis for the temperature Distribution During the Thawing of a Frozen Biological Organ. *A.I.Ch.E Symposium Series*, 75, pp.81-88.

Rubinsky, B. & Onik, G, 1991. Cryosurgery: recent advances on the application of cold medicine. *International Journal of Refrigeration*, 14.

Rubinsky, B. & Pegg, D., 1988. A Mathematical Model for the Freezing Process in Biological Tissue. *Proceedings of the Royal Society of London*, 234.

Rubinsky, B. & Shitzer, A., 1976. Analysis of a Stefan-Like Problem in a Biological Tissue Around a Cryosurgical Probe. *Journal of Heat Transfer*, 98(3).

Rubinsky, B. et al., 1994. Cryosurgical system for destroying tumors by freezing.

Rubinsky, B., Onik, G & Mikus, P., 2007. Irreversible electroporation: a new ablation modality - clinical implications. *Technology in Cancer Research and Treatment*, 6(1), pp.37-46.

Rubinsky, B. et al., 2008. Optimal Parameters for the Destruction of Prostate Cancer Using Irreversible Electroporation. *The Journal of Urology*, 180(6), pp.2668-2674.

Rui, J. et al., 1999. Effect of thermal variables on human breast cancer in cryosurgery. *Breast Cancer Research and Treatment*, 53(2), pp.185-192.

Rusby, J. et al., 2007. Breast duct anatomy in the human nipple: three-dimensional patterns and clinical implications. *Breast Cancer Research and Treatment*, 106, pp.171-179.

Sale, AJ, 1968. Effects of high electric fields on micro-organisms: III. Lysis of erythrocytes and protoplasts. *Biochim Biophys Acta*, 163(1), pp.37-43.

Sale, AJ & Hamilton, WA, 1968. Effects of high electric fields on micro-organisms. 3. Lysis of erythrocytes and protoplasts. *Biochim Biophys Acta*, 163(1), pp.37-43.

Sale, AJ & Hamilton, WA, 1967. Effects of high electric fields on microorganisms. 1. Killing of bacteria and yeasts. *Biochimica et Biophysica Acta*, 148, pp.781–788.

Saulis, G. & Venslauskas, M., 1993. Cell electroporation Part 1. Theoretical simulation of the process of pore formation in a cell. *Bioelectrochemistry and Bioenergetics*, 32, pp.221-235.

Schoellnast, H. et al., 2011. Acute and subacute effects of irreversible electroporation on nerves: experimental study in a pig model. *Radiology*, 260(2), pp.421-427.

Schoenbach, H. et al., 2000. Bacterial decontamination of liquids with pulsed electric fields. *IEEE Transactions on Dielectric and Electrical Insulation*, 7(5), pp.637–645.

Schröder, J., 1972. Altered Ratio Between Axon Diameter and Myelin Sheath Thickness in Regenerated Nerve Fibers. *Brain Research*, 45, pp.49-65.

Smith, J. & Fraser, J., 1974. An estimation of tissue damage and thermal history in the cryolesion. *Cryobiology*, 11(2), pp.139-147.

Somiari, S. et al., 2000. Theory and in vivo application of electroporative gene delivery. *Molecular Therapy*, 3(2), pp.178-87.

Srinivas, V. & Ananthasuresh, G., 2006. Analysis and Topology Optimization of Heat Sinks with a Phase-Change Material using a COMSOL Multiphysics Platform. *Excerpt from the Proceedings of the COMSOL Users Conference, Bangalore*.

Steinchen, A., Gallez, D. & Sanfeld, A., 1982. A viscoelastic approach to the hydrodynamic stability of membranes. *Journal of Colloid and Interface Science*, 85(1), pp.5-15.

Sun, L., Schiano, J. & Smith, N., 2003. Novel Adaptive Control System forUltrasound Hyperthermia Treatment of Prostate Disease. *IEEE Symposium on Ultrasonics*, 2, pp.1274–1277.

Takahashi, S. et al., 1997. Regeneration of Myoepithelial Cells in Rat Submandibular Glands After Yttrium Aluminium Garnett Laser Irradiation. *International Journal of Experiental Pathology*, 78, pp.91–99.

Takenaka, A. & Murakami, G., 2005. Variation in course of cavernous nerve with special reference to details of topographic relationships near prostatic apex: Histologic study using male cadavers. *Urology*, 65, pp.136-142.

Tatsutani, K et al., 1996. Effect of thermal variables on frozen human primary prostatic adenocarinoma cells. *Urology*, 48(3), pp.441-7.

Taylor, G. & Michael, D., 1973. On making holes in a sheet of fluid. *Journal of Fluid Mechanics*, 58(4), pp.625-639.

Teissie, J. & Rols, M., 1993. An experimental evaluation of the critical potential difference inducing cell membrane electropermeabilization. *Biophysical Journal*, 65(1), pp.409-413.

Teissie, J. et al., 2002. Recent biotechnological developments of electropulsation. A prospective review. *Bioelectrochemistry*, 55, pp.107-112.

Tsong, T., 1991. Electroporation of Cell Membranes. *BIophysical Journal*, 60, pp.297-306.

Valvano, J. & Chitsabesan, B., 1987. Thermal Conductivity and Diffusivityof Arterial Wall and Atherosclerotic Plaque. *Lasers in the Life Sciences*, 1, pp.219-229.

Vernier, P. et al., 2008. Nanosecond electric pulse-induced calcium entry into chromaffin cells. *Bioelectrochemistry*, 73(1), pp.1-4.

Villapecellin-Cid, M., Rao, L. & Reina-Tosina, J., 2003. Ranvier nodes impedance match with internodal transmission lines of myelinated axons. *Engineering in Medicine and Biology Society, 2003. Proceedings of the 25th Annual International Conference of the IEEE*, 2, pp.1905-1908.

Voller, V. & Prakash, C., 1987. A fixed grid numerical modelling methodology for convection-diffusion mushy region phase-change problems. *International Journal of Heat and Mass Transfer*, 30(8), pp.1709-1719.

Weaver, J., 2003. Electroporation of Biological Membranes from Multicellular to Nano Scales. *EEE Transactions on Dielectrics and Electrical Insulation*, 10.

Weaver, J., 2000. Electroporation of Cells and Tissues. *IEEE Transactions on Plasma Science*, 28, pp.24-33.

Weaver, J., 1993. Electroporation: A General Phenomenon for Manipulating Cells and Tissue. *Journal of Cellular Biochemistry*, 51, pp.426-435.

Weaver, J. & Chizmadzhev, Y., 1996a. Electroporation. In *Handbook of Biological Effects of Electromagnetic Fields*. Boca Raton: CRC Press, pp. 247-274.

Weaver, J. & Chizmadzhev, Y., 1996b. Theory of electroporation: a review. *Bioelectrochemistry and Bioenergetics*, 41, pp.135-160.

Weaver, J. & Mintzer, R., 1981. Decreased bilayer stability due to transmembrane potentials. *Physics Letters A*, 86(1), pp.57-59.

Wissler, E., 1998. Pennes' 1948 paper revisited. *Journal of Applied Physiology*, 85, pp.35-41.

Wright, N., 2003. On a Relationship Between the Arrhenius Parameters from Thermal Damage Studies. *Journal of Biomechanical Engineering*, 125, pp.300-304.

Wu, F. et al., 2003. A randomised clinical trial of high-intensity focused ultrasoundablation for the treatment of patients with localised breast cancer. *British Journal of Cancer*, 89, pp.2227 – 2233.

Wulff, W., 1974. The energy conservation equation for living tissue. *IEEE Transactions on Biomedical Engineering*, 21(6), pp.494-495.

Xiaoming, H. & Bischof, J., 2003. Quantification of temperature and injury response in thermal therapy and cryosurgery. *Critical reviews in biomedical engineering*, 31, pp.355-421.

Yao, C. et al., 2009. Window effect of pulsed electric field on biological cells. *IEEE Transactions on Dielectrics and Electrical Insulation*, 16(5).

Zimmerman, U., 1996. *The Effects of High Intensity ElectricField Pulses on Eukaryotic Cell Membranes: Fundamentals and Applications*, Boca Raton: CRC Press.